Electron Paramagnetic Resonance in Silicon

by

S. D. Lacey B.Sc.

Being a thesis
submitted to the University of Keele
for the Degree of Doctor of Philosophy

Department of Physics,
University of Keele,
Keele, Staffordshire.
September, 1971.

ABSTRACT

Electron Paramagnetic Resonance (E.P.R.) in silicon doped with the shallow Group V donors phosphorus and arsenic has been studied over the temperature range from 20 to 50°K. The range of donor concentrations examined was sufficient for exchange to be possible in the more highly doped samples, all samples exhibiting a resonance characteristic of bound donor electrons at 20°K.

The observed reduction in the hyperfine splitting with increasing temperature is interpreted as being due to the phonon-induced transitions of electrons between the various 1s hydrogen-like states. For phosphorus donors an estimate of 10.7 ± 0.4 meV is obtained for the valley-orbit splitting. The greater value of this splitting for arsenic donors results in an insignificant reduction in the hyperfine splitting for arsenic over the same temperature range.

Simultaneous with the reduction in the hyperfine splitting the linewidth and shape change. Although the above mechanism gives a calculated width of the correct order of magnitude, the increasing linewidth with temperature is better described by an activation energy of half the donor ionization energy. The exchange scattering of the bound donor electrons by conduction electrons is therefore thought to be the dominant source of the linewidth, such that with the increasing exchange frequency with temperature the hyperfine lines will eventually be averaged out and replaced by a single line. For phosphorus and arsenic donor concentrations of approximately 5.10^{17} cm^{-3} this narrowing single line was only observed for phosphorus. The difference in the donor ionization energies is thought sufficient to prevent its observation in the case of arsenic.

A possible alternative explanation of the above effects, due to the phonon-induced hopping of electrons from electronically occupied to neighbouring unoccupied sites, was also examined. Calculation demonstates that the experimental results cannot be interpreted in this fashion.

ACKNOWLEDGEMENTS

The author would like to express his thanks to the following:-

Professor D. J. E. Ingram, for providing facilities for research in the Physics Department.

Dr. G. Lancaster, for supervising the work.

All members of the Physics Department, for their encouragement and assistance.

Members of the technical staff, in particular Mr. A. G. Smallman.

Dr. M. Pollak, for the samples of compensated silicon.

The Plessey Company, for financing the purchase of liquid hydrogen.

Mrs. D. Webb, Mr. B. Bygrave and Mrs. J. Shrimpton, for assistance in producing this thesis.

The author's family, for their forbearance during the writing of this thesis.

The University of Keele, for the award of a Demonstratorship and Junior Research Fellowship.

CONTENTS

CHAPTER 6

CHAPTER 1

INTRODUCTION

The electrically active impurity and defect centres in silicon have been the subject of intensive fundamental studies, the stimulation for these studies having been the high level of investment of the electronics industry in silicon. One technique which has been used to advantage in elucidating the nature of these centres is that of Electron Paramagnetic Resonance, E.P.R.

The covalent nature of the bonding between the atoms in a perfect silicon crystal requires that each valence electron is paired with one whose magnetic dipole moment is aligned anti-parallel, so that the assembly of electrons has zero magnetic moment. But impurity, or extrinsic, conductivity in this Group IV material is usually achieved by the controlled addition of Group III or Group V elements. These elements act as acceptors or donors of electrons respectively. The "holes" or electrons associated with these impurities may either be constrained to their impurity centres, or, having been excited to the valence or conduction band, be free to move through the lattice. Unpaired electrons now exist, so that the assembly will have a finite magnetic moment, which should therefore be detectable in a magnetic field by the resonant absorption of energy.

Germanium was the first elemental semiconductor to be used in rectifiers and transistors, but the operational temperature limitation due to the materials energy band gap eventually led to the emergence of silicon as the material upon which industry has founded its active

electronic devices. E.P.R. in germanium is not possible to the fine limits of those in silicon, since various mechanisms broaden the resonance lines.

Before briefly summarizing the E.P.R. results in semiconducting III-V and II-VI materials, it is opportune to point out the difference between the so-called "Shallow" and "Deep" impurity centres. A shallow impurity, e.g., a Group V or III element in a Group IV semiconductor, has one unpaired electron or hole weakly bound to it. This electron or hole moves in a hydrogen-like orbit with a radius whose diameter is of the order of many lattice constants. Because the electron or hole is weakly bound, it may be easily excited to the conduction or valence band respectively. Even when bound to the impurity the behaviour of the electron or hole is determined mainly by the energy band structure and dielectric constant of the host lattice. By comparison, the deep centres have relatively high ionization energies, and the electrons or holes are effectively localized on the impurity ions. Their charge states may be varied by controlling the position of the Fermi level through the simultaneous incorporation of shallow donors or acceptors. The behaviour of the electrons or holes is now described by that of the free ion plus the effects of the surrounding atoms and ions of the solid.

In the semiconducting III-V materials doped with shallow impurities, electron magnetic resonance has only been observed for conduction electrons and holes. Conduction electron resonance in InSb, GaAs, InAs, GaP and $Ga_x In_{1-x} Sb$, and the resonance of conduction holes in GaAs, have been reported. For the II-VI materials ZnS and CdS incorporating shallow electron traps or donors e.g., halide ions, it is a

matter of some discussion whether the resonance is of bound electrons, or of those moving freely in the conduction band or a shallow impurity band.

The resonance of many deep impurities has been detected in silicon and germanium, and also in the III-V and II-VI materials. The iron transition group elements are the most common impurities to be studied, as they provide information on the covalent or ionic character of the host lattice. Some of these elements have been detected in silicon and germanium, GaAs, InAs and GaP, ZnS, ZnSe, ZnTe, CdS, CdTe, HgTe and $Cd_x Hg_{1-x}Te$. In fact, the first observation of magnetic resonance in semiconductors was of manganese in ZnS in 1951.

Two further sources of resonance which have been observed in silicon should be mentioned. Many paramagnetic centres created by irradiation with electrons, neutrons and ions have been studied, and resonances associated with the manner of the surface preparation have been detected.

Because of the spatial nature of the orbit and the low ionization energy of the shallow donor electron, two classes of resonance present themselves. The first is when the concentration of donors and the temperature are sufficiently low to prevent interaction between the bound electrons or to produce conduction electrons. In this case a spectrum characterized by the electron's interaction with its donor's nuclear spin is apparent. It has been shown that as the temperature is increased from 1.3 to 20°K the processes by which the electron may relax back to its Zeeman ground state after excitation by electro-

magnetic radiation are progressively via single phonon processes, two phonon processes, and a further two phonon process involving an excited state of the hydrogen-like approximation.

The second class of resonance is really the inverse of the first i.e., high donor concentrations, and/or high temperatures, such that the electron moves either in the conduction band or a shallow impurity band. A single spectral line is now observed. At temperatures greater than 100°K the dominant mechanism for the spin relaxation, through the spin-orbit coupling, is the same as that determining the electrons mobility i.e., scattering by phonons or impurities. At lower temperatures deviations from this mechanism were apparent.

Thus, an absence of explanation for the relaxation processes occurring in the temperature interval from 20 to 100°K stimulated the work to be described.

The thesis commences with a description of the basic resonance phenomenon, and, with a view to the situation in silicon, the various parameters which characterize the resulting spectrum. This is followed by the expansion of some of these points, a discussion on the semi-conductor to metal transition, and conduction processes which might influence the spin relaxation. The requirements and limitations associated with the detection of E.P.R. are then discussed, and how these factors are applied to the apparatus used. Finally, the results are presented and discussed in the light of suggested mechanisms.

CHAPTER 2

ELECTRON PARAMAGNETIC RESONANCE

In this chapter an account is given of the resonance phenomenon, along with the factors characterizing an observed spectrum. The account is biased towards the situation for Group V impurities in silicon, but not exclusively. Both classical and quantum mechanical descriptions are used, clarity dictating that description chosen for particular situations.

2.1 A Classical Description of Resonance

A magnetic moment $\underline{\mu}$ of a free particle, or a system of particles devoid of mutual interactions, is related to its total angular momentum $\underline{J}$ by a constant g, the "g factor", according to

$$\underline{\mu} = - g\beta \underline{J} \qquad \ldots\ldots\ldots\ldots\ldots 2.1$$

where β is the Bohr Magneton, while the minus sign relates the classical rotation of negative charge to the angular momentum direction. If this magnetic moment is now placed in a magnetic field $\underline{H}_o$, it will precess about this field at a fixed angle and at an angular frequency

$$\omega_o = \frac{g\beta}{\hbar} H_o, \qquad \ldots\ldots\ldots\ldots\ldots 2.2$$

or

$$\hbar\omega_o = g\beta H_o, \qquad \ldots\ldots\ldots\ldots\ldots 2.3$$

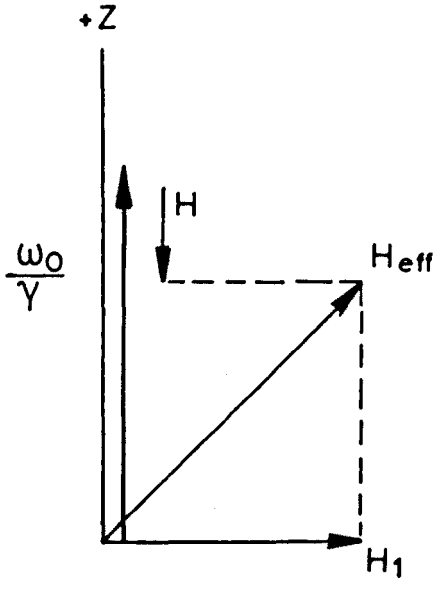

FIG. 2.1

H_{eff}, the Effective Field in the Rotating Frame of Reference, where $\gamma \equiv g\beta/\hbar$ (not to scale).

ω_o being the Larmor Angular Frequency.

Similarly, if this same magnetic moment is placed in the same magnetic field it will have a potential energy of

$$E = - \underline{\mu} \cdot \underline{H}_o \cdot \qquad \ldots\ldots\ldots\ldots \quad 2.4$$

The quantum mechanical description of the resulting $(2J + 1)$ Zeeman energy levels is given by

$$E_{M_J} = g\beta M_J H_o \qquad \ldots\ldots\ldots\ldots \quad 2.5$$

where M_J, known as the magnetic quantum number, is the projection of $\underline{J}$ along $\underline{H}_o$, and ranges from - J to + J in integral steps. The selection rule for magnetic dipole transitions is $\Delta M_J = \pm 1$, hence transitions taking place between the adjacent energy levels as specified in Equation 2.5 result in a resonance condition of

$$\hbar\omega_o = g\beta H_o. \qquad \ldots\ldots\ldots\ldots \quad 2.6$$

Thus Equations 2.3 and 2.6 suggest that a classical description is valid.

In the presence of a large magnetic field H and the favourably rotating component of an incident linearly polarized magnetic field perpendicular to H, of amplitude $2H_1$ and frequency ω_o, a magnetic dipole will precess about the effective field H_{eff} it observes in the frame of reference rotating at ω_o, as illustrated in Fig. 2.1[1]. As the field H is swept H_{eff} will pass through a condition in which its value is H_1 alone, at which point $H = H_o$ i.e., resonance occurs when the magnetic field is such that an isolated magnetic dipole moment would have a Larmor precession frequency of ω_o.

2.2 The Bloch Equations and Their Slow Passage Solution

If a system of magnetic dipoles is disturbed from equilibrium it will seek to return to that equilibrium. Bloch[2] advanced three equations to describe the dipoles' motion:

$$\left.\begin{aligned} \frac{dM_x}{dt} &= \gamma\,(\underline{H}_t \Lambda\, \underline{M})_x - \frac{M_x}{T_2} \\ \frac{dM_y}{dt} &= \gamma\,(\underline{H}_t \Lambda\, \underline{M})_y - \frac{M_y}{T_2} \\ \frac{dM_z}{dt} &= \gamma\,(\underline{H}_t \Lambda\, \underline{M})_z + \frac{(M_o - M_z)}{T_1} \end{aligned}\right\} \quad \ldots\ldots\ldots\ldots\ 2.7$$

where an assembly of moments is now considered i.e.,

$$\underline{M} = \sum_{\substack{\text{unit} \\ \text{volume}}} \underline{\mu}_1,$$

and $\underline{H}_t$ is the vector sum of $\underline{H}$ and $\underline{H}_1$. An exponential decay of M in the rotating frame is assumed. T_1, the spin-lattice relaxation time, describes the rate at which the component of M in the z direction returns to its equilibrium value, a process requiring the moments to exchange energy with the lattice. By comparison T_2, the spin-spin relaxation time, expresses the de-phasing of the angular motion of the individual moments contributing to the component of M perpendicular to the field, and is therefore described by a time different to that involving energy transfer.

If the thermal equilibrium value $\underline{M}_o$ is related to the susceptibility χ_o by

$$\chi_o = \frac{\underline{M}_o}{\underline{H}}, \qquad \text{..... 2.8}$$

and the complex susceptibility is given by

$$\chi = \chi' - i\chi'', \qquad \text{..... 2.9}$$

then, the steady state solution of Equation 2.7 for a field sweep through the resonance line taking much longer than the relaxation time T_1 i.e., the "Slow Passage Condition", gives

$$\chi' = \tfrac{1}{2}\chi_o \gamma H_o T_2 \left[\frac{T_2\,\gamma(H_o - H)}{1 + T_2^2\gamma^2(H_o - H)^2 + \gamma^2 H_1^2 T_1 T_2}\right] \qquad \text{..... 2.10}$$

$$\chi'' = \tfrac{1}{2}\chi_o \gamma H_o T_2 \left[\frac{1}{1 + T_2^2\gamma^2(H_o - H)^2 + \gamma^2 H_1^2 T_1 T_2}\right] \qquad \text{..... 2.11}$$

Now the average power absorbed per unit volume

$$P = 2\omega_o \chi'' H_1^2. \qquad \text{..... 2.12}$$

N.B. For a linearly polarized field of amplitude only H_1 this becomes

$$P' = \tfrac{1}{2}\omega_o \chi'' H_1^2. \qquad \text{..... 2.13}$$

Hence for the condition known as "non-saturation" i.e., when the spin-lattice relaxation processes are able to maintain equilibrium, or

mathematically

$$\gamma^2 H_1^2 T_1 T_2 \ll 1 + T_2^2 \gamma^2 (H_o - H)^2,$$

and for a sharp resonance i.e., $\gamma H_o T_2 \gg 1$,

$$P = \frac{\gamma^2 H_o^2 \chi_o T_2 H_1^2}{1 + T_2^2 \gamma^2 (H_o - H)^2} \qquad \ldots\ldots\ldots\ldots\ldots 2.14$$

This line is Lorentzian in shape, and has a full width at half height of

$$\Delta H_{\frac{1}{2}} = \frac{2}{\gamma T_2} . \qquad \ldots\ldots\ldots\ldots\ldots 2.15$$

For experimental reasons to be explained in Section 4.7 it is usual to modulate the magnetic field H with a small alternating field h_m ($< \Delta H_{\frac{1}{2}}$), and to consequently detect the derivative of P with respect to magnetic field. Thus it may be shown that

$$\Delta H_{pp} = \frac{2}{\sqrt{3}\, T_2 \gamma} \qquad \ldots\ldots\ldots\ldots\ldots 2.16$$

where ΔH_{pp} is the linewidth between the points of maximum gradient of the absorption curve, or rephrasing, the linewidth between absorption derivative extrema. It follows therefore that

$$\frac{\Delta H_{\frac{1}{2}}}{\Delta H_{pp}} = \sqrt{3} = 1.73 \qquad \ldots\ldots\ldots\ldots\ldots 2.17$$

for a Lorentzian line.

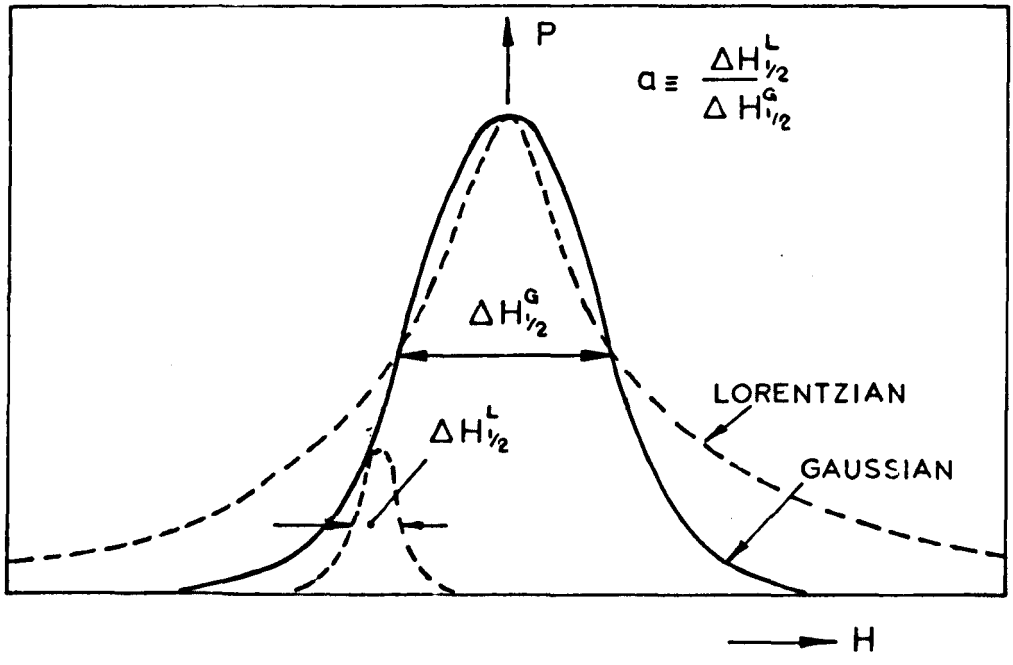

FIG. 2.2

Lorentzian and Gaussian Absorption Curves with the same $\Delta H_{1/2}$, showing one spin packet of the Gaussian.

The broadening of the above resonance lines can be ascribed to the fact that the two spin levels between which absorption is observed are not sharply defined. Such lines are designated "Homogeneously" broadened. Lines may be broadened for other reasons[3] (see Section 2.6) and will then generally speaking be Gaussian in shape and designated "Inhomogeneously" broadened. For a Gaussian line[4]

$$\frac{\Delta H_{\frac{1}{2}}}{\Delta H_{pp}} = 1.18. \qquad \ldots\ldots\ldots\ldots 2.18$$

A comparison in the shapes of the lines corresponding to the two types of broadening is given in Fig. 2.2.

2.3 Adiabatic Rapid Passage

Electron spin-lattice relaxation times in excess of two hours have been measured in silicon at very low temperatures, thus a field sweep through the resonance line occurs in a time short compared with T_1.

The above analysis would be inappropriate in this case. Bloch[2] has shown that during resonance the magnetic moment $\underline{M}$ will now preserve its angle with respect to $\underline{H}_{eff}$ (see Fig. 2.1), so preserving its interaction energy.

An upper limit to the rate of field sweep requires that the direction of $\underline{H}_{eff}$ should change only very slightly during one Larmor precession of $\underline{M}$ about it, or,

$$\left(\frac{1}{H_1}\right)\left|\frac{dH}{dt}\right| \ll \gamma H_1. \qquad \ldots\ldots\ldots\ldots 2.19$$

Similarly a lower limit may be fixed, imposed by the relaxation times. $\underline{M}$ must not decay before one precession about $\underline{H}_{eff}$, and the sweep must be fast enough to prevent $\underline{M}$ relaxing back to $\underline{M}_o$ before $\underline{H}_{eff}$ has been reversed. These conditions require

$$\gamma H_1 \gg \frac{1}{T_2} \qquad \ldots\ldots\ldots\ldots\ldots 2.20$$

and

$$\left(\frac{1}{H_1}\right)\left|\frac{dH}{dt}\right| \gg \frac{1}{T_1} . \qquad \ldots\ldots\ldots\ldots\ldots 2.21$$

For inhomogeneously broadened lines the situation is more complicated, but has been comprehensively analysed by Weger[5].

2.4 Spin-Lattice Relaxation

In Section 2.2 the concept of an interaction between the magnetic dipoles and the lattice was introduced, and its importance with respect to the observed susceptibilities and passage conditions is apparent.

The relaxation time may also be easily shown to be related to the probability per unit time, W, that a dipole will create or inelastically scatter phonons when making an emissive transition. For a spin $\frac{1}{2}$ system under thermal equilibrium

$$W = \frac{1}{2\,T_1} . \qquad \ldots\ldots\ldots\ldots\ldots 2.22$$

If this system is now subjected to an oscillating H_1 field as previously indicated, a further transition probability rate V must be introduced,

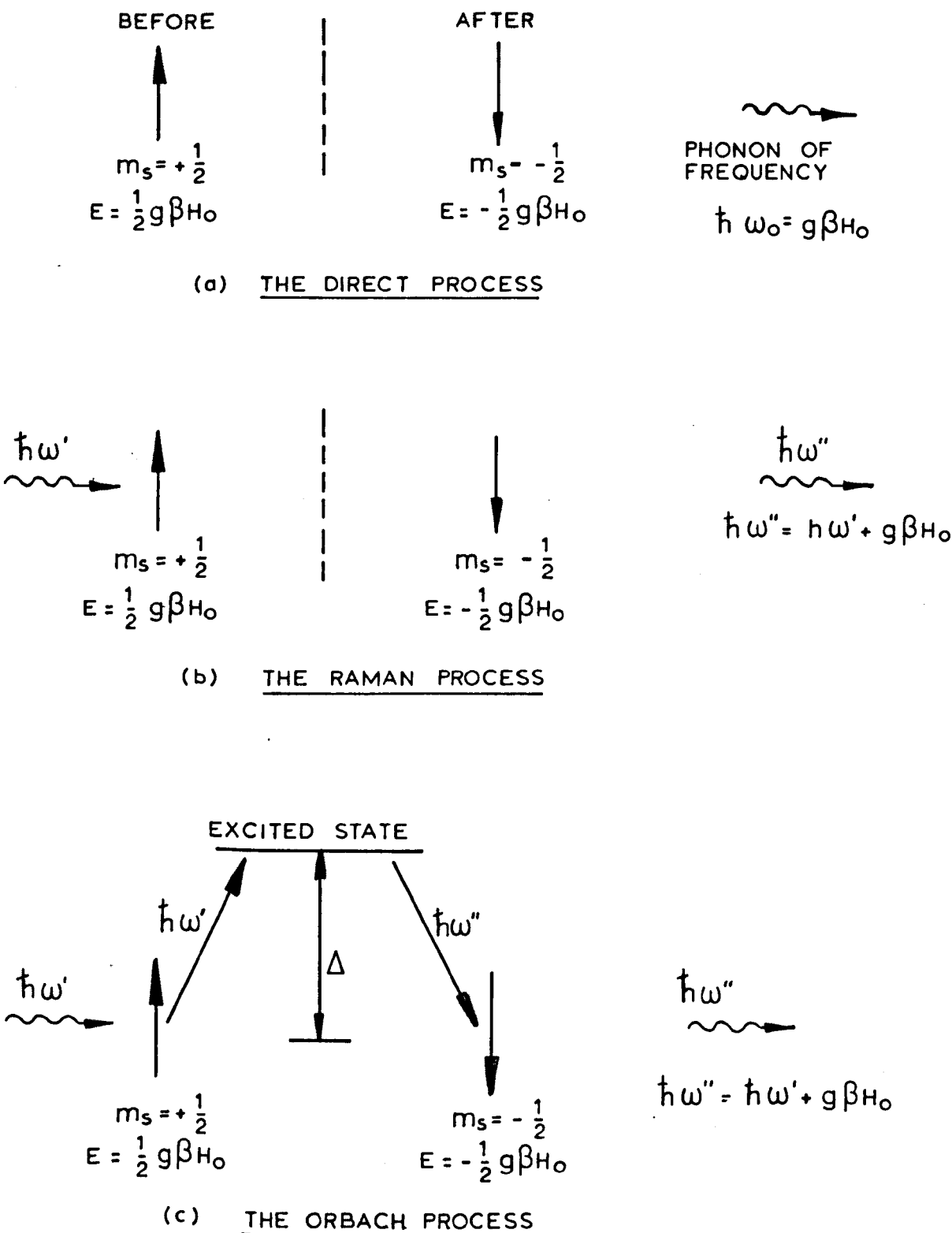

FIG. 2.3

Spin-Lattice Relaxation Processes.

being the same in both the upward and downward directions. It is now found that a spin temperature T_s may be defined by

$$T_s = T(1 + 2\ T_1\ V) \qquad \ldots\ldots\ldots\ldots\ 2.23$$

where T is the thermal equilibrium temperature under non-excited conditions. With increasing amplitude of the oscillating magnetic field H_1 there will be a related increase in V[6], such that when $V \geq \frac{1}{2T_1}$ saturation will begin to occur, resulting in a spin temperature increase above the thermal equilibrium temperature.

(a) The Direct Process

Pake[1] has reviewed the early work of Waller[7] on the coupling of spins to the lattice. He suggested that the small local magnetic field H_{loc} produced by neighbouring spins at the site of an individual spin can be modulated by the variation of the inter-spin distance due to phonons. This oscillatory field will have a comparitively large probability rate for inducing emissive transitions when the phonons have a frequency in the region of ω_o. Unfortunately phonon spectra indicate comparitively few phonons at those frequencies of interest i.e., in the region of 10 GHz. The relaxing spins in this Direct Process will then create phonons of energy $\hbar\omega_o$. This is illustrated in Fig. 2.3a, and calculation suggests

$$\frac{1}{T_1} \propto H_o^{\,2}\ T \qquad \ldots\ldots\ldots\ldots\ 2.24$$

where T is the temperature.

(b) The Raman Processes

Since there are few phonons at ω_o Waller further suggested an Indirect or Raman process in which inelastic scattering of higher frequency phonons occurs, as shown in Fig. 2.3b. This process usually dominates at higher temperatures than the above and Waller found

$$\frac{1}{T_1} \propto H_o^{\ 0}\, T^7 \ . \qquad \ldots\ldots\ldots\ldots\ldots\ 2.25$$

Direct and Raman Processes have also been shown to occur through the interaction between the crystalline electric field, modulated by phonons, and the spin-orbit coupling[8] (see Section 2.9). For the Direct Process

$$\frac{1}{T_1} \propto H_o^{\ 4}\, T \ , \qquad \ldots\ldots\ldots\ldots\ldots\ 2.26$$

and for the Raman Process

$$\left.\begin{aligned} &\frac{1}{T_1} \propto H_o^{\ 0}\, T^9 \ (\text{for } T \ll \theta_D) \\ &\frac{1}{T_1} \propto H_o^{\ 0}\, T^0 \ (\text{for } T \gtrsim \theta_D) \end{aligned}\right\} \qquad \ldots\ldots\ldots\ldots\ldots\ 2.27$$

where θ_D is the Debye temperature ($\theta_D = 658^\circ K$ for silicon).

A further Raman relaxation mechanism can occur when an excited state exists within a phonon energy from the upper Zeeman level of the ground state. Orbach[9] has shown that the excitation of the spin to

this excited state and its subsequent relaxation to the lower Zeeman level of the ground state gives

$$\frac{1}{T_1} \propto \exp\left(-\frac{\Delta}{kT}\right) \qquad \ldots\ldots\ldots\ldots\ldots 2.28$$

where Δ is the energy separation of the excited state and the ground state. Fig. 2.3c illustrates this.

Castner[10] has identified the above relaxation mechanisms in silicon containing shallow donor impurities, and has observed the various temperature regions in which each mechanism dominates.

2.5 Spin-Spin Relaxation

As was pointed out in the last Section each magnetic dipole experiences a local magnetic field H_{loc} which will differ in direction from dipole to dipole, and will vectorially add to the applied field H_o. Thus the energy levels will be broadened by an amount of the order of $g\beta H_{loc}$, and there will be a distribution of Larmor precession frequencies covering a range $\delta\omega_o \sim \gamma H_{loc}$. Hence two dipoles differing in precession frequency by $\delta\omega_o$ and initially in phase, will be out of phase in a time $\sim \frac{1}{\delta\omega_o} \sim T_2$, and thus destroy the component of total magnetic moment perpendicular to the field.

A further mechanism exists for assemblies containing only identical paramagnetic particles. The precessing dipoles will create at their neighbours site a periodic field of the resonance frequency under whose influence an exchange of the orientation of the moments is possible since the total energy will be conserved. This limitation on the

lifetime of each particle in a given Zeeman level leads again to broadening, and thus as in the above an increase in the observed line-width.

2.6 Inhomogeneously Broadened Resonance Lines

Portis[3] has suggested that in the following cases (a) hyperfine interaction (b) anistropy broadening (c) dipolar interaction between spins with different Larmor frequencies, and (d) inhomogeneities in the applied magnetic field, resonance lines may be broadened inhomogeneously, in that there will be a distribution of fields over the assembly of dipoles, and energy will be transferred only to those whose local field satisfies the resonance condition.

It is a useful illustration of homogeneous and inhomogeneous lines to compare their saturation behaviour, and the consequent determination of the relaxation times T_1 and T_2.

In a later chapter expressions will be derived for the signal which can be detected from resonance absorption in a sample, and it can be shown by an extension of Equation 4.7 that the signal voltage $V_R \propto \chi'' H_1$. The value of χ'' at the line centre, from Equation 2.11, is

$$\chi'' = \frac{\frac{1}{2} \chi_0 \gamma H_0 T_2}{1 + \gamma^2 H_1^2 T_1 T_2}, \qquad \ldots\ldots\ldots\ldots\ldots 2.29$$

and hence, below saturation level, the signal is proportional to the microwave field H_1, while for strong saturation $V_R \propto \frac{1}{H_1}$, and in this case the power absorbed is independent of H_1. By also examining the point at which the signal is a maximum, it may be seen that V_R

therefore has the form

$$V_R = \frac{X}{1 + X^2} \qquad \text{..... 2.30}$$

where $X = \gamma H_1 (T_1 T_2)^{\frac{1}{2}}$. Hence the saturation of a homogeneously broadened line yields the product $T_1 T_2$, while knowledge of the homogeneous linewidth ($\propto \frac{1}{T_2}$, see Equation 2.15) allows the separate calculation of T_1.

By comparison, in the inhomogeneous case the assumption is initially made that the processes for spin-spin interaction are weak as compared with the direct interaction of the dipoles with the lattice, that is spin diffusion is extremely slow and it is possible to saturate only a narrow portion of the line, namely the width determined by H_1 or T_2. For Lorentzian spin packets Castner[11] gives

$$\chi'' = \frac{\frac{1}{2} \chi_o \gamma H_o f (H - H_o)}{(1 + \gamma^2 H_1^2 T_1 T_2)^{\frac{1}{2}}} \qquad \text{..... 2.31}$$

where $f(H - H_o)$ is the normalized envelope function of the distribution of spin packets. Thus

$$V_R \propto \chi'' H_1 \propto (\frac{X}{(1 + X^2}2)^{\frac{1}{2}}. \qquad \text{..... 2.32}$$

In this case the absorption signal increases linearly below saturation, and then just flattens out for $X>1$.

Castner[11] continued to generalize the above case when the initial

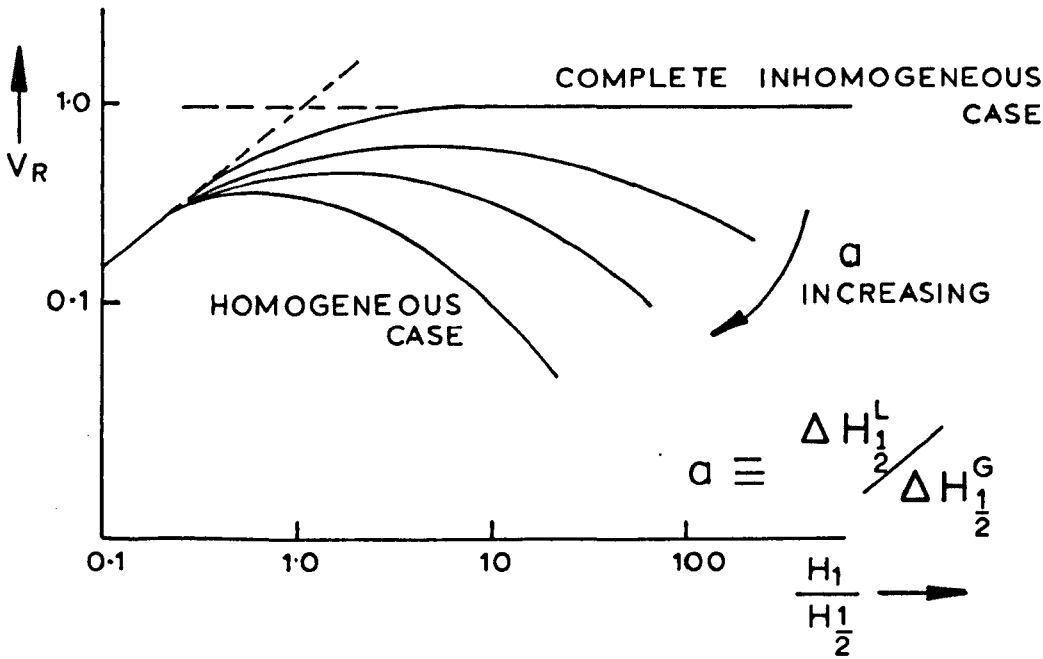

FIG. 2.4

Saturation behaviour during the transition from Inhomogeneous to Homogeneous Broadening.

assumption is not valid, and the spin packet width is approaching the envelope width. He defines a parameter $a \equiv \frac{\Delta H_{\frac{1}{2}}^{L}}{\Delta H_{\frac{1}{2}}^{G}}$ (see Fig. 2.2) being the ratio of the Lorentzian spin packet width to the inhomogeneous Gaussian width, and Fig. 2.4 shows the dependence of V_R upon the reduced microwave field $\frac{H_1}{H_{\frac{1}{2}}}$, where $H_{\frac{1}{2}} = \frac{1}{\gamma (T_1 T_2)^{\frac{1}{2}}}$, for increasing a. T_2, $(T_1 T_2)^{\frac{1}{2}}$ and T_1 may be independently determined through a, $H_{\frac{1}{2}}$, and the very high power saturation of the whole Gaussian envelope, respectively.

This theory has been applied to the measurement of the Raman spin-lattice relaxation of shallow donors in silicon when $T_1 < 10^{-4}$ sec[10]. For $T_1 > 10^{-3}$ sec the adiabatic population inversion technique has been used.

2.7 Exchange and Motional Narrowing of Resonance Lines

The influence of exchange between the magnetic dipoles, or motion of the dipoles, upon the resonance linewidth and shape is often best described by the Method of Moments.

The n^{th} moment M_n with respect to the centre of the line H_o is defined as

$$M_n = \frac{\int_{-\infty}^{+\infty} (H - H_o)^n \, g(H) \, dH}{\int_{-\infty}^{+\infty} g(H) \, dH} \qquad \text{..... 2.33}$$

where g(H) is the lineshape function. If, as is often the case, g (H) is symmetrical with respect to H_o all odd moments will vanish.

A Gaussian curve, for example, described by

$$g(H) = G \exp\left[- 0.693 \left(\frac{H - H_o}{\frac{1}{2} \Delta H_{\frac{1}{2}}} \right)^2 \right]$$

has moments[4]

$$\left.\begin{aligned} M_2 &= 0.721 \ (\tfrac{1}{2} \Delta H_{\frac{1}{2}})^2 \\ M_4 &= 1.56 \ (\tfrac{1}{2} \Delta H_{\frac{1}{2}})^4 \end{aligned}\right\} \qquad \ldots\ldots\ldots\ldots 2.34$$

and hence

$$\frac{M_4}{(M_2)^2} = 3.0 \ . \qquad \ldots\ldots\ldots\ldots 2.35$$

For a Lorentzian line no second or higher moments can be defined since the corresponding integrals diverge. This is overcome by truncating the curve at $b = |H - H_o|$, with $b >> \Delta H_{\frac{1}{2}}$, and assuming $g(H)$ is zero outside this region. Kittel and Abrahams[12] find

$$\left.\begin{aligned} M_2 &\simeq \frac{b \ \Delta H_{\frac{1}{2}}}{\pi} \\ M_4 &\simeq \frac{b^3 \ \Delta H_{\frac{1}{2}}}{3\pi}, \end{aligned}\right\} \qquad \ldots\ldots\ldots\ldots 2.36$$

and hence $$\frac{M_4}{(M_2)^2} = \frac{\pi}{3} \cdot \frac{b}{\Delta H_{\frac{1}{2}}} >> 1.$$

Thus an inspection of the ratio $\frac{M_4}{(M_2)^2}$ for spectral lines can point to the lineshape function.

The exchange interaction between the magnetic moments of two

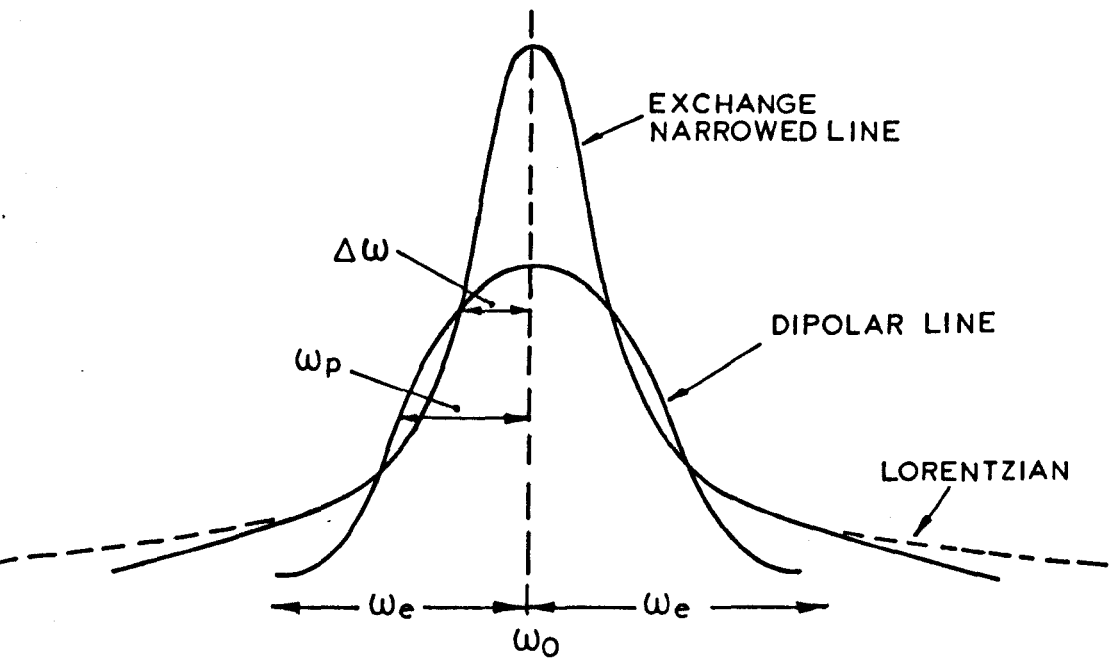

FIG. 2.5

The Exchange Interactions influence on Lineshape.

electrons has the form

$$\mathcal{H}_{ex} = -2 J_{ij} \underline{S}_i \cdot \underline{S}_j \qquad \ldots\ldots\ldots\ldots 2.37$$

where $\underline{S}i$ and $\underline{S}_j$ are the spin angular momenta of the two electrons, and J_{ij} is the exchange integral, having a value which is a function of the degree of overlap of the electron wave functions, and thus as an approximation, only nearest neighbours need be considered. Van Vleck[13] has shown that the addition of the exchange interaction to the dipolar interaction leaves the second moment unchanged, but the fourth moment increases as J^2, providing $J > \frac{\beta^4\beta^4}{r_o^6}$, where r_o is the nearest-neighbour distance. The resulting change in the lineshape is shown in Fig. 2.5, which indicates the importance of the wings in the calculation of the fourth moment. Van Vleck's calculations suggest, and Anderson and Weiss[14] confirm, that the exchange narrowed Gaussian line is Lorentzian shaped in the centre, but falls off more rapidly in the wings. In frequency terms this occurs at $\omega_o \pm \omega_e$, where $\omega_e \sim \frac{J}{\hbar}$. For a dipolar half-linewidth of ω_p, an exchange narrowed half-linewidth of

$$\Delta\omega = \frac{\omega_p^2}{\omega_e} \qquad \ldots\ldots\ldots\ldots 2.38$$

is obtained. They further show that when $\omega_e >> \omega_o$, $\mathcal{H}_{ex}$ is no longer a small perturbation on the Zeeman and dipolar Hamiltonians (see Section 2.9), and the spin states are mixed. This leads to a half-linewidth of

$$\Delta\omega = \frac{10}{3} \cdot \frac{\omega_p^2}{\omega_e} \cdot \qquad \ldots\ldots\ldots\ldots 2.39$$

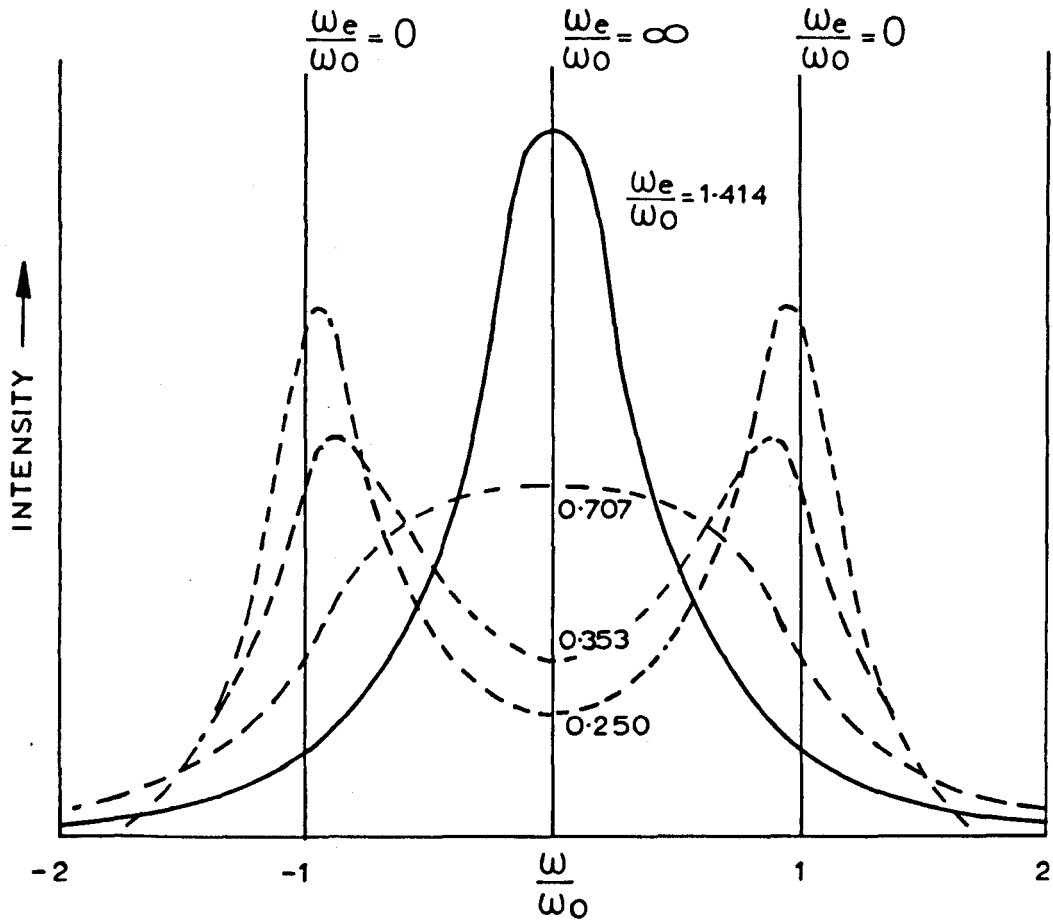

FIG. 2.6

Exchange or Motional Narrowing of a Pair of Lines.

Anderson[15] has extended the work of Anderson and Weiss[14] to include the case of ionic diffusion (i.e., motion) in solids. His model assumes that the precessing moments give rise to a radiated electromagnetic wave which is undergoing frequency modulation because the magnetic interactions between moments act to change the frequency of precession. The frequency modulation is changing in a random way in time due to the effect of motion on the magnetic interactions.

For the example in which there are only two possible environments, with frequency shifts of $\pm \omega_o$ from the centre of gravity, and these frequencies are equally probable, Anderson[15] shows that the two lines at $\pm \omega_o$ draw together as the jump rate ω_e increases, but always have the half-width of ω_e. The maxima of the lines occur at

$$\omega_{max} = \pm \sqrt{\omega_o^2 - 2\,\omega_e^2}\ , \qquad \ldots\ldots\ldots\ldots\ 2.40$$

$$\text{for} \quad \left(\frac{\omega_o}{\omega_e}\right)^2 > 2\ .$$

When the jumping pre-dominates i.e., $\omega_e > \omega_o$, only a single line will be exhibited of half-width

$$\Delta\omega \simeq \frac{\omega_o^2}{2\omega_e}\ , \qquad \ldots\ldots\ldots\ldots\ 2.41$$

which shows the usual exchange narrowing. These spectral changes are shown taking place in Fig. 2.6.

At the same time as Van Vleck suggested the importance of exchange on the lineshape, Bloembergen, Purcell and Pound[16] observed the

narrowing of nuclear magnetic resonance (N.M.R.) lines due to the motion of atoms in liquids and some solids. They also demonstrated an equation of the form of Equation 2.38 was valid, when ω_e is replaced by $\frac{1}{\tau_c}$, where τ_c would be the mean time for the existance of the ion in any one of two possible environments, or more generally, it represents a time such that at the end of the interval τ_c the environment is little changed, or remains correlated. Hence the shorter τ_c i.e., the more rapid the motion, the narrower the line.

2.8 Resonance Lineshapes for Conduction Electrons

The observation of resonance only in those metals having a small spin-orbit coupling constant was explained by Elliott[17] to be due to the fact that the relaxation time is inversely proportional to the spin-orbit coupling interaction energy, and hence for strong coupling the resonance is broadened beyond detection.

For those conductors in which resonance has been observed Dyson[18] and Feher and Kip[19] have shown that in general two experimental situations arise. These situations are dependent upon the relative values of the parameters T_T (the time an electron takes to traverse the sample), T_D (the time it takes to diffuse through the skin depth), and T_1 and T_2.

(a) Thin sample, $T_T \ll T_D$: For samples satisfying

$$\theta < 4\delta \qquad \text{..... 2.42}$$

where θ is the sample thickness, and δ the classical skin depth, the lineshape is Lorentzian and independent of diffusion rates.

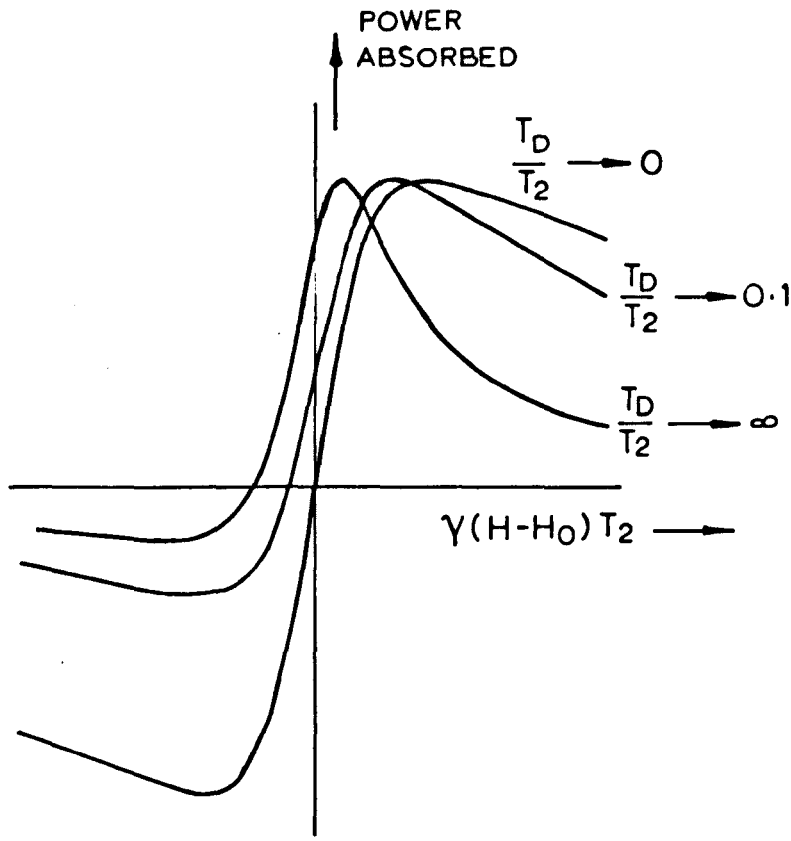

FIG. 2.7
The Dysonian Lineshape.

In this case samples are fine particles or thin films, the most common being the suspension of particles of alkali metals in ammonia.

(b) Thick sample, $T_T >> T_D$ and $T_T >> T_2$: The value of the ratio $\frac{T_D}{T_2}$ is important in this case. As the diffusion time becomes small compared with the relaxation time, the absorption curves assume the appearance of the derivative of a normal absorption curve as shown in Fig. 2.7. Metals of high conductivity satisfy the condition $\frac{T_D}{T_2} \to 0$, but at low temperatures the lineshape may be modified by passing into the anomalous skin effect region. $\frac{T_D}{T_2} \to \infty$ corresponds to thick films with slowly diffusing magnetic dipoles as found for example in materials containing paramagnetic impurities.

2.9 The Spin Hamiltonian

The assumption of free particles within a magnetic field made in the derivation of Equation 2.5 must now be modified to include the effect of the surrounding lattice upon an ion sitting within it. In addition the effect of spin-orbit coupling must be taken into account.

The concept of the rotation of the electron's negative charge gives rise to its magnetic dipole moment. On the other hand, a magnetic dipole is also produced by the movement of the electron in its orbit. Thus an interaction between these two dipoles is possible. This is called the spin-orbit interaction and may be expressed as

$$\mathcal{H} = \lambda \underline{L} \cdot \underline{S} \qquad \ldots\ldots\ldots\ldots\ldots 2.43$$

where λ is the spin-orbit coupling constant. The importance of this term for a paramagnetic ion sitting within a lattice depends upon the value of λ compared to the splitting of the energy levels by the crystal field. If the ground state arising from the crystal field and spin-orbit effects is split into $(2S' + 1)$ levels in a magnetic field, then S' is called the effective spin[20]. The admixture of states by the spin-orbit interaction results in the state represented by S' having orbital contributions. This will be reflected in a departure from the "free-spin" value of g, equal to 2.0023. This orbital contribution to S' also depends on the crystal field, so that the g value may well be anisotropic[21].

As an example of the effect of spin-orbit coupling consider the structure of the valence band in silicon. The valence band wave functions of silicon are formed from three valence p states of atomic silicon, $(1s^2\ 2s^2\ 2p^6\ 3s^2\ 3p^2)$ and thus the band is expected to be three fold degenerate (excluding spin). The spin-orbit coupling removes this degeneracy, leaving a doubly and a non-degenerate level, the former uppermost[17, 22].

In summary therefore, it may be concluded that observations made upon the ground states of ions may be described by a Hamiltonian containing spin only operators.

(a) Isolated Donors in Silicon

By way of an example consider the bound donor electron in silicon, and assume for the present (see Section 3.2) that its wave function is 1s like (spherically symmetric) and of a sufficient radius to include

many unit cells of the lattice within which a 5% abundant silicon isotope, Si^{29}, having a nuclear spin of $\frac{1}{2}$ is randomly distributed. The Spin Hamiltonian may be written[23]

$$\mathcal{H} = -\underline{\mu}_e \cdot \underline{H} - \underline{\mu}_D \cdot \underline{H} - \left(\frac{8\pi}{3}\right)\underline{\mu}_e \cdot \underline{\mu}_D |\psi(0)|^2$$

$$+ \left(\frac{8\pi}{3}\right)\sum_1 \underline{\mu}_e \cdot \underline{\mu}_1 |\psi(\underline{r}_1)|^2 - \sum_1 \underline{\mu}_1 \cdot \underline{H}$$

$$+ \sum_1 \frac{1}{(\underline{r}-\underline{r}_1)^3}\left\{\underline{\mu}_1 \cdot \underline{\mu}_e - \frac{3[\underline{\mu}_1 \cdot (\underline{r}-\underline{r}_1)][\underline{\mu}_e \cdot (\underline{r}-\underline{r}_1)]}{(\underline{r}-\underline{r}_1)^2}\right\} \quad \text{..... 2.44}$$

where $\underline{\mu}_e$, $\underline{\mu}_D$ and $\underline{\mu}_1$ are respectively the magnetic moments of the electron, impurity nucleus and Si^{29} nucleus at the l^{th} lattice point. $\psi(\underline{r}_1)$ is the electronic wave function at the l^{th} lattice point, with $\underline{r}$ being measured with respect to the donor nucleus.

Terms one, two and five represent the Zeeman interactions of the electron, donor and Si^{29} nuclei, while the third represents the Fermi-Segrè hyperfine interaction, consequent upon the electron wave function having a finite probability density, $|\psi(0)|^2$, of being at the site of the donor nucleus. Similarly term four is this same interaction between the electron and the Si^{29} nuclei. The last term represents the dipole-dipole interaction of the electron with the Si^{29} nuclei.

The first three terms may be re-written in the following form

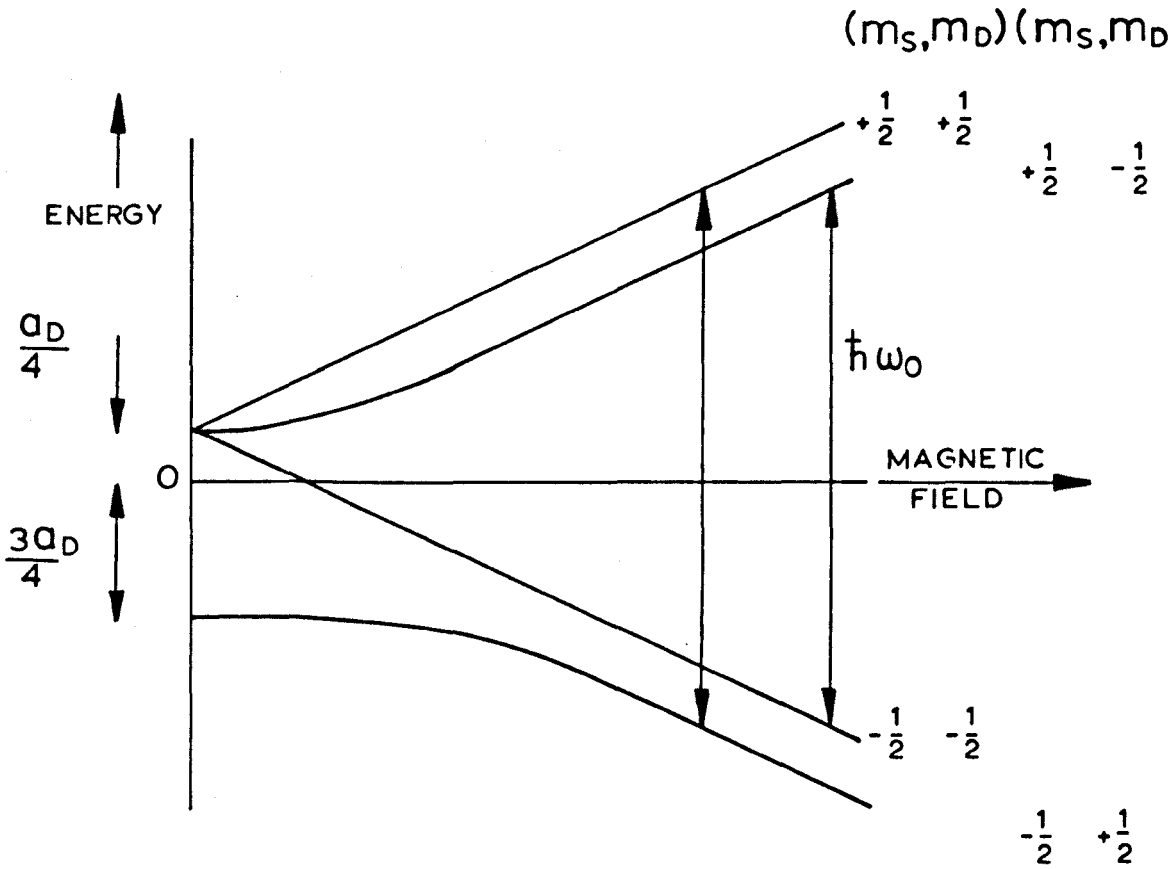

FIG. 2.8

The Magnetic Energy Levels of Phosphorus ($I_D = \frac{1}{2}$) in Silicon.

$$\mathcal{H}' = g\beta\, \underline{s} \cdot \underline{H} - \left(\frac{\mu_D}{I_D}\right) \underline{I} \cdot \underline{H} + a_D\, \underline{s} \cdot \underline{I} \qquad \ldots\ldots\ldots\ldots\ldots 2.45$$

where $$a_D = \left(\frac{16\pi}{3}\right)\left(\frac{\mu_D}{I_D}\right)\mu_e \left|\psi(o)\right|^2. \qquad \ldots\ldots\ldots\ldots\ldots 2.46$$

The Breit-Rabi[24] solution of this shortened version of Equation 2.44 is shown in Fig. 2.8[25]. In the high field approximation

$$E = g\beta H m_s + a_D m_s m_D - \left(\frac{\mu_D}{I_D}\right) H m_D, \qquad \ldots\ldots\ldots\ldots\ldots 2.47$$

where m_s and m_D are the magnetic quantum numbers for the electron and donor, and I_D is the spin of the donor nucleus. The selection rules for a magnetic dipole transition require $\Delta m_s = \pm 1$ and $\Delta m_D = 0$. Thus $(2 I_D + 1)$ hyperfine lines are exhibited, separated, in magnetic field terms, by

$$\frac{a_D}{g\beta}. \qquad \ldots\ldots\ldots\ldots\ldots 2.48$$

The effect of the terms neglected in Equation 2.44 is merely to broaden the hyperfine lines inhomogeneously.

(b) Interacting Donors in Silicon

When the concentration of phosphorus donors is above 6.10^{16} cm^{-3} approximately, new lines appear between those indicated above. Slichter[26] and Jérome and Winter[27] have shown that the proximity of the donors is such that exchange can occur, and Equation 2.45 may

be modified to include this. Then

$$\mathcal{H} = g\beta\,(\underline{s}_1 + \underline{s}_2)\cdot\underline{H} + J\,\underline{s}_1\cdot\underline{s}_2 +$$

$$a_D\,(\underline{s}_1\cdot\underline{I}_1 + \underline{s}_2\cdot\underline{I}_2) - \left(\frac{\mu_D}{I_D}\right)(\underline{I}_1 + \underline{I}_2)\cdot\underline{H} \quad \ldots\ldots\ldots\ldots 2.49$$

where $\underline{s}_1$ and $\underline{s}_2$ are the electronic spins of the two interacting donors of nuclear spin $\underline{I}_1$ and $\underline{I}_2$. If $J \gg a_D$ the total electronic spin may be defined by $|\underline{S}|^2 = |\underline{s}_1 + \underline{s}_2|^2$, and hence two electronic states result, a triplet $S = 1$ and a singlet $S = 0$. Therefore Equation 2.49 becomes

$$\mathcal{H} = g\beta\,\underline{S}\cdot\underline{H} + \tfrac{1}{2}J\left[S\,(S+1) - \tfrac{3}{2}\right]$$

$$+ \frac{a_D}{2}\,\underline{S}\cdot(\underline{I}_1 + \underline{I}_2) - \left(\frac{\mu_D}{I_D}\right)(\underline{I}_1 + \underline{I}_2)\cdot\underline{H}. \quad \ldots\ldots\ldots\ldots 2.50$$

The high field, lowest order solution of this equation gives

$$E = g\beta\,H\,M_s + \tfrac{1}{2}J\left[S\,(S+1) - \frac{3}{2}\right]$$

$$+ \frac{a_D}{2}\,(M_s\,m_{D_1} + M_s\,m_{D_2}) - \left(\frac{\mu_D}{I_D}\right)H\,(m_{D_1} + m_{D_2}) \quad \ldots\ldots\ldots 2.51$$

where M_s may take the values ± 1, 0 for the triplet, and 0 for the singlet. The selection rules now require $\Delta S = 0$, $\Delta M_s = \pm 1$, $\Delta m_{D_1} = \Delta m_{D_2} = 0$, giving $(4\,I_D + 1)$ lines with a spacing of $\frac{a_D}{2g\beta}$. The relative intensity of the lines will be 1-2-3-4 ..... 4-3-2-1.

For phosphorus, of the three lines, only the central one will be observed, the others being masked by the isolated donor hyperfine lines.

The second order solution of Equation 2.50 introduces terms which enable the determination of the exchange integral J by the ENDOR technique[23]. This double resonance technique offers an improved resolution over that of electron spin resonance alone. The coupling is shown to be anti-ferromagnetic, and is of the order of 15 GHz[27] for a phosphorus concentration of 8.10^{16} cm^{-3} (cf. a_D = 118 MHz).

A broad background line simultaneously observed has been shown to be due to those pairs for which $J \sim a_D$[28, 29]. Similar effects have been observed for three and four atom clusters[30].

REFERENCES

1. G. E. Pake, Paramagnetic Resonance (Benjamin) 1962.
2. F. Bloch, Phys. Rev. 70 (1946) 460.
3. A. M. Portis, Phys. Rev. 91 (1953) 1071.
4. C. P. Poole Jr., Electron Spin Resonance (Wiley) 1967 .
5. M. Weger, Bell System Tech. J. 39 (1960) 1013.
6. C. P. Slichter, Principles of Magnetic Resonance (Harper and Row) 1963.
7. I. Waller, Z. Physik 79 (1932) 370.
8. J. H. Van Vleck, J. Chem. Phys. 7 (1939) 72.
9. R. Orbach, Proc. Phys. Soc. (London) A77 (1961) 821.
10. T. G. Castner Jr., Phys. Rev. 130 (1963) 58.
11. T. G. Castner Jr., Phys. Rev. 115 (1959) 1506.
12. C. Kittel and E. Abrahams, Phys. Rev. 90 (1953) 238.
13. J. H. Van Vleck, Phys. Rev. 74 (1948) 1168.
14. P. W. Anderson and P. R. Weiss, Revs. Mod. Phys. 25 (1953) 269.
15. P. W. Anderson, J. Phys. Soc. Japan 9 (1954) 316.
16. N. Bloembergen, E. M. Purcell and R. V. Pound, Phys. Rev. 73 (1948) 679.
17. R. J. Elliott, Phys. Rev. 96 (1954) 266.
18. F. J. Dyson, Phys. Rev. 98 (1955) 349.
19. G. Feher and A. Kip, Phys. Rev. 98 (1955) 337.
20. A. Abragam and M. H. L. Pryce, Proc. Roy. Soc. (London) A205 (1951) 135.
21. C. J. Ballhausen, Introduction to Ligand Field Theory (McGraw-Hill) 1962 .

22. L. Liu, Phys. Rev. 126 (1962) 1317.

23. G. Feher, Phys. Rev. 114 (1959) 1219.

24. G. Breit and I. I. Rabi, Phys. Rev. 38 (1931) 2082.

25. A. Honig and E. Stupp, Phys. Rev. 117 (1960) 69.

26. C. P. Slichter, Phys. Rev. 99 (1955) 479.

27. D. Jérome and J. M. Winter, Phys. Rev. 134 (1964) 1001.

28. J. R. Marko, Phys. Letts. 27A (1968) 119.

29. T. Shimizu, J. Phys. Soc. Japan 25 (1968) 1021.

30. G. Feher, R. C. Fletcher and E. A. Gere, Phys. Rev. 100 (1955) 1784.

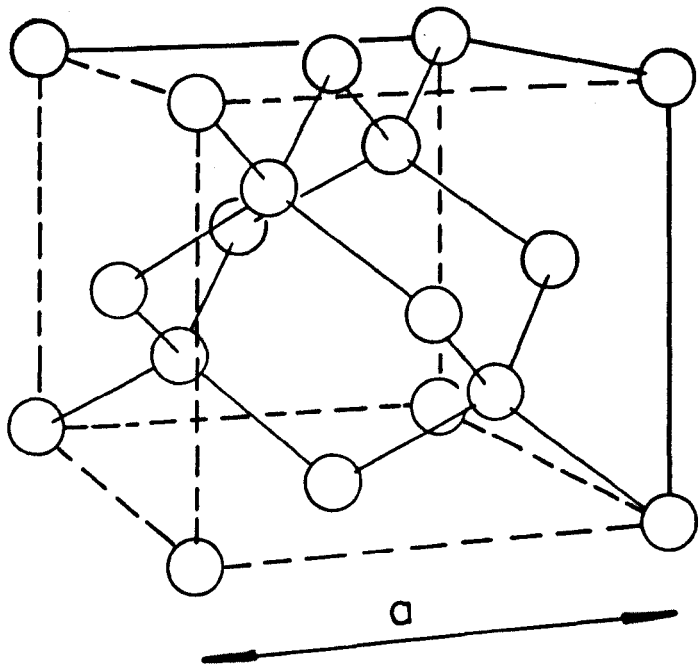

FIG. 3.1

The Silicon Crystal Lattice.

CHAPTER 3

ELECTRON PARAMAGNETIC RESONANCE IN N-TYPE SILICON

This chapter commences with a brief outline of the theoretical determination of the electronic band structure of silicon. The shallow "hydrogen-like" states introduced by donor impurity atoms and the magnetic resonance of electrons in such states are then described. To follow, there is an account of the electronic conduction mechanisms in silicon, and how they influence the magnetic resonance.

3.1 The Crystal Structure and Energy Band Structure of Silicon

The silicon crystal lattice is of the diamond type and is illustrated in Fig. 3.1. It is formed by covalent bonding between the four sp^3 hybridized, tetrahedrally co-ordinated orbitals, produced by the linear combination of the valence atomic orbitals (L.C.A.O.) 3s and 3p. This crystal symmetry is reflected in the region of the reciprocal lattice known as the first Brillouin Zone. Within this region the electronic wave vector $\underline{k}$ has its minimum, or reduced, value. The important symmetry lines within this region are designated Γ (at the centre of the zone) - X in the <100> directions and Γ - L in the <111> directions.

It is difficult to treat mathematically a many-particle system such as a crystal. This has led to the assumption being made that a "single particle" approximation may be used in which each electron,

described by its wave function $\psi(\underline{r})$, can be regarded as moving independently in a static potential field $V(\underline{r})$. The form of $V(\underline{r})$ is such that it takes the electron's average interaction with the rest of the crystal into account. The Schroedinger wave equation may then be written

$$\mathcal{H}\psi(\underline{r}) = \left[\frac{\underline{p}^2}{2m_o} + V(\underline{r})\right]\psi(\underline{r}) = E\psi(\underline{r}) \quad \ldots\ldots\ldots\ldots\ldots 3.1$$

where $\underline{p}$ is the electron momentum operator and E the energy eigenvalue. Since the potential $V(\underline{r})$ has the periodicity of the lattice it may be shown that solutions of Equation 3.1 always have the Bloch form

$$\psi(\underline{r}) = e^{i\underline{k}\cdot\underline{r}}\, U_{\underline{k}}(\underline{r}) \quad \ldots\ldots\ldots\ldots\ldots 3.2$$

i.e., $U_{\underline{k}}(\underline{r})$ modulates the plane wave $e^{i\underline{k}\cdot\underline{r}}$ with the period of the lattice. Thus the eigenvalues depend on $\underline{k}$, and the electronic band structure may be described by an $E(\underline{k})$ plot in the first Brillouin Zone.

The solution of the Schroedinger Equation 3.1 has been attempted in two main fashions. Either the form of the crystal potential is assumed along with various wave functions, allowing quantitative estimates of the form and ordering of bands; or group and perturbation theories are used to provide a catalogue of possible bands, the ultimate determination of the correct one being left to experiment.

Herman[1, 2] and Callaway[3] have reviewed the various methods

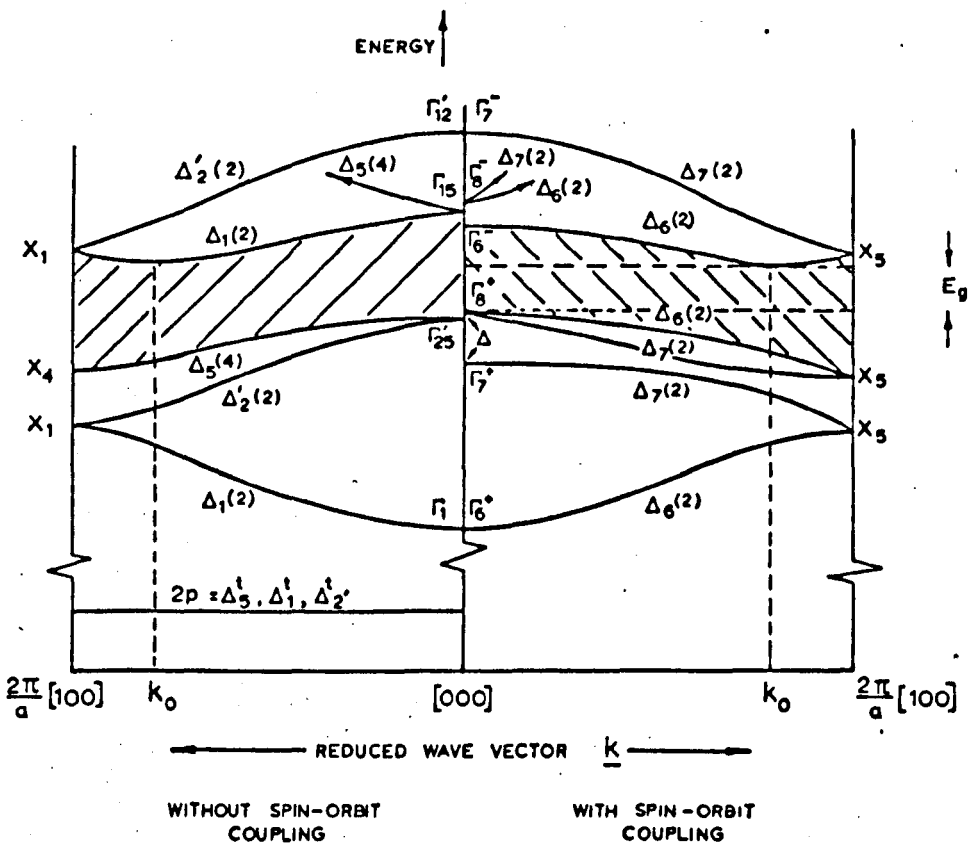

FIG. 3.2

The Energy Bands of Silicon Along the ⟨100⟩ Directions of the Brillouin Zone. Numbers in parentheses are degeneracies. (not drawn to scale)

used in the first category. The principal methods are the use of orthogonalized plane waves (O.P.W.), the cellular method, the tight binding approximation, and the pseudo-potential method. To the left of Fig. 3.2 is shown the silicon band structure calculated by this last method[4]. A summary of group and perturbation theoretical methods used in energy band calculations is given by Long[5].

Initial energy band calculations using the numerical and group theoretical methods ignored the effects of spin-orbit coupling. Elliott[6] pointed out this omission and modified the Schroedinger equation to

$$\mathcal{H}\psi(\underline{r}) = \left\{\frac{\underline{P}^2}{2m_o} + V(\underline{r}) + \frac{\hbar^2}{4m_o^2 c^2}(\nabla V \wedge \underline{P}) \cdot \underline{\sigma}\right\}\psi(\underline{r}) = E\psi(\underline{r}) \qquad \ldots\ldots 3.3$$

where $\underline{\sigma}$ is the Pauli spin operator. Spin-orbit coupling effects are greatest when the electron is close to a real lattice point, when the potential is roughly spherically symmetric, and the last term in $\mathcal{H}$ in Equation 3.3 may be re-written

$$\mathcal{H}_{so} = \frac{\hbar^2}{4m_o^2 c^2}\frac{1}{r}\frac{dV}{dr}\underline{L} \cdot \underline{S} \qquad \ldots\ldots\ldots\ldots 3.4$$

which is of the form of Equation 2.43. $\mathcal{H}_{so}$ is normally sufficiently small to be considered a perturbation, only having a significant effect when responsible for the resolution of an energy degeneracy. This is illustrated to the right of Fig. 3.2.

By way of an example consider the Γ_{25}' basis functions for the valence band maximum at $k = 0$. They represent the six p-states

which are degenerate without spin-orbit coupling. Inclusion of this factor removes the degeneracy between the four fold degenerate $P_{\frac{3}{2}}$ state, and the two fold $P_{\frac{1}{2}}$ state, separating them by an energy Δ, which has been measured by optical techniques to be 0.04 eV[7,8]. The degeneracy of the Δ_6 and Δ_7 valence bands at k = 0, gives rise to constant energy surfaces which have a "warped" spherical shape.

Having previously noted the valence band maximum occurs at k = 0, it has been deduced that the conduction band minima lie in the six <100> directions at $k_o = 0.85 \frac{2\pi}{a}$ [9, 10], although recent measurements using ENDOR suggest that k_o cannot be defined to within $0.15 \frac{2\pi}{a}$ of this point[11]. Therefore, there is an indirect energy gap E_g, which is 1.12 eV at room temperature[12]. Introducing now the electron effective mass defined by

$$m^*_{ij} = \hbar^2 \left(\frac{\partial^2 E}{\partial k_i \, \partial k_j} \right)^{-1}, \qquad \text{..... 3.5}$$

then, in the region of the [001] ellipsoidal conduction band minimum the electron energy with respect to that minimum is given by

$$E = \frac{\hbar^2}{2m_{||}} (k_z - k_o)^2 + \frac{\hbar^2}{2m_{\perp}} (k_x^2 + k_y^2) \qquad \text{..... 3.6}$$

where $m_{||}$ (= 0.98 m_o) and $m_{\perp}$ (= 0.19 m_o) are the effective masses parallel and perpendicular to the axis, respectively.

3.2 Shallow Impurity States

The introduction of the Group V impurities phosphorus, arsenic and antimony into silicon gives rise to impurity states having an ionization energy small compared to the indirect band gap, and such impurities are therefore described by the adjective "shallow".

Kohn and Luttinger[13] and Kohn[14] have calculated the energy spectrum of these donors using the Effective Mass Theory or Approximation (E.M.A.). In this approximation the donor electron is considered to observe a potential $U(\underline{r})$ in addition to the $V(\underline{r})$ used in Equation 3.1, and for large r

$$U(\underline{r}) = -\frac{e^2}{\kappa r} \qquad \ldots\ldots\ldots\ldots\ldots 3.7$$

where κ is the dielectric constant of silicon (= 11.40 ± .05 at liquid helium temperatures[15]). It can be shown that the wave functions of the donor states are given by

$$\psi(\underline{r}) = \sum_{j=1}^{6} a_j F_j(\underline{r})\, \phi_j(\underline{r}) \qquad \ldots\ldots\ldots\ldots\ldots 3.8$$

where the sum is over the six equivalent minima, a_j are numerical coefficients, $\phi_j(\underline{r})$ is the Bloch wave at the j^{th} minimum, and $F_j(\underline{r})$ are "hydrogen-like" envelope functions. The Schroedinger equation may then be solved by using Wannier functions. These functions are Fourier transforms of the Bloch functions, and have the properties of being localized to the lattice points, are functions of position only, and the functions on different lattice points are orthogonal.

The eigenvalue equation for the "hydrogen-like" levels corresponding to the [001] axis then becomes

$$\left[-\frac{\hbar^2}{2m_{\parallel}}\frac{\partial^2}{\partial z^2}-\frac{\hbar^2}{2m_{\perp}}\left(\frac{\partial^2}{\partial x^2}+\frac{\partial^2}{\partial y^2}\right)-\frac{e^2}{\kappa r}\right]F(\underline{r}) = E\,F(\underline{r}). \quad \ldots\ldots\ldots 3.9$$

Since there will be six equivalent solutions for the six minima the donor levels might be expected to be six fold degenerate. For the most tightly bound states the assumed form for $U(\underline{r})$ breaks down, and the Hamiltonian must reflect the tetrahedral symmetry at each donor site i.e., be invariant under the symmetry group T_d. The irreducible representations of this symmetry group then decompose the 1s ground states into

$$1s = A_1 + E + T_2 \quad \ldots\ldots\ldots\ldots\ldots 3.10$$

which are one, two and three fold degenerate respectively. The coefficients α_j have been evaluated and it has been concluded that for small $\underline{r}$ the 1s (A_1), 1s (E) and 1s (T_2) states are principally s -, d -, and p - like respectively. The 1s (A_1) state is the only one having $|\psi(o)|^2$ non-zero, and it alone therefore has a Fermi-Segrè or contact hyperfine interaction with the donor nucleus. Consequently its deviation from the simple E.M.A. is greatest. Likewise the d- and p-natures of the 1s (E) and 1s (T_2) states are reflected in a small, but finite shift from the E.M.A. position. Putting $U(\underline{r}) = -\frac{\Delta Z e^2}{r}$ for small $\underline{r}$, where ΔZ is the excess charge of the donor

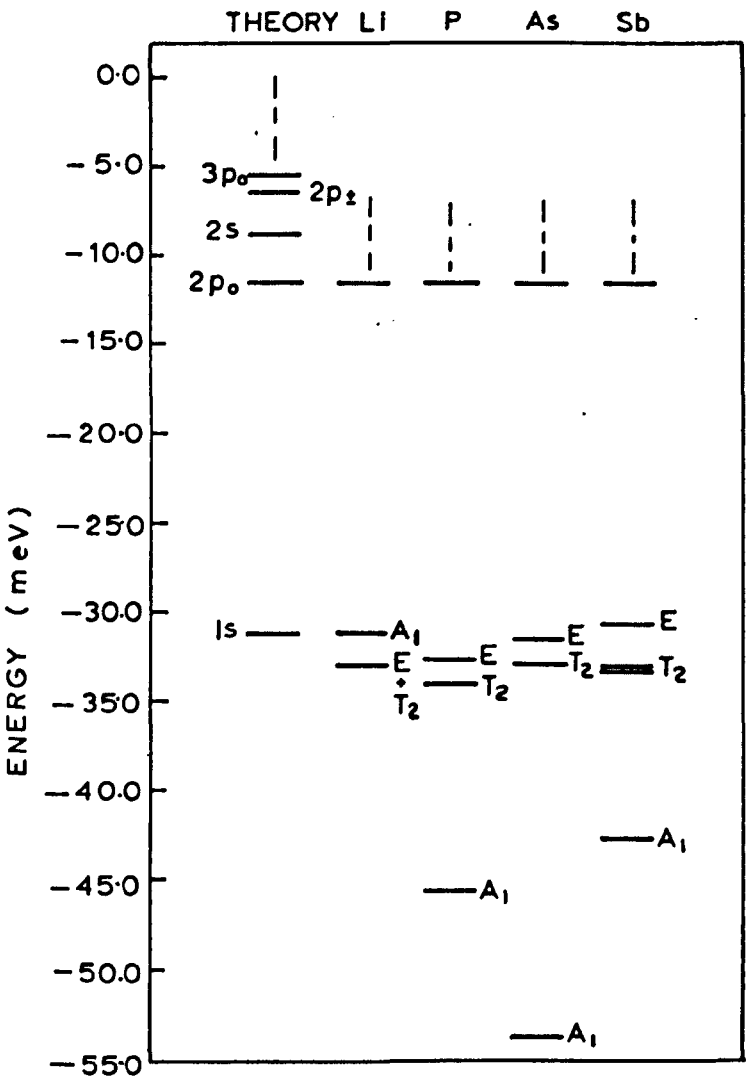

FIG. 3.3

Energy Levels of Donors in Silicon.

nucleus over that of silicon, good agreement is then found between the calculated and measured values of $|\psi(0)|^2$.

The separation of the 1s (A_1) state from the 1s (T_2) state is referred to as the valley-orbit or chemical splitting, and varies between the different donor species. A comparison between the E.M.A. energy levels of donors in silicon[15], and those determined experimentally is given in Fig. 3.3, while the valley-orbit splittings are tabulated in Table 3.1[16, 17]. Spin-orbit coupling is known to remove the degeneracy of the 1s (T_2) state for antimony-and bismuth-doped silicon[16, 17], and to be important in the spin-lattice relaxation of shallow donors[18].

Phillips[19] has recently reviewed the limitations of the E.M. A. which predicts a unique binding energy depending only on host-crystal parameters such as dielectric constant and effective mass. Generally speaking, effort to improve the E.M.A. has been in three directions, either to the formulation of a systematic theory starting from the many-electron Hamiltonian[20], or to the form of the central-cell potential[21], or to the form of $U(\underline{r})$ using such techniques as the Quantum-Defect method[22]. The first method[20] suggested that as $r \to \infty$ an additional term varying as r^{-2} may be present in the Coulombic potential, while the second involves the pseudo-potential theory[21], successfully applied to impurity states in inert gas crystals, but more difficult to apply to silicon due to a non-filled valence shell. Morita and Nara[23] were first to theoretically account for the dependence of the valley-orbit splitting on the species of the donor impurity. They used a method which estimated the strain field about

Donor	Valley-Orbit Splitting $1s\ (A_1) - 1s\ (T_2)$	
	(meV)	(^oK)
Sb	9.55	111
P	11.6	135
As	21.1	245
Bi	34	394

TABLE 3.1

The Valley-Orbit Splitting of Donors in Silicon.

a donor due to its distorting the silicon lattice. Phillips[19] proposes three basic mechanisms to account for this dependence, namely differences in the bond strengths between impurity and host, the difference in core-core repulsive forces, and the difference in p-d hybridization. He believes electronegativity (the power to attract an electron) to be the most important parameter determining the central-cell interactions.

3.3 g-Values of Donor Electrons

The Spin Hamiltonian for isolated donors has been given in Equation 2.44, and it has been shown that $(2I_D + 1)$ hyperfine lines separated by $\frac{a_D}{g\beta}$ are observed e.g., for phosphorus-$(I = \frac{1}{2})$ doped silicon, two lines separated by 42 gauss result.

Due to the axial symmetry of the conduction band minima or valleys, the g factor of each valley has two principal values $g_{||}$ and $g_{\perp}$. Roth[24], using the admixture of the nearby spin-orbit-split valence band into the conduction band, calculated

$$g_{||} - 2 = -\left(\frac{\delta}{E_{gd}}\right)\left(\frac{m_o}{m_{\perp}} - 1\right) \qquad \text{..... 3.11}$$

and

$$g_{\perp} - 2 = -\left(\frac{\delta}{E_{gd}}\right)\left(\frac{m_o}{m_{||}} - 1\right) + \Delta g_{\perp}, \qquad \text{..... 3.12}$$

where E_{gd} is the direct energy separation of the two bands at the conduction band valley at k_o, $\Delta g_{\perp}$ is a small correction term, and δ is the spin-orbit splitting of the valence band at k_o, estimated by Roth to be $\frac{2}{3}$ of the splitting Δ at $k = 0$. Although this "two-band"

model was successful for germanium, Elliott[6] explained that the failure of the above equations for silicon is due to the small spin-orbit splitting of the Δ_5 valence band (splits into Δ_6 and Δ_7 - see Fig. 3.2) at k_o, and that the contribution of the Δ_5 band to the deviation, δg_{11}, of g_{11} from the isotropic average of the valleys, g_o, is positive, while the observed deviation is negative.

Liu[25] has proposed that the deep-lying 2p state, because of its large spin-orbit splitting, makes the dominant negative contribution both to δg_{11} and $\delta g_{\perp}$. Contrary to the estimate of Roth, the author deduces from Liu[25] that $\delta \sim \frac{1}{40} \Delta$.

The g factor observed is an average taken over the six equivalent valleys, and for the 1s (A_1) state, where the coefficients α_j are equal

$$g_o = \frac{1}{3} g_{11} + \frac{2}{3} g_{\perp}. \qquad \text{..... 3.13}$$

Under the application of a uniaxial stress the six valleys may be unequally populated, and give rise to an anisotropic g value. This is a consequence of the strain admixture of the anisotropic 1s (E) state into the 1s (A_1) state. The valley re-population g shift is a function of g_{11}, $g_{\perp}$, and the "valley strain" given by[26]

$$\Xi_u \frac{S'}{E_{12}} \qquad \text{..... 3.14}$$

where Ξ_u is the deformation potential for pure shear, E_{12} is the valley-orbit splitting, and S' is the strain. Simultaneous to the

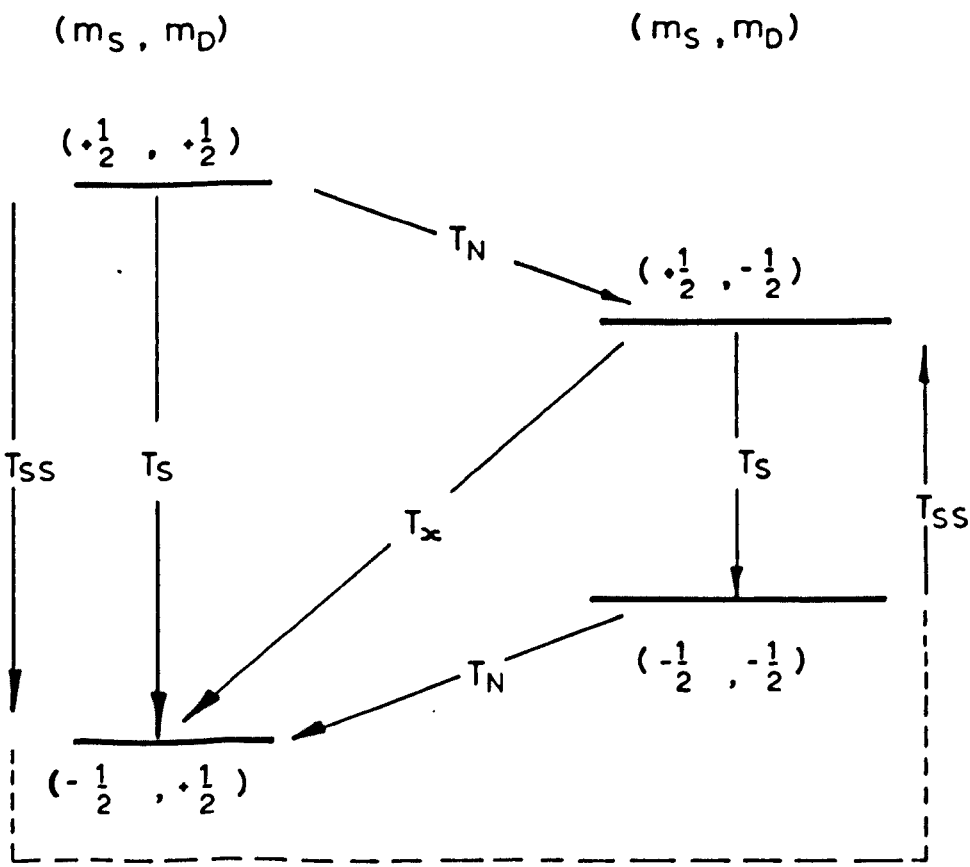

FIG. 3·4

Spin - Lattice Relaxation Processes in Phosphorus – Doped Silicon.

valley re-population effect, a g-shift also occurs due to the strain admixture of the Δ_2' band. The two effects may be resolved by choosing a particular stress axis, enabling $g_{||}$ and $g_{\perp}$ to be determined. The g shifts are observed to increase for donor impurities of increasing ionization energy.

The strain admixture of the "hyperfine-less" 1s (E) state into the 1s (A_1) state also gives rise to a reduction in the hyperfine splitting a_D, from which the valley-orbit splitting and by inference the deformation potential can be determined. Wilson and Feher[26] obtained a value of 11 eV for Γ_{4u} which is in disagreement with the value of 7.8 eV measured by photoexcitation[27], and of 8.3 eV measured through piezo-resistance[28], but in agreement with 11.3 eV obtained by piezo-optic measurements[29]. Kleiner[30] has demonstrated that the discrepancy between the photoexcitation and E.P.R. values cannot be accounted for by the neglect in the latter experiments of the dipolar hyperfine coupling. This coupling will be discussed later in Section 6.4.

3.4 Spin-Lattice Relaxation of Bound Donor Electrons

There has been considerable theoretical and experimental investigation of this subject. The available relaxation processes for bound electrons in phosphorus-doped silicon[31] are shown in Fig. 3.4.

The "vertical" T_s mechanism is the one which has been most studied. This is due to its short-circuiting effect over the other mechanisms since $T_s << T_x$ and T_N. These latter processes require a change in the donor nuclear magnetic quantum number, while the T_{ss}

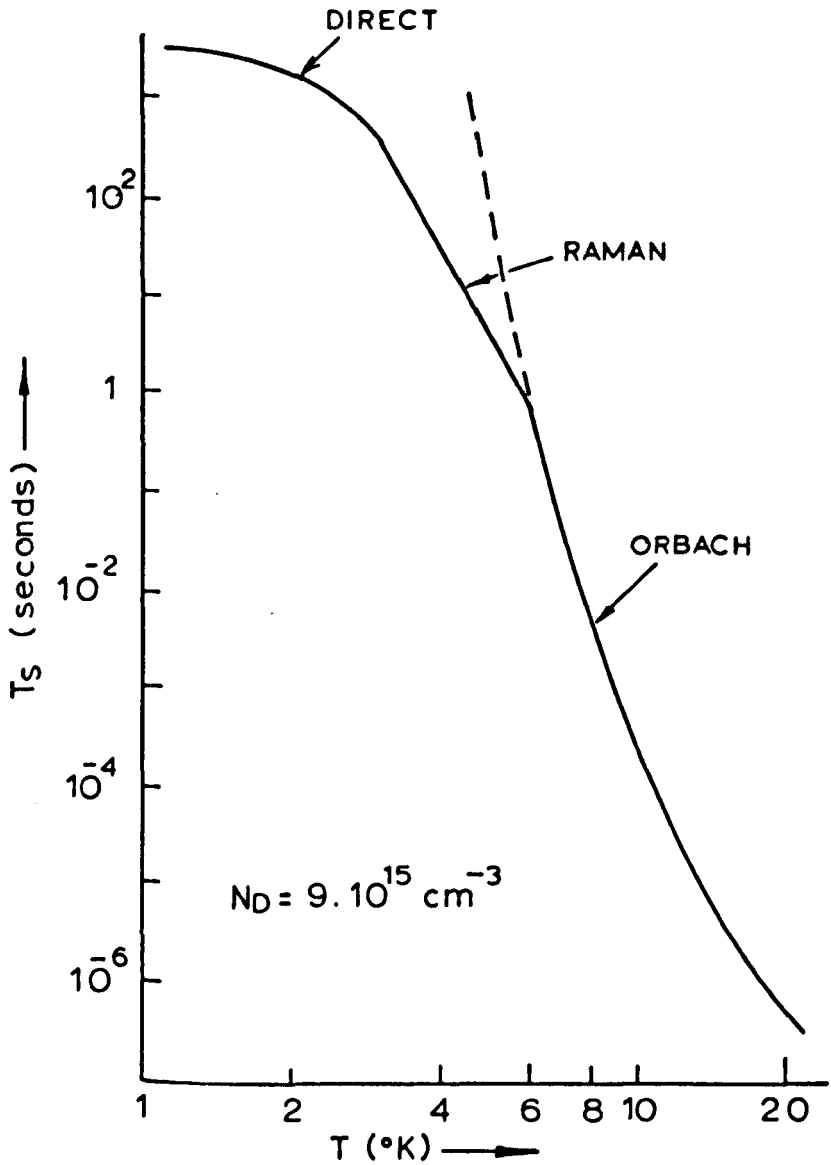

FIG. 3.5

Spin-Lattice Relaxation Time T_S for Phosphorus-Doped Silicon.

mechanism, possibly involving spin-exchange, is only effective when the number of free electrons is increased, by illumination for example. Castner[32] has represented the T_s processes by

$$\frac{1}{T_s} = A H_o^4 T + B H_o^2 T^7 + C T^9 + D \exp\left(-\frac{\Delta E}{kT}\right). \quad \ldots\ldots\ldots\ldots 3.15$$

The first term represents a direct process and has been explained by Roth[24] and Hasegawa[33]. They suggest that through the electron's spin-orbit interaction and the time varying strain imposed by the phonons the g factor will be modulated, there being two contributions. Firstly, due to the strain admixture of the 1s (E) state into 1s (A_1) state the populations of the six conduction band valleys will be modulated, and secondly this strain will cause the admixing of higher lying bands into the conduction band. These mechanisms dominate in phosphorus-doped silicon up to 2.4°K. Between this temperature and 6°K the power law Raman region is entered with an exponent closer to 9 than 7, and within limits there is no magnetic field dependence. The dominance of the T^9 term suggests a relaxation process involving the spin-orbit interaction (see Section 2.4b), although no satisfactory explanation in these terms has so far been published. Castner[18] does mention a private communication from Roth, Hasegawa and Nakayama who have demonstrated a T^9 process having the correct dependences and order of magnitude if the impurity potential is included and note is taken of the breakdown in the E.M.A.

In the temperature region up to 20°K Castner[32] shows that the

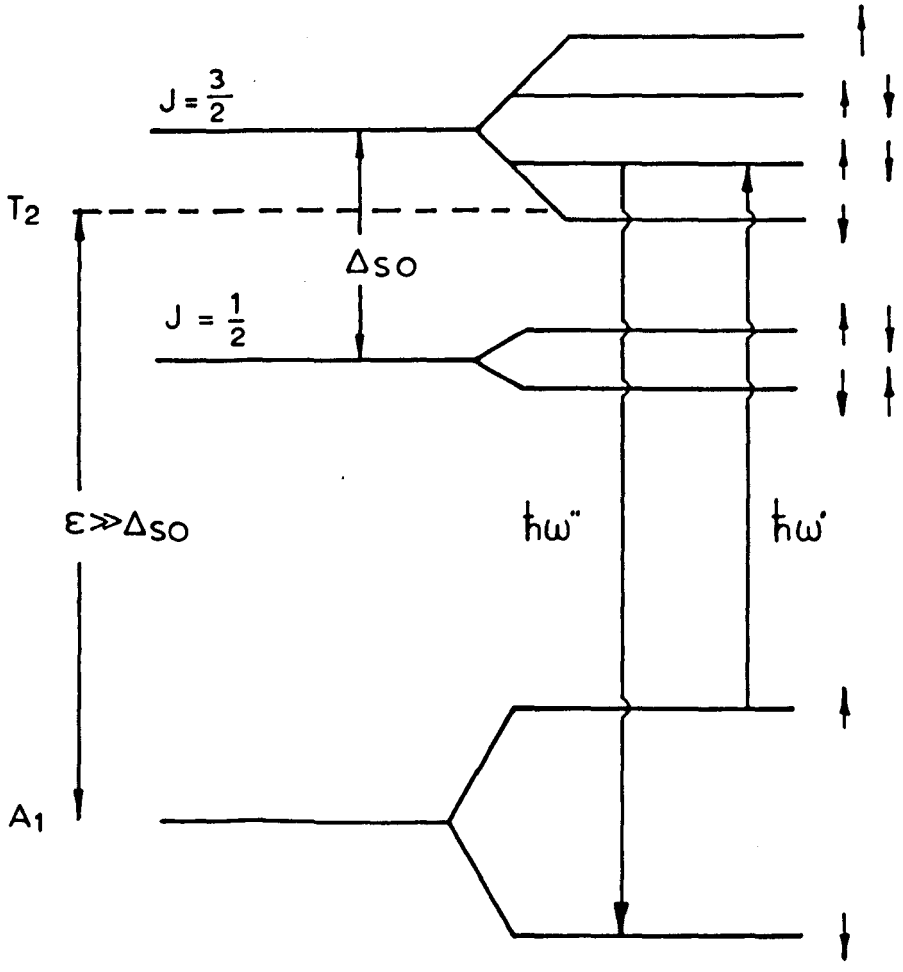

FIG. 3.6

The Influence of the Spin-Orbit and Zeeman Interactions upon the $1s$ (A_1 and T_2) States.

exponential or Orbach process is dominant. The three regions and measured relaxation times are shown in Fig. 3.5. Good agreement is found between the calculated splitting of the 1s (A_1) and 1s (E and T_2) states and the energy ΔE.

The dependence of T_s upon the atomic number of the impurity led Castner[18] to suggest that the relaxation mechanism is due to the spin-orbit interaction associated with the 1s (T_2) state. He writes the Hamiltonian in the form

$$H = H_{\text{eff. mass}} + U(\underline{r}) + \lambda_{\text{imp}}(r)\, \underline{L}.\underline{S} + g\beta H_o S_z \quad \ldots\ldots\ldots\ldots\ 3.16$$

where $U(\underline{r})$ is the additional potential the donor experiences, including the atomic potential of the donor $U_{\text{imp}}(\underline{r})$ which dominates the spin-orbit interaction. Since the 1s (E) states contain much less admixture of opposite-spin states than the 1s (T_2) states, and being higher in energy will be less populated, the 1s (T_2) states are thought to dominate the relaxation. In a magnetic field the energy states are as indicated in Fig. 3.6, where the pure spin states are represented by $\uparrow$ and $\downarrow$, the the admixed states by $\uparrow\downarrow$ and $\downarrow\uparrow$.

Thus the Orbach process may be represented by phonon-absorption transitions from either one of the A_1 Zeeman states to the four T_2 impure-spin states followed by phonon emission back to the other A_1 Zeeman state. The matrix elements determining the Raman spin-lattice relaxation transition probability depend mostly on Umklapp intervalley scattering between opposite conduction band minima i.e., an emitted or absorbed phonon of wave vector $0.3\frac{\pi}{a}$. Such a mechanism

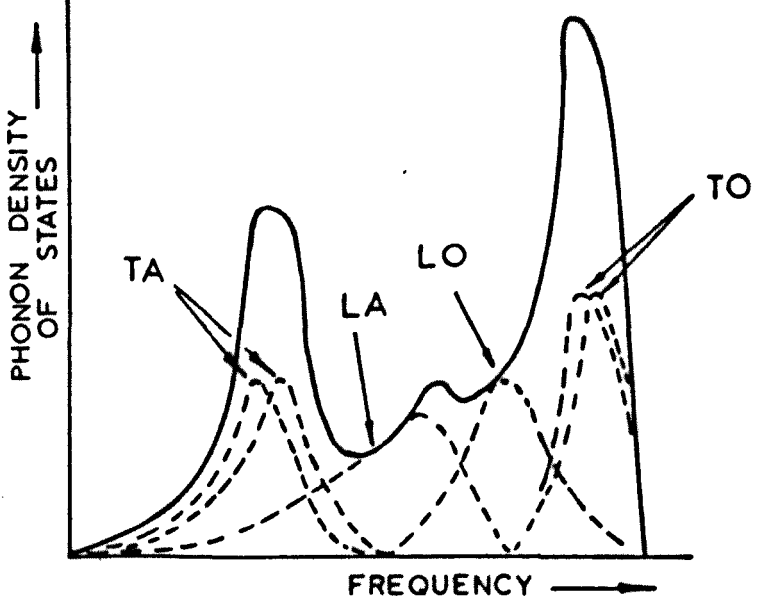

FIG. 3·7a.

Phonon Frequency Distribution of a Diamond Like Lattice.

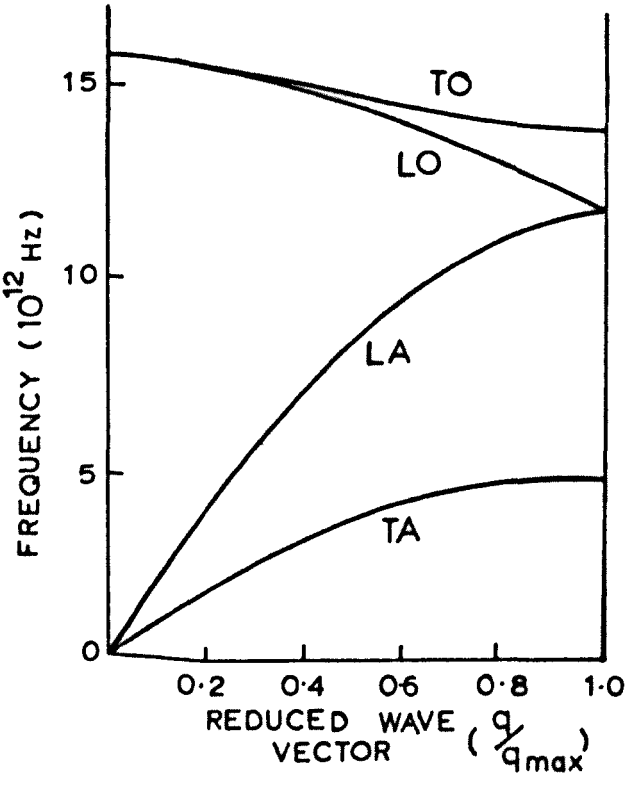

FIG. 3·7b

Dispersion Curves for Phonons Propagating in the [001] direction in Silicon at Room Temperature.

would be insignificant at low temperatures, with the consequent domination of other processes.

A simplification in the calculation of the electron-phonon interaction is achieved by recognizing that this interaction is manifested in the measured level-widths of the 1s (T_2) states, assumed to arise from spontaneous phonon emission. For a phosphorus donor concentration of $1.5 \cdot 10^{16}$ cm^{-3}, and using estimated values of 0.022 and 0.2 meV for the spin-orbit splitting and level-widths respectively, the calculated rate constant D is approximately a factor of two higher than the experimentally measured value of $0.020 \cdot 10^{10}$ sec^{-1}.

The calculated phonon frequency distribution curve for a diamond-like lattice[34] is shown in Fig. 3.7a., along with the measured dispersion curve for silicon, Fig. 3.7b. The Roth-Hasegawa expression for the direct process involves the summation of the inverse fifth powers of the velocities of the longitudinal and transverse acoustic phonons. Since the latter term exceeds the former by an order of magnitude, this process is dominated by transverse, long wavelength acoustic phonons. Similarly, transverse phonons dominate in the Raman T^9 process, the breakdown occurring in this mechanism when the phonon wave vector q times the donor electron orbital radius a_o approaches unity. The Orbach process requires higher frequency phonons i.e., short wavelengths, and in the temperature region of interest these will be in the middle of the frequency distribution and from the density of states it should be noted that these will be longitudinal.

The spin-lattice relaxation time is also a function of the concentration of donors. Feher and Gere[31] observed a rapid increase in the direct process when the concentration of phosphorus donors exceeded 10^{16} cm^{-3}, and Castner's[18] calculations for the Orbach process degrade with increasing concentration. Igo[36] has also measured the dependence of the relaxation time upon the degree of compensation. His results are in agreement with the theory of Sugihara[37], who proposed that relaxation occurs via an electron hopping process from neutral to charged impurities accompanied by spin reversal. The importance of such fast relaxing pairs has been further studied by Yang and Honig[38]. They investigated two fast relaxing centres, neutral donor pairs of less than average separation, and neutral-ionized pairs as proposed by Sugihara[37]. The neutral pairs fast-relaxing mechanism is the phonon modulation of the exchange coupling, the isolated spins being relaxed via spin diffusion to these centres. The temperature and magnetic field dependence associated with this mechanism is through the variation of the concentration of these centres with the above parameters, the former because high exchange-energy pairs populate a non-magnetic singlet state as the temperature is lowered, and the latter through the relative heat capacities of the Zeeman and exchange systems.

3.5 Impurity Conduction and the Semiconductor to Metal Transition

In 1961 Mott and Twose[39] reviewed the theories of impurity conduction in semiconductors. These theories were developed from

Mott's hypothesis[40] that at T = 0°K a crystalline array of atoms would exhibit a sudden discontinuity in its conductivity with decreasing lattice parameter.

Impurity conduction can be defined as a conduction process in which the electron or hole moves between neighbouring donors or acceptors without activation into the conduction or valence bands. It may be divided into two classes (i) motion of an electron (in an n-type conductor) from an occupied donor site to an unoccupied neighbouring site that has been produced by compensation with acceptors, (ii) a concentration of donors sufficient for there to be a high degree of electron orbital overlap between neighbouring sites, establishing an impurity band.

The first case implies a phonon-induced electron hopping motion, and has been described theoretically by Miller and Abrahams[41]. If a low concentration of donors N_D is partially compensated by N_A acceptors, an energy difference Δ exists between the $(N_D - N_A)$ occupied sites and the N_A unoccupied ones, due to the local field produced by nearby ionized acceptors and donors. Considering only the singlet ground states of the donors, the activation energy for hopping, Δ, was calculated by Miller and Abrahams[41] to be

$$\Delta = \left(\frac{e^2}{\kappa}\right)\left(\frac{4\pi N_D}{3}\right)^{\frac{1}{3}}(1 - 1.35\,K^{\frac{1}{3}}) \qquad \ldots\ldots\ldots\ldots 3.17$$

where $K = \frac{N_A}{N_D}$, and the second term is the reciprocal of the average separation between donors, $\frac{1}{R}$. At a given donor concentration the activation energy has a minimum value for K = 0.5. The calculated

hopping rate for silicon is given by

$$u = \left(\frac{\xi_u^{\,2}}{\pi \rho C^5 \hbar^4}\right)\left(\frac{2e^2}{3\kappa a^2}\right)^2\left(\frac{1}{6}\right)\left(\frac{\pi a}{4R\left[\left(\frac{a}{b}\right)^2-1\right]}\right)^{\frac{1}{2}} R^2 e^{\frac{-2R}{a}} \cdot \Delta \cdot \coth\frac{\Delta}{2kT}, \quad 3.18$$

where ρ is the density, and C the velocity of longitudinal phonons. The quantities a and b are the perpendicular and parallel radii of the electron orbit respectively. They are given by $a = \hbar\left(\frac{2m_\perp}{E_{obs}}\right)^{-\frac{1}{2}}$, and $b = \left(\frac{m_\perp}{m_{||}}\right)^{\frac{1}{2}} a$, E_{obs} being the observed ionization energy. For phosphorus-doped silicon a = 21.1Å and b = 9.3 Å. Myszkowski[42] has extended the calculations of Miller and Abrahams and demonstrated that observation of higher impurity conductivity (at fixed N_D) for donors having a small valley-orbit splitting is accountable by the inclusion of the excited states.

The conductivity of a sample can be expressed by[43]

$$\sigma = \sum_{i=1}^{3} \sigma_i^{(o)} \exp\left[-\frac{\varepsilon_i}{kT}\right], \quad \ldots\ldots\ldots\ldots 3.20$$

where ε_i is the activation energy of the i^{th} conduction process, and $\sigma_i^{(o)}$ is the extrapolated value of σ_i for $\frac{1}{T} \to 0$. ε_1 is the familiar donor ionization energy, ε_2 is an activation energy in the intermediate concentration range of uncertain origin, and ε_3 is the hopping energy Δ. D.C. measurements of the conductivity[44,45] have shown fair agreement in the experimental ε_3 with the theories of Mott and Miller and Abrahams. Measurement of the effect of hopping upon the complex conductivity of n-type silicon at low temperatures[46] showed a

frequency dependence $\sim \omega^{0.8}$ in the range $10^2 - 10^5$ Hz. A polarization model is used, in which the application of an electric field alters the potential around the minority impurity in a time ~ hopping time. By applying a current at 10^5 Hz Amitay and Pollak[47] have attempted to measure a Hall voltage which could be attributed to the hopping conduction, none was apparent. Photon-induced hopping has also been observed[48,49]. In the microwave and far-infra-red regions the absorption has two contributions, a direct absorption without phonon participation, plus a direct absorption accompanied by the emission of a single longitudinal acoustical phonon.

Evidence for the influence of hopping upon E.P.R. spectra is given by Wilson[50], in the linewidth decrease with increasing donor concentration in compensated germanium. The line narrowing was consistent with the application of Miller and Abrahams' hopping rate to the standard motional narrowing equation (see Equation 2.41). Zhurkin et al[51] have observed a similar linewidth reduction in silicon, and have pointed out that at fixed compensation ratio and increasing donor concentration, the hopping and exchange energies will be comparable at some point. Microwave double resonance experiments on ionized impurity pairs[52] have confirmed the theoretical considerations of the hydrogen-like molecule-ion approximation[53], the fluctuating field due to hopping causing the change with time of the bonding and anti-bonding states. The coupling between the nuclear spins of the isotope Si^{29} and the lattice has been studied by Jérome and Winter[54]. They conclude that the hopping motion modulates the dipolar coupling of the electronic spins and the nuclear

spins, effecting a direct relaxation mechanism of the nuclear Zeeman levels.

The second category of impurity conduction can be described in a manner similar to the tight-binding approximation (bearing in mind the aperiodic ~~nature~~ distribution of the donors or acceptors), in that an impurity band, or continuum of electron states, will be formed with increasing concentration (i.e., decreasing separation) of donors or acceptors, the width of this band increasing until it merges with the nearest intrinsic band, at which point $\epsilon_1 = 0$. Mott's criterion for the transition concentration at the band formation is given by

$$N^{\frac{1}{3}} a_o \simeq 0.2. \qquad \ldots\ldots\ldots\ldots 3.20$$

Hence for phosphorus-doped silicon, $a_o \simeq 16$ Å, $N \sim 2.10^{18}$ cm^{-3}.

Alexander and Holcomb[55] have reviewed the data available on this transition. Hall effect, N.M.R., and E.P.R. measurements at low temperatures confirm that the transition takes place in the range $2.5 - 4.0 \cdot 10^{18}$ cm^{-3}. It is thought that the transition occurs at $3 \cdot 10^{18}$ cm^{-3}, the distribution in each technique being accounted for by a Poisson distribution of local donor densities. Mott's hypothesis appears to be supported if due account is taken of this distribution[56]. The donor concentration at which the impurity band merges with the conduction band (or the Fermi level reaches the conduction band) has been firmly identified to be at 2.10^{19} cm^{-3}. The presence of localised magnetic moments[57], has been suggested to occur in the intermediate concentration range. This is not supported

by static measurements of the spin susceptibility[58], which are thought to present more accurate data than that determined from E.P.R. Two other theories for this region have been advanced (i) the D^- band model[59], and (ii) an "inhomogeneity" model, in which the impurity states are regarded as spatial mixtures of the metallic and non-metallic regions[60]. The second model is thought to account for the differences observed in the susceptibility determined from E.P.R. and static techniques, in that the para - and dia-magnetic susceptibilities for the two phases will sum in different fashions. The activation energy $\mathcal{E}_2$ is postulated to arise from a band formed by those electrons in the excited hydrogenic states of those donors in non-metallic regions.

3.6 Conduction Electron Resonance

The first reported observation of E.P.R. in silicon[61] in 1953 was of conduction electrons in a sample containing $\sim 2.10^{18}$ phosphorus donors cm^{-3}.

Since the averaged g factor is isotropic, powdered samples may be conveniently used. This prevents microwave cavity damping, and in order that the lineshape is not distorted the condition imposed by Equation 2.42 is normally adhered to i.e., a requirement to work with powdered samples having a thickness less than four times the classical skin depth. This powdering of the sample gives rise to surface state lines[10,62-64], the most prominent having a g-value of 2.006. Fortunately it may usually be removed by etching the sample. Recent measurements by Kodera[65] on rod shaped samples of phosphorus-doped

silicon in the concentration range $10^{17} - 10^{19}$ cm^{-3} indicated that the lineshapes were consistent with the Dyson theory, although to explain the inconsistency between the diffusion time T_D (see Section 2.8) derived by line-fitting and that calculated from the mobility, a model is proposed in which two types of electronic motion are possible, namely rapid motion in an impurity cluster and slow transitions between the clusters.

The importance of the spin-orbit coupling of conduction electrons has already been mentioned (see Section 3.1). Elliott[6] has shown that through this interaction a mechanism exists for the conduction electron spin-lattice relaxation, in that relaxation can occur during the scattering of electrons by both phonons and ionized impurities. The longitudinal and transverse relaxation times T_1 and T_2 may be equated in this context, since at the temperatures of interest the frequency characteristic of the phonons is very much greater than the Larmor frequency so that to the spins the surroundings appear isotropic[66]. Elliott demonstrated that the momentum relaxation time τ is related to the spin-lattice relaxation time by

$$T_1 \simeq \frac{\tau}{(\Delta g)^2} \qquad \text{..... 3.21}$$

where Δg is the deviation of the g value from the free spin value. At high temperatures phonon scattering dominates and therefore $\tau \propto T^{-\frac{1}{2}}$ approximately. Using a different approach, Yafet[67] considered the phonon modulation of the electron spin-orbit interaction and deduced

$$T_1 \propto T^{-\frac{5}{2}}, \qquad \ldots\ldots\ldots\ldots\ldots 3.22$$

in agreement with the results of Lancaster, Van Wyk and Schneider[68] at temperatures above 77°K.

Most of the more recent papers on conduction electron resonance in phosphorus-doped silicon have been devoted to spectral changes apparent with increasing N_D at certain fixed temperatures. Many of the results are discussed with respect to the degeneracy temperature at a particular concentration, or vice versa. This temperature is defined through the consideration that at the lowest temperatures the conduction electrons will occupy states over a bandwidth of $(E_F - E_c)$, where E_F and E_c are the Fermi and conduction band energies respectively. This is equated to kT_{deg}, or numerically

$$T_{deg} = 4.2 \cdot 10^{-11} \, n_{deg}^{\frac{2}{3}}, \qquad \ldots\ldots\ldots\ldots\ldots 3.23$$

where n_{deg} is the degeneracy electron concentration, and T_{deg} is the degeneracy temperature.

In a series of papers Kodera has discussed the effect of doping on the spectrum over the concentration range $1.10^{17} - 5.10^{19}$ cm^{-3} at room and liquid nitrogen temperatures. A summary [69], concludes that at room temperature the concentration dependence of the spin-lattice relaxation time is related to the Brooks-Herring relaxation time for ionized impurity scattering. By comparison at 77°K the linewidth displays a minimum at a concentration of $1.8 \cdot 10^{18}$ cm^{-3}.

The lineshape is Lorentzian in both cases, the g value decreasing monotonically at room temperature, but decreasing only above 3.10^{18} cm^{-3} at 77°K. These latter figures may be compared with n_{deg} of $2.1 . 10^{19}$ and $2.2 . 10^{18}$ cm^{-3} respectively. Thus below these concentrations the electrons are non-degenerate, but, in particular, above $2.2 . 10^{18}$ cm^{-3} at 77°K the electrons are degenerate and may move in the conduction or impurity bands. Below this concentration Kodera proposes that electrons are "localized" within clusters of increasing size. He notes there is no change in the ratio $\frac{\Delta H_{\frac{1}{2}}}{\Delta Hpp}$ (see Section 2.2) with concentration, although the ratio is observed to change from 1.55 to 1.78 on cooling to 77°K ($\frac{\Delta H_{\frac{1}{2}}}{\Delta Hpp}$ = 1.73 for a Lorentzian line, and 1.18 for a Gaussian). Similar measurements by Gränacher and Czaja[70] are in general agreement with Kodera[69], but they conclude that the importance of electronic motion in the impurity band at 77°K causes the Elliott theory to be inappropriate at this temperature. At the two above temperatures Kodera[71] studied the absorption intensity, confirming the above model, qualitative agreement alone being found at concentrations greater than 5.10^{18} cm^{-3} at 77°K. The g value variation with concentration is reminescent of that observed in InSb[72], where the formula of Roth et al[73] for the g factor in terms of the effective mass, reflects the increasing non-parabolicity of the conduction band with increasing concentration of donors.

The transition from the observation of the hyperfine lines alone to conduction electrons alone with increasing concentration of donors

at liquid helium temperatures is reported in several papers[74-76]. Maekawa and Kinoshita [74] describe the gradual growth of a wide central line as the cluster size increases, the hyperfine lines disappearing at a phosphorus concentration of 7.10^{17} cm^{-3}, a value in agreement with that estimated theoretically[56]. Measurement of the exchange interaction energy for clusters of small numbers are in agreement with those of Jérome and Winter as described in Section 2.9b. Just prior to the disappearance of the hyperfine lines a transition region is observed in which the central line grows in intensity but decreases in width. The combined effects of hopping and exchange are postulated to account for this. In the region $7.10^{17} - 3.10^{18}$ cm^{-3} this line narrows considerably from $\Delta H_{pp} \sim 4$ gauss to 0.4 gauss. The analysis here is similar to that for germanium[50] i.e., hopping, the linewidth being given by

$$\Delta H_{pp} \propto \exp\left[\frac{2R}{a_o}\right] \tanh\left[\frac{\Delta}{2kT}\right] \qquad \ldots\ldots\ldots\ldots 3.24$$

where the terms have been previously defined. Δ is found to be in the range $4 - 7^{\circ}K$ i.e., 0.34 - 0.60 meV. Intensity measurements are interpreted to suggest the existence of anti-ferromagnetic coupling between the donor electrons. Lifetime broadening of the line occurs above 3.10^{18} cm^{-3} due to motion in the impurity band. No change in g values for these measurements at X band (9.3 GHz) was noted throughout the concentration range.

Observation[75] of spectral changes at a higher frequency, 46 GHz, and a lower temperature, $1.5^{\circ}K$, indicate that in a sample with

$N_D \sim 2.5 \cdot 10^{17}$ cm^{-3} a broad background line is apparent in addition to the hyperfine, two, three and four donor cluster lines and is shifted to the low field side of the centre of the hyperfine lines by 10 gauss. With increasing concentration this line increases in size and narrows while moving closer to the centre of the original hyperfine lines. At $1.7 \cdot 10^{18}$ cm^{-3} two lines are apparent, one lying at the central field. Above 2.10^{18} cm^{-3} a single line is observed increasing in width with donor concentration. The shift in the broad background line is thought to be due to a ferromagnetic exchange interaction between clusters of donors which are within themselves coupled anti-ferromagnetically. At the higher concentrations the central line is associated with electrons in the impurity band.

At liquid helium temperatures Kodera[76] noted the changes in a central line with concentration. This line was Lorentzian shaped, and had a constant g value equal to that determined by Feher[10] of 1.99875 for conduction electrons, and different to that for the hyperfine lines. He concludes therefore that the line does not arise from exchange coupling, but is due to motion in clusters as previously advanced for higher temperatures.

Lancaster, Van Wyk and Schneider[68] noted a linewidth increase in some samples as the temperature decreased below approximately 77°K. An order of magnitude calculation assuming relaxation via spin-orbit coupling to the donor impurities resulted in a linewidth approximately ten times too large, although the temperature dependence would be correct. In Chapter 6 an account is given of an examination of samples in this temperature region below 77°K but above 20°K where it

is possible to observe the spectral changes occurring in samples exhibiting hyperfine structure at 20°K. The results are discussed with respect to various theories.

REFERENCES

1. F. Herman, Rev. Mod. Phys. 30 (1958) 102.
2. F. Herman, Proc. I.R.E. 43 (1955) 1703.
3. J. Callaway, Solid State Physics 7 (Eds. Seitz and Turnbull) (Academic Press) 1958.
4. L. Kleinman and J. C. Phillips, Phys. Rev. 118 (1960) 1153.
5. D. Long, Energy Bands in Semiconductors (Wiley) 1968).
6. R. J. Elliott, Phys. Rev. 96 (1954) 266.
7. S. Zwerdling, K. J. Button, B. Lax and L. M. Roth, Phys. Rev. Letts. 4 (1960) 173.
8. T. Staflin, J. Phys. Chem. Solids 27 (1966) 65.
9. J. C. Phillips, Phys. Rev. 112 (1958) 685.
10. G. Feher, Phys. Rev. 114 (1959) 1219.
11. E. B. Hale and R. L. Mieher, Phys. Rev. 184 (1969) 751.
12. D. Long, J. Appl. Phys. 33 (1962) 1682.
13. W. Kohn and J. M. Luttinger, Phys. Rev. 98 (1955) 915.
14. W. Kohn, Solid State Physics 5 (Eds. Seitz and Turnbull) (Academic Press) 1957.
15. R. A. Faulkner, Phys. Rev. 184 (1969) 713.
16. R. L. Aggarwal and A. K. Ramdas, Phys. Rev. 140 (1965) 1246.
17. H. J. Zeiger, W. E. Krag and L. M. Roth, M.I.T., Lincoln Lab. Reports, July 15, 1962 (Unpublished).
18. T. G. Castner Jr., Phys. Rev. 155 (1967) 816.
19. J. C. Phillips, Phys. Rev. 1 (1970) 1540.
20. L. J. Sham, Phys. Rev. 150 (1966) 720.
21. J. Hermanson and J. C. Phillips, Phys. Rev. 150 (1966) 652.

22. H. B. Bebb, Phys. Rev. 185 (1969) 1116.

23. A. Morita and H. Nara, J. Phys. Soc. Japan 21, Supplement, (1966) 234.

24. L. M. Roth, Phys. Rev. 118 (1960) 1534.

25. L. Liu, Phys. Rev. 126 (1962) 1317.

26. D. K. Wilson and G. Feher, Phys. Rev. 124 (1961) 1068.

27. W. E. Krag, W. H. Kleiner, S. Fischler and H. J. Zeiger, Bull. Am. Phys. Soc. 9 (1964) 705.

28. J. E. Aubrey, W. Gubler, T. Henningsen and S. H. Koenig, Phys. Rev. 130 (1963) 1667.

29. K. J. Schmidt-Tiedemann, Proc. Int. Conf. on Physics of Semiconductors, Exeter, (1962) 191.

30. W. H. Kleiner, Solid State Research, M.I.T., Lincoln Lab. Reports, 1969 (Unpublished).

31. G. Feher and E. A. Gere, Phys. Rev. 114 (1959) 1245.

32. T. G. Castner Jr., Phys. Rev. 130 (1963) 58.

33. H. Hasegawa, Phys. Rev. 118 (1960) 1523.

34. H. M. J. Smith, Philos. Trans. 241A (1948) 105.

35. B. N. Brockhouse, Phys. Rev. Letts. 2 (1959) 256.

36. T. Igo, J. Phys. Soc. Japan 21 (1966) 874.

37. K. Sugihara, J. Phys. Soc. Japan 18 (1963) 961.

38. G. Yang and H. Honig, Phys. Rev. 168 (1968) 271.

39. N. F. Mott and W. D. Twose, Advan. Phys. 10 (1961) 107.

40. N. F. Mott, Canad. J. Phys. 34 (1956) 1356.

41. A. Miller and E. Abrahams, Phys. Rev. 120 (1960) 745.

42. A. Myszkowski, J. Phys. Chem. Solids 28 (1967) 105.

43. E. A. Davis and W. Dale Compton, Phys. Rev. 140 (1965) 2183.

44. K. R. Atkins, R. Donovan and R. H. Walmsley, Phys. Rev. 118 (1960) 411.

45. N. A. Penin, B. G. Zhurkin and B. A. Volkov, Soviet Phys. - Solid State 7 (1966) 2580.

46. M. Pollak and T. H. Geballe, Phys. Rev. 122 (1961) 1742.

47. M. Amitay and M. Pollak, J. Phys. Soc. Japan 21, Supplement (1966) 549.

48. J. Dlinowski and J. Mycielski, Phys. Rev. 140 (1965) 1024.

49. L. J. Neuringer, R. C. Milward and R. L. Aggarwal, J. Phys. Soc. Japan 21, Supplement (1966) 582.

50. D. K. Wilson, Phys. Rev. 134 (1964) 265.

51. B. G. Zhurkin, N. A. Penin and Prem Swarup, Soviet Phys. - Solid State 8 (1967) 2839.

52. A. Koma and S. Tanaka, J. Phys. Soc. Japan 22 (1967) 139.

53. S. Tanaka, A. Koma and M. Kobayashi, J. Phys. Soc. Japan 22 (1967) 127.

54. D. Jérome and J. M. Winter, J. Phys. Chem. Solids 27 (1966) 129.

55. M. N. Alexander and D. F. Holcomb, Rev. Mod. Phys. 40 (1968) 815.

56. D. F. Holcomb and J. J. Rehr, Jr., Phys. Rev. 183 (1969) 773.

57. Y. Toyozawa, J. Phys. Soc. Japan 17 (1962) 986.

58. W. Sasaki, S. Maekawa and J. Kinoshita, J. Phys. Soc. Japan 22 (1967) 928.

59. C. Yamanouchi, J. Phys. Soc. Japan 18 (1963) 1775.

60. N. Mikoshiba, Rev. Mod. Phys. 40 (1968) 833.

61. A. M. Portis, A. F. Kip, C. Kittel and W. H. Brattain, Phys. Rev. 90 (1953) 988.

62. G. Lancaster and E. E. Schneider, Proc. Int. Conf. on Semiconductor Physics, Prague (1960) 589.

63. G. K. Walters and T. L. Estle, J. Appl. Phys. 32 (1961) 1854.

64. M. F. Chung and D. Haneman, J. Appl. Phys. 37 (1966) 1879.

65. H. Kodera, J. Phys. Soc. Japan 28 (1970) 89.

66. R. K. Wangsness and F. Bloch, Phys. Rev. 89 (1953) 728.

67. Y. Yafet, Solid State Physics 14 (Eds. Seitz and Turnbull) (Academic Press) 1963.

68. G. Lancaster, J. A. Van Wyk and E. E. Schneider, Proc. Phys. Soc. 84 (1964) 19.

69. H. Kodera, J. Phys. Soc. Japan 21 (1966) 1040.

70. I. Grünacher and W. Czaja, J. Phys. Chem. Solids 28 (1967) 231.

71. H. Kodera, J. Phys. Soc. Japan 26 (1969) 377.

72. R. A. Isaacson, Phys. Rev. 169 (1968) 312.

73. L. M. Roth, B. Lax and S. Zwerdling, Phys. Rev. 114 (1959) 90.

74. S. Maekawa and N. Kinoshita, J. Phys. Soc. Japan 20 (1965) 1447.

75. K. Morigaki and S. Maekawa, Proc. Int. Conf. on Physics of Semiconductors, Moscow, (1968).

76. H. Kodera, J. Phys. Soc. Japan 27 (1969) 1197.

CHAPTER 4

THE DETECTION OF ELECTRON PARAMAGNETIC RESONANCE

In Chapter 2 the condition for resonance was described. The means by which resonance may be observed will now be considered, and a theoretical estimate produced for the sensitivity of the resulting spectrometer. In conclusion, various spectrometer systems and components will be discussed.

4.1 Introduction

A paramagnetic sample illuminated with electromagnetic radiation of angular frequency ω_o will absorb energy at the resonant magnetic field H_o given by Equation 2.3,

$$\hbar\omega_o = g\beta H_o. \qquad \ldots\ldots\ldots\ldots\ 4.1$$

The average power absorbed per unit volume from a linearly polarized field is given by Equation 2.13,

$$P = \tfrac{1}{2}\omega_o H_1^2 \chi'', \qquad \ldots\ldots\ldots\ldots\ 4.2$$

where the symbols have been previously defined. The discussion in this chapter will be devoted to the consideration of power absorption, but the techniques are, in general, applicable to dispersion also.

In order to maximize the power absorption Equation 4.2 suggests

the use of oscillating magnetic fields of large amplitude and high frequencies, the latter demanding high magnetic fields. The state of development of these requirements has led to most advances in E.P.R. being made at microwave frequencies in the range 9 to 35 GHz. Fortunately, techniques available at these frequencies have enabled some enhancement of the magnitude of the oscillating magnetic fields, for instance by using a resonant cavity.

Several assumptions will be made in the analysis which follows. They are, a condition of non-saturation, and a sample small in comparison to a wavelength and placed in the maximum H_1 field.

4.2 Resonant Cavity Q Changes Associated with Absorption

The power absorbed at resonance will result in a change in the quality factor Q of the cavity, where the Q of the cavity into which a paramagnetic sample is placed is given by[1]

$$Q = \omega_0 \frac{\text{Energy Stored}}{\text{Average Power Dissipated}},$$

$$= \omega_0 \frac{1/8\pi \int_{V_c} H_1^2 \, dV_c}{P_1 + \frac{1}{2}\omega_0 \int_{V_s} H_1^2 \, \chi'' \, dV_s} \qquad \ldots\ldots\ldots\ldots 4.3$$

where P_1 is the power dissipated in the cavity in the absence of any paramagnetic losses, V_s is the sample volume, and V_c the cavity volume.

Assuming that the paramagnetic losses are small compared with P_1, then

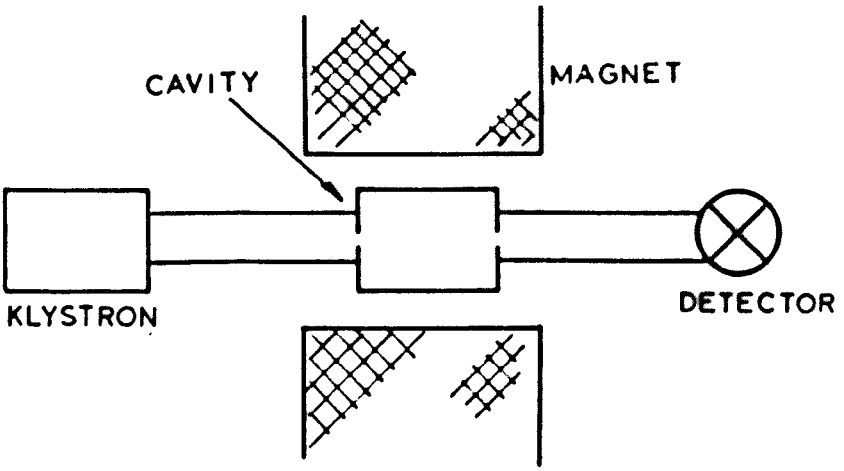

FIG. 4.1

Transmission Cavity Spectrometer.

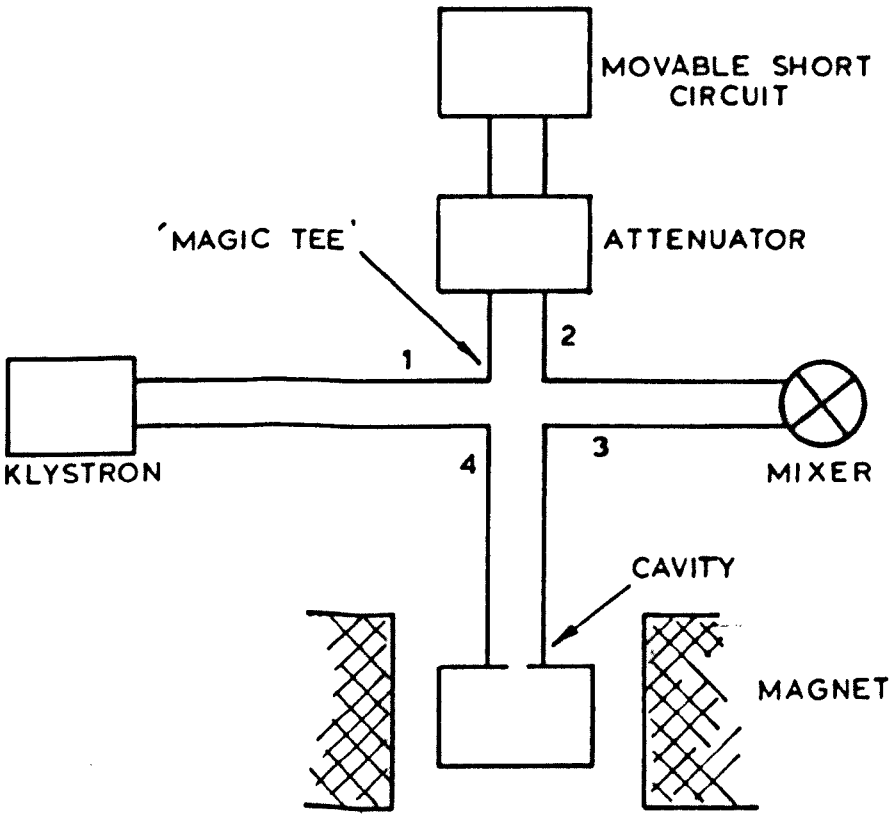

FIG. 4.2

Reflection Cavity Spectrometer.

$$Q = Q_o \left(1 - 4\pi \frac{\int_{V_s} H_1^2 \chi'' \, dVs}{\int_{V_c} H_1^2 \, dVc}\right), \qquad \ldots\ldots\ldots\ldots 4.4$$

which may be written

$$Q = Q_o \left(1 - 4\pi \chi'' \eta Q_o\right), \qquad \ldots\ldots\ldots\ldots 4.5$$

giving

$$\Delta Q = 4\pi \chi'' \eta Q_o^2, \qquad \ldots\ldots\ldots\ldots 4.6$$

where Q_o is the cavity Q in the absence of paramagnetic losses, and η is the filling factor, which is a measure of the fraction of the microwave energy within the cavity that interacts with the sample.

4.3 Types of Spectrometer

As previously indicated resonant cavities are usually used in E.P.R., and the mode of their usage allows the classification of most spectrometers into one or two types, Transmission Cavity, or Reflection Cavity.

(a) Transmission Cavity Spectrometer

This is shown in a simplified form in Fig. 4.1. A reflex klystron produces coherent microwaves which are coupled into a cavity via a small hole or iris. Likewise, power is coupled out to the detector, which is usually a silicon or germanium diode. The sample is placed within the cavity at a position of maximum microwave magnetic field, consistent with this field being perpendicular to the steady field within which the cavity is situated. At resonance, a decrease

in the power detected will be observed due to absorption by the sample.

(b) Reflection Cavity Spectrometer

Detection effeciency may be seriously limited by an inability to change the power incident upon the cavity and detector independantly, as above. In order to overcome this, use is made of a reflection cavity, Fig. 4.2.

The main element of this system is the "Magic Tee" which has the property, that if arms 2 and 4 are matched i.e., no power is reflected, all the power incident within arm 1 will be divided equally between these arms, and no power will reach arm 3. This division of power is true for any incident arm providing a similar symmetry is adopted.

If attenuation is now removed from arm 2 power will be reflected and can then reach the detector, so biasing it to a point of optimum efficiency, without altering the power coupled into the cavity. When resonance occurs the cavity impedance changes, so that power is reflected, and hence detected.

4.4 Determination of the Sensitivity of a Reflection Cavity Spectrometer in the Case of Limiting Thermal Noise

A resonant cavity is the microwave analogue of a radio-frequency tuned circuit, and equivalent circuits may be employed in the determination of optimum operating conditions for various configurations of microwave apparatus. The theoretical aspects of E.P.R. spectrometer sensitivity have been discussed extensively by various authors[1-12]. Here the analysis of Feher[1] is followed for a reflection cavity

placed in one arm of a magic tee microwave bridge, and considering the case of a linear detector (rectified crystal current proportional to the square root of the microwave power incident), Buckmaster and Dering[13] obtain

$$\frac{\Delta V \text{ refl.}}{V} = \pm \pi \chi'' \eta Q_0 \quad \ldots\ldots\ldots\ldots 4.7$$

where + and - refer to the degree of coupling of the cavity to the external waveguide, ΔV refl. is the change of voltage at the detector, and V is the voltage available at the input arm of the magic tee.

Nyquist (see Van der Ziel[14]) has shown that for a system of internal resistance R_o, terminated by an equal resistance, the root-mean-square (R.M.S.) noise voltage generated at temperature T, is

$$V_{R.M.S.} = (4 R_o kT \Delta f)^{\frac{1}{2}},$$

where Δf is the bandwidth of the system; although a receiver matched to an impedence R_o has an equivalent noise voltage at its input of[10]

$$V_n = \tfrac{1}{2} (4 R_o kT \Delta f)^{\frac{1}{2}}. \quad \ldots\ldots\ldots\ldots 4.8$$

For the limit of detectibility χ''_{min}, the E.P.R. signal ΔV refl. is equated to this noise voltage. Hence

$$\tfrac{1}{2} (4 R_o kT\Delta f)^{\frac{1}{2}} = V \pi \chi''_{min} \eta Q_o,$$

or $$\chi''_{min} = \frac{(4 R_o kT\Delta f)^{\frac{1}{2}}}{2 \pi \eta Q_o V} . \qquad \ldots\ldots\ldots\ldots 4.9$$

But for a matched generator

$$P_o = \frac{V^2}{R_o} \qquad \ldots\ldots\ldots\ldots 4.10$$

where P_o is the available power of the oscillator. Combining Equations 4.9 and 4.10 gives

$$\chi''_{min} = \frac{(kT\Delta f)^{\frac{1}{2}}}{\pi \eta Q_o P_o^{\frac{1}{2}}} . \qquad \ldots\ldots\ldots\ldots 4.11$$

This expression may now be converted into a more useful form by assuming the sample exhibits an unsaturated Lorentzian line at H_o, of peak to peak width ΔH_{pp}, and obeys the Curie Law. Thus

$$N_{min} = \frac{3 V_s kT_s}{\pi \eta Q_o g^2 \beta^2 S(S+1)} \left(\frac{\Delta H_{pp}}{H_o}\right) \left(\frac{3 kT\Delta f}{P_o}\right)^{\frac{1}{2}} \qquad \ldots\ldots\ldots 4.12$$

where N_{min} is the minimum number of spins observable in a sample of volume V_s at a temperature T_s, of "g factor" g, and of spin S.

It is now usual to state the sensitivity as the minimum number of spins observable per unit linewidth, for 1 milliwatt incident upon the cavity, and for a bandwidth of 1 Hz. Therefore, making the following assumptions $T_s = T = 300^{\circ}K$, $H_o = 12.5$ kilogauss, $P_o = 2$ milliwatt, $g = 2$, $S = \frac{1}{2}$ and $\Delta f = 1$ Hz, yields

$$N/_{\Delta H_{pp}} = 3.1\ 10^{13} \frac{V_s}{\eta Q_o} . \qquad \ldots\ldots\ldots\ldots 4.13$$

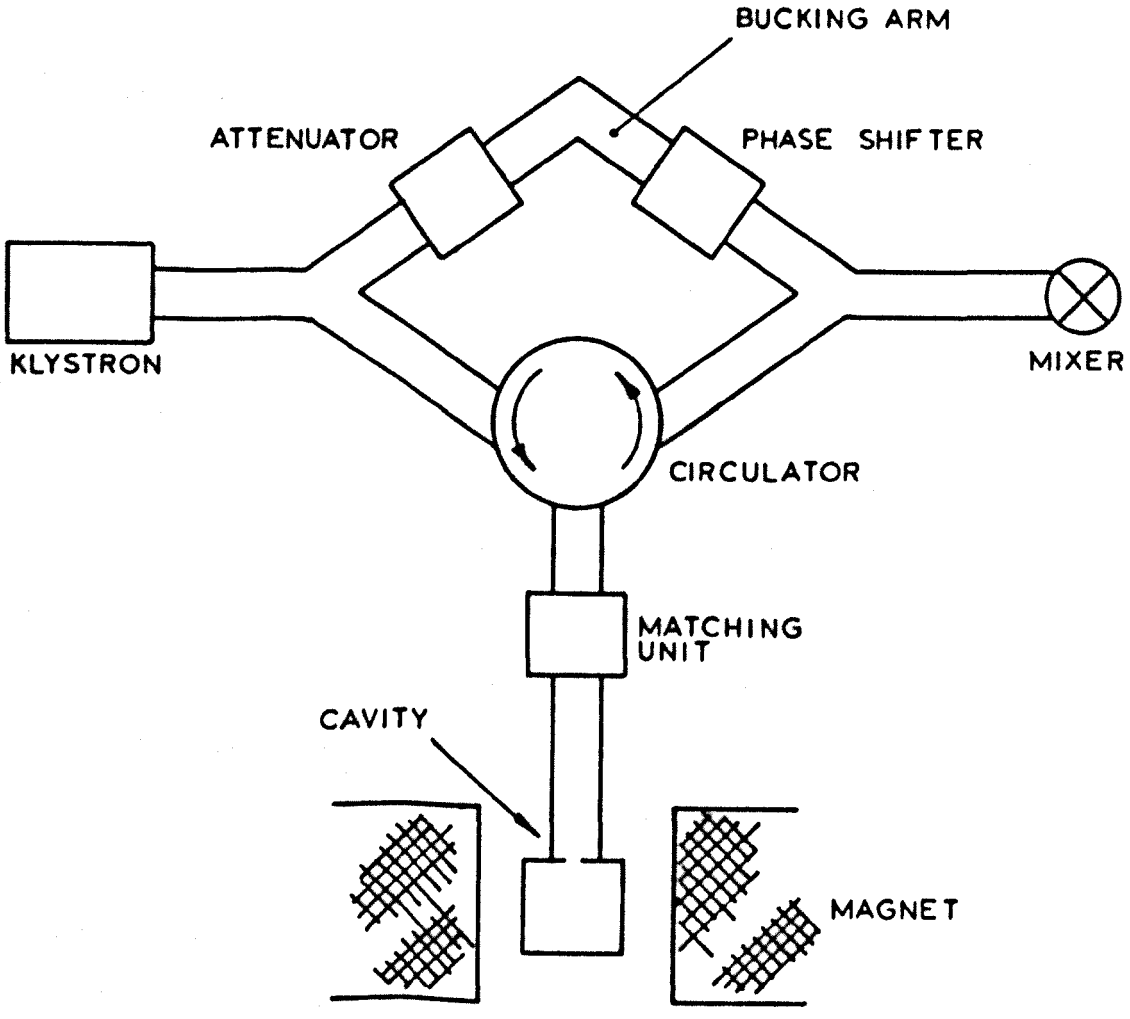

FIG. 4.3

Reflection Cavity Spectrometer using a Circulator.

If the use of a cylindrical TE_{011} cavity is assumed for which[15]

$$\eta \simeq 12.33 \left[\frac{V_s}{V_o}\right] \frac{2}{3}, \qquad \ldots\ldots\ldots\ldots\ldots 4.14$$

and the cavity has a diameter of 1.09 cm, and length 1.26 cm, exhibiting a Q_o of 5000, then

$$N/\Delta H_{pp} = 9.10^8 \text{ spins gauss}^{-1}. \qquad \ldots\ldots\ldots\ldots\ldots 4.15$$

Thus an expression has been deduced, Equation 4.12, for the minimum number of observable spins, and from this an order of magnitude of detectibility has been calculated.

A circulator used in place of the magic tee offers higher sensitivity since all the power reflected from the cavity at resonance will pass to the detector, as shown in Fig. 4.3. Faulkner[16,17] has discussed this point, and suggested various microwave circuits in which this component may be used.

To this point the introduction of noise into the system other than thermal noise has been neglected. This may be corrected by multiplying Equation 4.8 by the square root of a Noise Factor F^* (>1), which will be discussed later.

The various terms of Equation 4.12 will now be considered, including their interdependence, and consequent optimisation.

4.5 Factors to be Maximised (V_s, η, Q_o and ω_o)

The filling factor η is a function of the ratio of the sample

Spectrometer Conditions	N_{min}/V_s (η = const.)	N_{min} (V_s = const.)
Constant Microwave Power, P_ω.	$\frac{1}{\omega_o^{3/2}}$	$\frac{1}{\omega_o^{5/2}}$
Constant Energy Density at Sample. ($\langle H_1^2 \rangle_{sample}$ = const.) ($\langle H_1^2 \rangle_{cavity}$ = const.)	$\frac{1}{\omega_o^{3/4}}$	$\frac{1}{\omega_o^{11/4}}$
Constant Energy Density in Waveguide Outside Sample. ($\langle H^2 \rangle_{waveguide}$ = const.)	$\frac{1}{\omega_o^{1/2}}$	$\frac{1}{\omega_o^{7/2}}$

TABLE 4.1

Dependence of the Detectibility on Microwave Frequency.

volume V_s to cavity volume V_c mitigated by a factor which describes the part of the total microwave magnetic field in the cavity interacting with the magnetic sample. Because of this, a sample is always placed in a cavity where the microwave magnetic field is strongest and most uniform. Since most magnetic samples exhibit dielectric loss, there is an optimum sample size for maximum sensitivity, for as the sample size is increased, there is an increasing interaction with the microwave electric field and the dielectric loss increases, and this in turn reduces the total Q of a cavity.

Feher[1] has shown that for a rectangular TE_{10} mode cavity the optimum sample size when placed on an end plate, is such that the total Q of the cavity with sample is one third less than the Q without the sample. He also points out that the analysis is only valid as long as the noise is not a function of Q_o, and that the sample is not saturated.

The frequency dependence of Equation 4.12 has been studied by Poole[15], and is summarized in Table 4.1. For the usual experimental situation in which there is plenty of sample available, and the limiting factor is the amount that can be put into the cavity without appreciably lowering the Q, at constant incident power, a factor of two increase in frequency produces about a factor of three increase in sensitivity. Whereas for a constant sample size (e.g., small single crystal) and a constant microwave power, a factor of twenty-two increase for a similar frequency rise would be expected. Again, no account being taken of noise in the system or detector.

Automatic frequency control is normally applied to the microwave

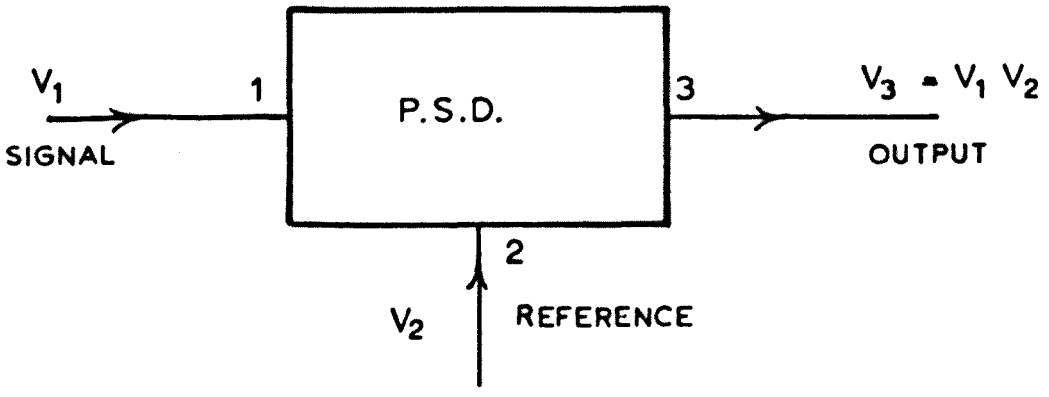

FIG. 4.4
Phase Sensitive Detector.

source in order to stabilize the frequency to that of the sample cavity, or to a very high Q reference cavity. An extensive list of references is given by Harvey[18], the most popular system being that due to Pound[19], and its modification by Tuller, Galloway and Zaffaranos[20].

4.6 Factors to be Minimized (T_s, T and Δf)

A decrease in the temperature of the sample T_s will both increase the power absorption i.e., lowering N_{min}, and the cavity Q_o, assuming both are within the refrigerant. It is not usual to lower the temperature of the detector, although this would produce a sensitivity increase.

To reduce the noise factor of the system (as will be discussed in Section 4.7) it is usual to modulate the magnetic field H_o at some frequency say f_m, typically 100KHz, such that from the microwave detector there is a voltage whose amplitude and phase it is desired to measure. A Phase Sensitive, or Lock-In, Detector is designed to do just this, and many circuits have been suggested[21-31], the most common to date being due to Schuster[21].

The basic phase sensitive detector is shown in Fig. 4.4. Suppose that the reference voltage $V_2 = V_o \cos 2\pi f_m t$ and the signal voltage is $V_1 = V_s \cos (2\pi f_m t + \phi)$, then the d.c. output is

$$V_{dc} = \tfrac{1}{2} V_s V_o \cos\phi. \qquad \ldots\ldots\ldots\ldots 4.16$$

If the reference phase is chosen to make $\phi = 0$ then

$$V_{dc} = \tfrac{1}{2} V_s V_o. \qquad \ldots\ldots\ldots\ldots\ 4.17$$

Hence this circuit is essentially a mixer with zero intermediate frequency (i.f.).

Robinson[10] has drawn a comparison between the effective noise bandwidth offered by a phase sensitive detector, and straight rectification. Suppose there is a signal at f_m of known phase in a background of noise, in a bandwidth Δf_m. If this input is rectified and the resultant d.c. output applied to a meter of bandwidth Δf_b, the effective bandwidth of the system is $(2\Delta f_m \Delta f_b)^{\frac{1}{2}}$. Whereas the effective noise bandwidth of the phase sensitive detector is Δf_b.

If the following is taken as an example, $\Delta f_m = 2$ KHz, and $\Delta f_b = 1$ Hz, then the simple detector has $\Delta f_{eff} = 63$ Hz i.e., a 63-fold improvement for the phase sensitive detector.

4.7 The Noise Factor, F*

Noise will be introduced into a spectrometer at many points. Bosch and Gambling[32] have performed a detailed study of noise in microwave power sources and have shown that the sideband noise spectrum consists of contributions from (i) background noise, (ii) amplitude modulation (a.m.) noise, and (iii) frequency modulation (f.m.) noise. They have shown that the f.m. noise is the dominant contribution in klystrons at sideband frequencies below 10 MHz.

A contribution to this f.m. noise is the result of electrode supplies to klystrons which do not provide ideal d.c. voltages. The

most sensitive electrode of a reflex klystron is the reflector which may have a frequency/voltage sensitivity of 100 KHz volt^{-1} to 10 MHz volt^{-1}. Using 1 MHz volt^{-1} as an example, a reflector supply with less than 100 microvolts ripple is necessary if it is required to keep the reflector supply induced f.m. noise below 100 Hz.

Microphonics at the cavity due to its immersion in a boiling liquid refrigerant, and eddy currents induced in the walls of the cavity at high modulation fields, both contribute to the noise of the system, principally at sideband frequencies up to 500 Hz. Similarly microphonics in any part of the system will degrade the spectrometer sensitivity.

The most important source of noise in the majority of spectrometers is the so-called Flicker Noise in the point contact semiconductor detector (in this case being used as a mixer). This will be discussed further after deduction of the form of the Noise Factor F*.

Torrey and Whitmer[33] define the noise figure of a network as

$$F = \frac{\frac{dNo}{So}}{\frac{dNi}{Si}} \qquad \ldots\ldots\ldots\ldots\ldots 4.18$$

where $\frac{dNi}{Si}$ is the incremental noise to signal power ratio at the input, and $\frac{dNo}{So}$ is a similar quantity at the output. If it is assumed that the input noise power of a network is the Johnson noise $kT\Delta f$, then

$$dNo = GkT\Delta f + (F - 1)\, GkT\Delta f \qquad \ldots\ldots\ldots\ldots\ldots 4.19$$

where G is the power gain $\frac{So}{Si}$. This means the network adds $(F - 1)$ $GkT\Delta f$ to the amplified input.

Friis[34] developed a method to determine the overall noise figure of n cascaded networks, and showed

$$F_{1,2,\ldots n} = 1 + (F_1 - 1) + \frac{(F_2 - 1)}{G_1} + \frac{(F_3 - 1)}{G_1 G_2} + \ldots \qquad \ldots\ldots 4.20$$

From which it is apparent that the noise figure of the first stage F_1, is of particular importance, assuming the power gains G_1, G_2 .... are large.

Application of the Friis formula to the case in hand gives F', the noise figure of the composite system of mixer plus i.f. pre-amplifier,

$$F' = \frac{FdGd + Fa - 1}{Gd}, \qquad \ldots\ldots\ldots\ldots 4.21$$

where Fd is the mixer noise figure at the particular i.f. used, Gd is the conversion gain, which is the ratio of the power at the i.f. to that at the microwave frequency (since Gd < 1, the reciprocal is often used, L, the conversion loss), and Fa is the noise figure of the i.f. pre-amplifier.

If the following definition is adopted

$$FdGd = t, \qquad \ldots\ldots\ldots\ldots 4.22$$

then this represents the factor by which the microwave mixer introduces more noise into the system than a Johnson source at the same temperature, and as a consequence is usually called the Noise Temperature Ratio, or just Noise Temperature.

To Equation 4.21 must now be added the noise figure of the klystron

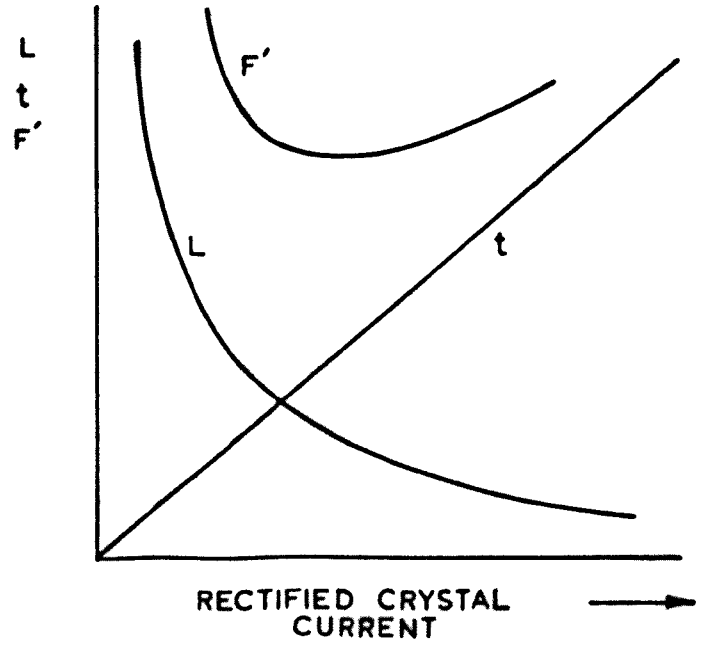

FIG. 4.5a

The Dependence of Noise Temperature Ratio, Conversion Loss and Overall Noise Figure as a Function of Rectified Crystal Current.

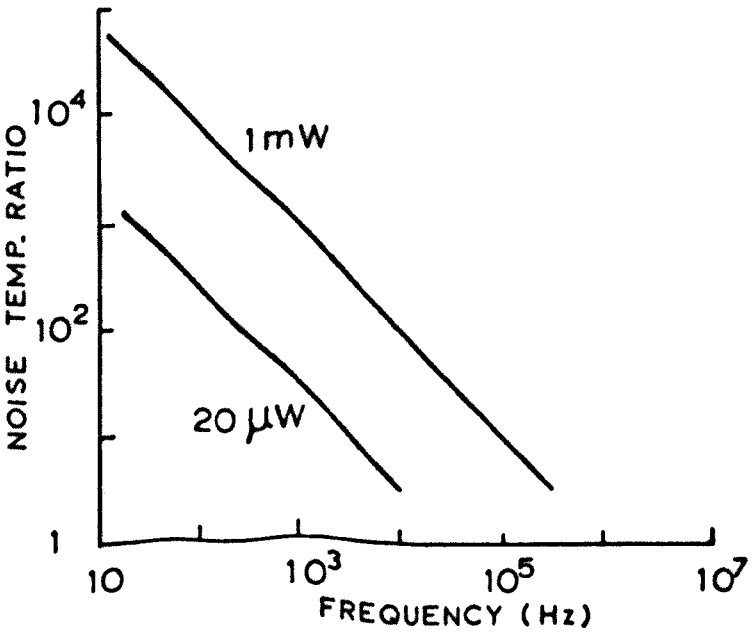

FIG. 4.5b

The Frequency Dependence of the Noise Temperature Ratio of Crystal Mixer IN23WE at Two Incident Microwave Power Levels.

F_k. Thus the complete Noise Factor, F*, becomes

$$F^* = F_k + \frac{FdGd + Fa - 1}{Gd}, \qquad \ldots\ldots\ldots\ldots 4.23$$

or

$$F^* = F_k + L(t + Fa - 1). \qquad \ldots\ldots\ldots\ldots 4.24$$

The noise temperature ratio of the mixer is principally determined by the Flicker Effect, although shot noise is present. Flicker noise is thought to be due to trapping states, which are more likely to arise at surfaces or interfaces, although bulk effects are not precluded. Torrey and Whitmer[33], Strandberg, Johnson and Eshbach[35], Ingram[4], and Buckmaster and Dering[13] have shown that for a square law detector,

$$t - 1 = A_{SL} \frac{P_{RF}^2}{f_m}, \qquad \ldots\ldots\ldots\ldots 4.25$$

and for a linear detector

$$t - 1 = A_L \frac{P_{RF}}{f_m}, \qquad \ldots\ldots\ldots\ldots 4.26$$

where A_{SL} and A_L are experimentally determined parameters which characterize a particular crystal mixer. Hence the common expression of Flicker noise as "$\frac{1}{f}$ noise".

Fig. 4.5a shows the general crystal characteristics[33], and Fig. 4.5b the frequency dependence of the noise temperature ratio at two incident microwave power levels for a 1N23WE crystal mixer[13]. The minimum in the overall noise figure at finite powers, demonstrates

the necessity of being able to separately bias the crystal mixer if easily saturated samples are being examined, as inferred in Section 4.3b.

Fig. 4.5b would suggest the use of as high an i.f. as possible, but this is counter-balanced by the fact that the noise of a given type of i.f. amplifier increases with frequency. Strum[36] has demonstrated that the noise figure of the mixer plus amplifier exhibits a broad minimum in the region of 30 MHz.

Modulation of the magnetic field H_o at this frequency is not very practical, and broadening of the resonance line can occur, brought about by a modulation of the Larmor precession frequency. For a $g = 2$ resonance, the necessary restriction on frequency is

$$f_m << 2.8.10^6 \Delta H_{\frac{1}{2}} \text{ Hz}, \qquad \ldots\ldots\ldots\ldots 4.27$$

where $\Delta H_{\frac{1}{2}}$ is the linewidth in gauss. Hence the narrowest lines that can be examined, at for example the following frequencies, are

Modulation Frequency, f_m	Minimum Linewidth
100 Hz	0.04 Milligauss
100 KHz	36 Milligauss
30 MHz	10 Gauss

4.8 Superheterodyne Detection

This technique employs the mixing of two frequencies in order to obtain a high i.f. (~ 30 MHz) so that the noise figure of the system may be minimized.

Spectrometers operating on this principle may be divided into three types, viz. (i) two microwave sources with automatic frequency

control between them, (ii) very stabilized sources, or (iii) one klystron.

England and Schneider[37] were first to use superheterodyne detection in paramagnetic resonance, and their spectrometer was of the first type, as were many of the earlier ones[1,5,8,38-42].

When highly stabilized microwave sources are used, the i.f. is devoid of drift because the sources are stabilized. This may be achieved by using for example the harmonic of a stable quartz oscillator,[42] or a phase locking system[43-46], which may be capable of locking the klystron frequency to within a few cycles.

A single-klystron spectrometer using superheterodyne demodulation was first described by Llewellyn, Whittlestone and Williams[47], who generated the local oscillator power by frequency modulation of the microwave power source to produce a 10 MHz sideband which was separated from the carrier by a system of resonant cavity filters. Similarly 45 MHz sidebands have been produced by a crystal modulator[48], using a fraction of the power for the local oscillator, the remainder being coupled to the cavity. Buckmaster and Dering[49] have pointed out that failure to remove the modulation sidebands from the signal power, or the carrier and one sideband from the local oscillator power, will result in a degradation of the noise figure of the system, and have described their own spectrometer[50] which uses a ferrite single sideband generator to produce the intermediate frequency. Zwarts and van Ormondt[51] have also described a system using only one of the sidebands, and Patanker[52] has demonstrated a variant on this system, using double sideband demodulation.

4.9 The Magnetic Field, H_o

As pointed out by Coles[53] in his review of magnet systems for E.P.R., a spectrometer comprises two virtually independent sections, namely the microwave system (including the associated electronics) and the magnet system.

For frequencies of 9 GHz (X band) and 35 GHz (Q band), magnetic fields of the order of 3300, and 12500 gauss respectively, are necessary for $g \approx 2$ resonances. If $2 < g < 2$ corresponding lower or higher fields are required, and the magnet must also be able to reach fields sufficient to examine wide lines.

The magnetic field must also be homogeneous over the sample volume. A rule of thumb is that the variation in the strength over the sample, ΔH_o, should be less than one quarter to one fifth of the line width ΔHpp. Hence for certain free radicals which exhibit line widths as low as 20 milligauss at X band, a homogeneity of 5 milligauss is required, equivalent to 1ppm. This would be achieved using plane pole pieces of at least 8" diameter, and parallel to within 1 or 2 microns across the diameter. Coned pole pieces may be used to obtain higher fields with the same magnet, but there is a reduction in the volume exhibiting the same homogeneity.

As pointed out in Section 4.6, detection sensitivity can be increased by decreasing the bandwidth of the meter following the phase sensitive detector. A network of variable time constant is normally used, and thus it must be ensured that the stability of the magnetic field during this time is of the same order. Water cooled electromagnets are normally used, having sophisticated current control circuits, with

facilities for current/field sweeps through the resonance.

For frequencies higher than Q band e.g., O band (70 GHz), g = 2 resonances require fields at the limit of electromagnets with finite gaps and homogeneity, so that the timely arrival of superconducting magnets able to achieve 25000 gauss with ease, has coincided with the development of microwave components able to provide sufficient power for use in E.P.R.

4.10 General Discussion

To this point conventional spectrometers have been described, but as with any technique there are variations on a theme, which will now be briefly reviewed.

For the examination of samples exhibiting high dielectric loss at microwave frequencies, e.g., metals, highly doped semiconductors, and water, several spectrometers operating in the hundreds of megahertz region have been reported, and are reviewed by Hill and Wyard[54]. Collingwood and White[55] have suggested the use of a helical resonator for such spectrometers, so that convenience of use is improved, smaller resonators are possible, and a higher Q can be achieved for samples needing irradiation at the resonance frequency.

Helices have also been used in place of cavities at microwave frequencies, since modulation and optical irradiation may be easily introduced, and in double resonance experiments, the helix can also serve as the N.M.R. coil. Also, since the helix is broadbanded, it is not necessary to stabilise the source as precisely as in the cavity case, and f.m. noise[32] becomes unimportant. It has been shown[9]

that about the same sensitivity as cavity spectrometers is attainable, provided the helix is no more than a few half wavelengths long. Webb[56] and Pearlman and Webb[57] discuss the practicallities of their manufacture and use.

Payne[58] has used a 100 milliwatt travelling wave tube in a "self-stabilized" oscillator-spectrometer system, where the cavity is the frequency determining element of the feedback network. A directional coupler at the amplifier output is used to sample the microwave power. His system was able to achieve a sensitivity comparable to conventional spectrometers, without frequency stabilization or superheterodyne detection.

The usefulness of low-noise microwave pre-amplifiers for improving sensitivity has been examined by many, e.g.,[59,60], who have concluded that the expected increase was seldom yielded since it was difficult to avoid saturation effects in the pre-amplifier. Buckmaster and Dering[61] have shown that the use of a pre-amplifier is justified only if its noise figure $F_p < F'$ (Equation 4.21), and its gain $G_p > 10^2$. They further indicate that the ultimate sensitivity of any balanced bridge spectrometer is independent of the cavity Q and the microwave power in the cavity, but is proportional to the square root of the product of the output bandwidth and the standard deviation of the microwave oscillator f.m. noise spectrum, in the absence of sample saturation effects.

Detectors other than conventional crystal rectifiers have been used, the most common being the bolometer (or barretter)[1,62]. Because it has a long response time, a field modulation frequency of less than 1 KHz is used, and although it can be as sensitive as a crystal detector,

it is less often used, partly due to its ease of "burn-out". Schmidt and Solomon[63], using a crude bolometer in intimate contact with the sample, have detected the temperature rise on resonance, and predict a sensitivity of 10^6 spins for favourable samples (e.g., conduction electrons in metals and semiconductors) at liquid helium temperature. Tunnel and backward diodes, which exhibit greater reverse conduction than forward, have recently been used as detectors. Tunnel detectors offer a $\frac{1}{f}$ noise "corner" as much as three decades in frequency below that of crystal detectors, and an i.f. impedance in the range 50-150 ohms which is compatible with standard transmission lines[64]. Germanium backward diodes used as mixers at X band are less noisy than conventional diodes with low power local oscillators[65], although gallium arsenide backward diodes for millimetre wave applications exhibit $\frac{1}{f}$ noise to frequencies approaching 200 MHz[66]. Hot carrier diodes, which consist of a rectifying metal-semiconductor contact or Schottky barrier, are also beginning to be used as detectors, and have a $\frac{1}{f}$ noise "corner" of the order of 1 KHz. Indium antimonide has been used as a photoconductive detector in the millimetre and sub-millimetre region. Although practically less convenient, since a temperature of the order of $4^{\circ}K$ and a magnetic field of the order of 6000 gauss is necessary[67], it has a short response time.

Solid state microwave power sources and circuits are now becoming commercially available. An X band spectrometer with a Gunn diode mounted inside the sample cavity has been exhibited[68]. The f.m. noise is worse than that of a klystron close to the carrier frequency but falls off more rapidly with modulation frequency than that of the

klystron. Avalanche diode generators are also being developed, but again are noisier than klystrons[69].

Enhancement of the signal to noise of a spectrum may be achieved by repeated scanning of the spectrum, averaging the results in a computer of average transients. An increase of a factor $m^{\frac{1}{2}}$ may be obtained for m sweeps. This instrument has also been used in spectrometers studying transient paramagnetic species[70]. Glarum[71] has demonstrated that spectra resolution may be increased by simultaneously modulating the magnetic field H_o at f_m (typically 100 KHz), $\frac{fm}{3}$, $\frac{fm}{5}$ etc., while continuing to detect at f_m; and Fourier transform analysis[72] has been used in the interpretation of spectra showing poorly resolved hyperfine structure due to several nuclear species.

The advantages offered by using a balanced mixer detector will be discussed in the following chapter, suffice to say at present, that if at low modulation frequencies the major noise source is the klystron, sensitivity may be improved by using such a system.

REFERENCES

1. G. Feher, Bell System Tech. J. 36 (1957) 449.
2. B. Bleaney and K. W. H. Stevens, Rept. Prog. Phys. 16 (1953) 109.
3. D. J. E. Ingram, Spectroscopy at Radio and Microwave Frequencies (Butterworths Scientific Publications) 1955.
4. D. J. E. Ingram, Free Radicals as Studied by Electron Spin Resonance (Butterworths Scientific Publications) 1958.
5. H. Misra, Rev. Sci. Instrum. 29 (1958) 590.
6. K. A. Müller, Bull. Ampere, 9e année (Numéro spécial) (1960) 342.
7. J. P. Goldsborough and M. Mandel, Rev. Sci. Instrum. 31 (1960) 1084.
8. D. T. Teaney, M. P. Klein and A. M. Portis, Rev. Sci. Instrum. 32 (1961) 721.
9. T. H. Wilmshurst, W. A. Gambling and D. J. E. Ingram, J. Electron. Control 13 (1962) 339.
10. F. N. H. Robinson, Noise in Electrical Circuits (O.U.P.) 1962.
11. H. Misra, Indian J. Pure Appl. Phys. 1 (1963) 37.
12. J. S. Hyde, Paper presented at Seventh Annual N.M.R.-E.P.R. Workshop, Varian Associates, Palo Alto, Calif., 1963.
13. H. A. Buckmaster and J. C. Dering, Canad. J. Phys. 43 (1965) 1088.
14. A. Van der Ziel, Noise (Prentice-Hall Inc) 1954.
15. C. P. Poole, Jnr., Electron Spin Resonance (Wiley) 1967.
16. E. A. Faulkner, J. Sci. Instrum. 39 (1962) 135.
17. E. A. Faulkner, Lab. Pract. 13 (1964) 1065.
18. A. F. Harvey, Microwave Engineering (Academic Press) 1963.
19. R. V. Pound, Rev. Sci. Instrum. 17 (1946) 490.

20. W. G. Tuller, W. C. Galloway and F. P. Zaffarano, Proc. I.R.E. 36 (1948) 794.

21. N. A. Schuster, Rev. Sci. Instrum. 22 (1951) 254.

22. H. L. Cox Jr., Rev. Sci. Instrum. 24 (1953) 307.

23. E. A. Faulkner, J. Sci. Instrum. 37 (1959) 321.

24. E. A. Faulkner and R. H. O. Stannett, Elect. Enging. 36 (1964) 159.

25. M. J. Wright, Elect. Engng. 34 (1962) 698.

26. B. V. Rollin, J. Sci. Instrum. 41 (1964) 239.

27. P. Williams, J. Sci. Instrum. 42 (1965) 474.

28. Y. Beers, Rev. Sci. Instrum. 36 (1965) 696.

29. E. A. Faulkner and D. W. Harding, J. Sci. Instrum. 43 (1966) 97.

30. D. P. Ryan, Rev. Sci. Instrum. 37 (1966) 486.

31. J. P. Stuart and W. Derbyshire, J. Sci. Instrum. 44 (1967) 62.

32. B. G. Bosch and W. A. Gambling, J. Brit. I.R.E. 24 (1962) 389.

33. H. C. Torrey and C. A. Whitmer, Crystal Rectifiers (McGraw-Hill) 1948.

34. H. F. Friis, Proc. I.R.E. 32 (1944) 419.

35. M. W. F. Strandberg, H. R. Johnson and J. R. Eshbach, Rev. Sci. Instrum. 25 (1954) 776.

36. P. D. Strum. Proc. I.R.E. 41 (1953) 875.

37. T. S. England and E. E. Schneider, Nature 166 (1950) 437.

38. J. M. Hirshon, and G. K. Fraenkel, Rev. Sci. Instrum. 26 (1955) 34.

39. C. Ryter, R. Lacroix and R. Extermann, Onde Élect. 35 (1955) 490.

40. A. A. Manenkov and A. M. Prokhorov, Radiotekh. i Elektron. 1 (1956) 469.

41. A. C. Rose-Innes, J. Sci. Instrum. 34 (1957) 276.

42. K. D. Bowers, R. A. Kamper and R. B. D. Knight, J. Sci. Instrum. 34 (1957) 49.

43. R. L. Poynter and G. R. Steffensen, Rev. Sci. Instrum. 34 (1963) 77.

44. H. J. McAleer, Proc. I.R.E. 47 (1959) 1137.

45. H. A. Buckmaster and J. C. Dering, J. Sci. Instrum. 43 (1966) 554.

46. W. R. Day, Microwave J. 10 (1967) 35.

47. P. M. Llewellyn, P. E. Whittlestone and J. M. Williams, J. Sci. Instrum. 39 (1962) 586.

48. G. Brown, D. R. Mason and J. S. Thorp, J. Sci. Instrum. 42 (1965) 648.

49. H. A. Buckmaster and J. C. Dering, J. Sci. Instrum. 43 (1966) 404.

50. H. A. Buckmaster and J. C. Dering, Canad. J. Phys. 45 (1967) 107.

51. C. M. S. Zwarts and D. van Ormondt, J. Sci. Instrum. 43 (1966) 317.

52. A. V. Patankar, J. Sci. Instrum. 44 (1967) 354.

53. B. A. Coles, Lab. Pract. 13 (1964) 1073.

54. M. J. Hill and S. J. Wyard, J. Sci. Instrum. 44 (1967) 433.

55. J. C. Collingwood and J. W. White, J. Sci. Instrum. 44 (1967) 509.

56. R. H. Webb, Rev. Sci. Instrum. 33 (1962) 732.

57. M. R. Pearlman and R. H. Webb, Rev. Sci. Instrum. 38 (1967) 1264.

58. J. B. Payne, I.E.E.E. Trans. MTT-12 (1964) 48.

59. C. H. Townes, Phys. Rev. Lett. 5 (1960) 428.

60. W. A. Gambling and T. H. Wilmshurst, Phys. Lett. 5 (1963) 228.

61. H. A. Buckmaster and J. C. Dering, J. Sci. Instrum. 44 (1967) 430.

62. R. Beringer and J. G. Castle, Phys. Rev. 78 (1950) 581.

63. J. Schmidt and I. Solomon, J. Appl. Phys. 37 (1966) 3719.

64. R. B. Mouw and F. M. Schumacher, Microwave J. 9 (1966) 27.

65. T. H. Oxley, J. Electron. Control 17 (1964) 1.

66. C. A. Burrus and D. T. Young, Solid State Electron. 9 (1966) 49.

67. E. H. Putley, Proc. I.E.E.E. 51 (1963) 1412.

68. Institute of Physics and the Physical Society, Exhibition, 1969.

69. F. E. Chapman and R. E. Michel, Rev. Sci. Instrum. 38 (1967) 1170.

70. E. W. Firth and D. J. E. Ingram, J. Sci. Instrum. 44 (1967) 821.

71. S. H. Glarum, Rev. Sci. Instrum. 36 (1965) 771.

72. R. H. Silsbee, J. Chem. Phys. 45 (1966) 1710.

CHAPTER 5

EXPERIMENTAL TECHNIQUES

Following a description of the commercial spectrometer and various small modifications which were made to it, an account will be given of its conversion to one with balanced mixer detection. The proton resonance frequency meter for magnetic field measurement, type of cavity, and low temperature techniques used will also be outlined.

5.1 The Commercial Spectrometer

The spectrometer was a Hilger and Watts Ltd. ESR 2 Q-band Microspin Spectrometer[1]. It operated in the wavelength range 8.4 to 8.8 mm, and was of the reflection cavity type as described in Section 4.3b, displaying the E.P.R. signal in many ways depending upon its amplitude. For large signals a video mode could be employed, when the absorption (or dispersion) signal was viewed on an oscilloscope as the magnetic field H_o was swept at 50 Hz about the resonance point. When higher sensitivity was necessary, a high frequency modulation f_m of 100 kHz was available, the first derivative of the resonance curve being traced by a pen recorder, in addition to the oscilloscope display, as the external magnetic field was slowly swept. Combinations of these two modes of display were also possible.

A block diagram of the spectrometer is shown in Fig. 5.1, and a system description will now follow.

(a) The Klystron and Automatic Frequency Control

An E.M.I. R5146 klystron provided approximately 30 milliwatts of

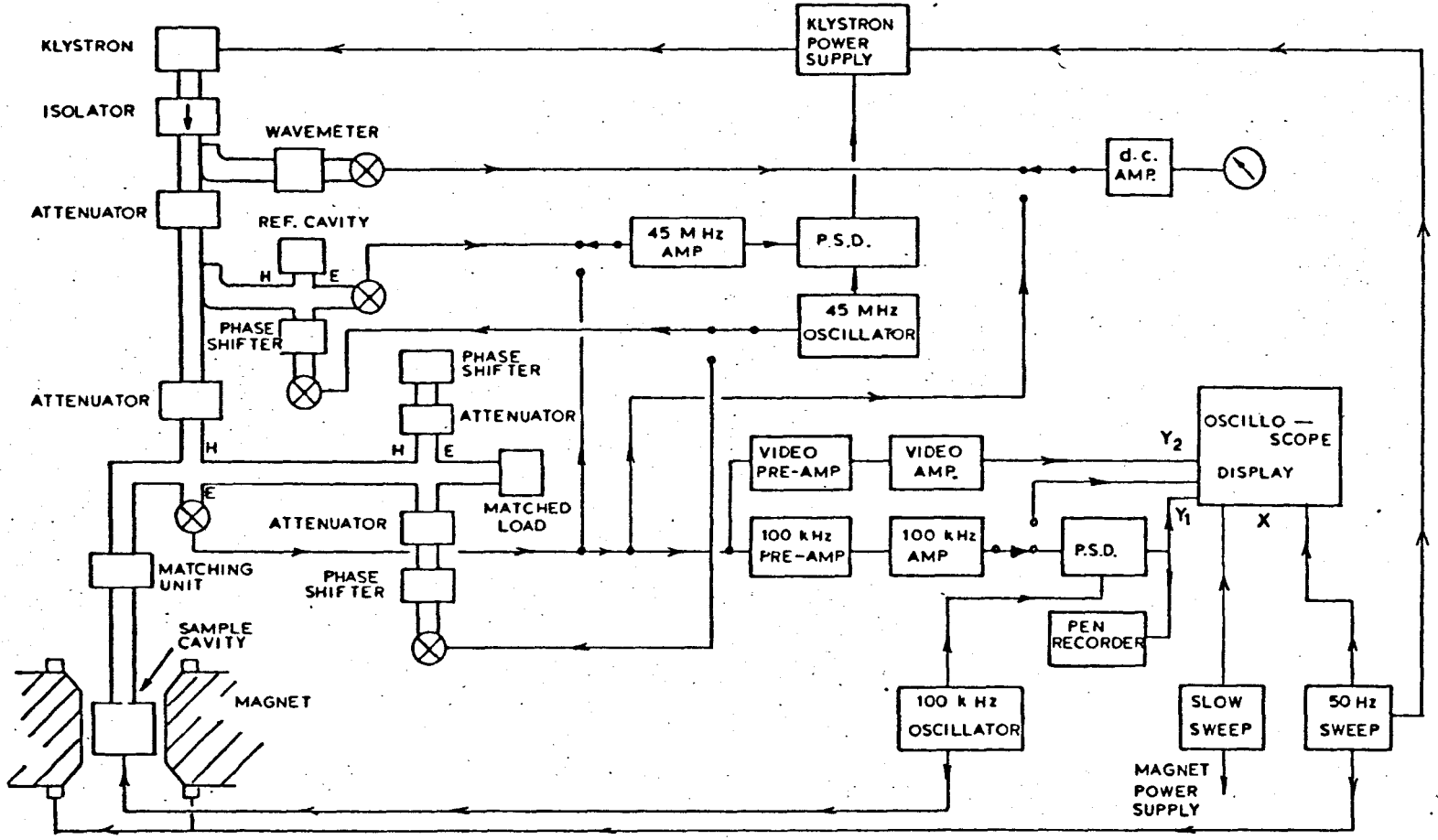

FIG. 5.1 The Commercial Spectrometer.

microwave power. Its associated stabilized power supplies had a reflector ripple voltage of approximately 12 mV peak to peak, and since the klystron had a frequency/voltage sensitivity of 2 MHz volt^{-1}, f.m. noise was produced over a bandwidth of 24 KHz.

In order to facilitate the tuning of the cavity to the klystron maximum power point, or klystron tuning if the cavity resonant frequency was not adjustable, a 50 Hz modulator was added into the spectrometer. Deriving its input from the 'X' sweep of the oscilloscope display unit, approximately 100 V of variable phase could be applied to the klystron reflector. This was sufficient to display a whole klystron mode, having a half-power points width of 30 V, or 60 MHz.

Two automatic frequency control systems were built into the spectrometer, one locking the frequency to an external high Q cavity and the other locking to the sample cavity. Both were of the modified equal arm Pound type[2] using an i.f. of 45 MHz, and are shown in Fig. 5.1. For the external cavity system a stability of 1 in 10^6 (35 KHz in 35 GHz) was claimed at constant temperature. Successful operation of the sample cavity system was not achieved, since lock could not be maintained when attenuation was removed from the opposite arm of the magic tee in order to bias the signal mixer crystal.

The microwave frequency was monitored using a calibrated wavemeter.

(b) Video Detection

The video pre-amplifier was mounted in close proximity to the signal mixer crystal. It had a gain of 20 dB (X10) and a bandwidth of 15 Hz to 10 KHz, and fed the video amplifier of the same bandwidth but of gain 80 dB (X10^4). As a separate proton resonance system was

used, a circuit modification at this point enabled the video amplifier output to be coupled into the Microspin "Proton Resonance Amplifier" (or second oscilloscope 'Y' trace), which allowed the display of the 100 KHz signal envelope when the field was simultaneously modulated at 50 Hz.

(c) High Frequency Detection

A 100 KHz crystal-controlled oscillator was able to feed up to 4 amps peak to peak into a low impedance modulation loop situated within the sample cavity (see Section 5.4). It also provided 10 V R.M.S. as a source for a reference phase-shifter and amplifier.

The 100 KHz pre-amplifier was also mounted close to the signal mixer crystal. Its input impedance was approximately 500 ohms, providing match for the SHM8 silicon mixer crystals used throughout the spectrometer. These mixer crystals had an overall noise figure of 17 dB. The pre-amplifier had a double triode used in cascode fashion at the input, so that roughly, the gain of a single pentode was available, but only at the cost of the noise figure of a triode, since partition noise would not be present. The amplifier provided a gain of 67 dB (X $2.2 \cdot 10^3$), with a bandwidth of 2.5 KHz centred at 100 KHz.

The signal was then fed to the main amplifier such that inclusion of the pre-amplifier gave an overall gain of approximately 128 dB (x $2.5 \cdot 10^6$), the bandwidth reducing to 2 KHz. Under these conditions the noise of the amplifiers was proportional to 0.3 μV appearing at the input to the pre-amplifier, which was equivalent to a pre-amplifier noise figure of 7.3 dB, taking Equation 4.20 into account. The output of the main amplifier may either be directly displayed on the oscilloscope, or be

switched to the phase sensitive detector. This was of the Schuster type[3], having a pentode signal amplifier connected in cascode with a double triode, such that the reference voltage was able to switch the signal between the anode loads of the triodes. At the output of the phase sensitive detector an RC time constant network in the range 3 m sec to 6 sec provided the effective bandwidth of the system.

A Honeywell "Electronik" potentiometric strip chart recorder of 10 mV sensitivity was used to provide a permanent record of the spectrum, while simultaneously the spectrum was displayed on the oscilloscope. Repetitive slow field sweeps of 5 sec duration, and single sweeps in the range 1 to 20 mins were available. Slow sweep amplitudes were of 10 to 250 gauss, although this could be increased by using an external field sweep unit.

When the spectrometer sensitivity was measured at $77^{o}K$ using a known volume of crushed 1.10^{16} cm^{-3} phosphorus-doped silicon, with a cavity Q of 5000, and a bandwidth of $\frac{1}{6}$ Hz, a signal to noise ratio of 27:1 and a linewidth of 6.8 gauss resulted. This was equivalent to a sensitivity of $2.2 . 10^{10}$ spins $gauss^{-1}$. If this is converted to the conditions appertaining to Section 4.4 (assuming the linewidth does not change) the sensitivity becomes

$$4.1.10^{11} \text{ spins gauss}^{-1}. \qquad \ldots\ldots\ldots\ldots 5.1$$

This figure should be compared with Equation 4.15 increased by the noise figure of the spectrometer F*. Bosch and Gambling[4] and Johnson, Smith and Calder[5] have shown that for a reflex klystron the a.m. and f.m. noise powers at 100 KHz off the carrier are typically -140 to

-150 dB Hz^{-1}. Hence for 1 milliwatt bias power onto the mixer crystal the klystron noise figure[6] F_k is 21 dB. Estimating the mixer conversion loss as 6 dB[7], gives

$$F^* = 23 \text{ dB}. \qquad \ldots\ldots\ldots\ldots\ldots 5.2$$

Thus Equation 5.1 must be compared with

$$1{\cdot}2.10^{10} \text{ spins gauss}^{-1}. \qquad \ldots\ldots\ldots\ldots\ldots 5.3$$

The non-attainment of theoretical sensitivity may be accounted for by such factors as microphonics introduced by the internal modulation loop, the discrimination of klystron f.m. noise by the sample cavity[8], and 15 milliwatts may have been an over estimate for the power reaching the cavity.

5.2 Balanced Mixer Detection

To enable the observation of inhomogeneously broadened lines under slow passage conditions, Weger[9] has deduced restrictions which must apply, and they include

$$\sqrt{T_1 T_2} \ll \frac{H_1}{2\pi f_m \Delta H_{\frac{1}{2}}} \qquad \ldots\ldots\ldots\ldots\ldots 5.4$$

where the symbols have been previously defined. Hence in the case of phosphorus-doped silicon where long relaxation times can be found, high modulation frequencies are unfavourable.

Thus modifications to the spectrometer were commenced such that modulation frequencies below 100 kHz would be available. An

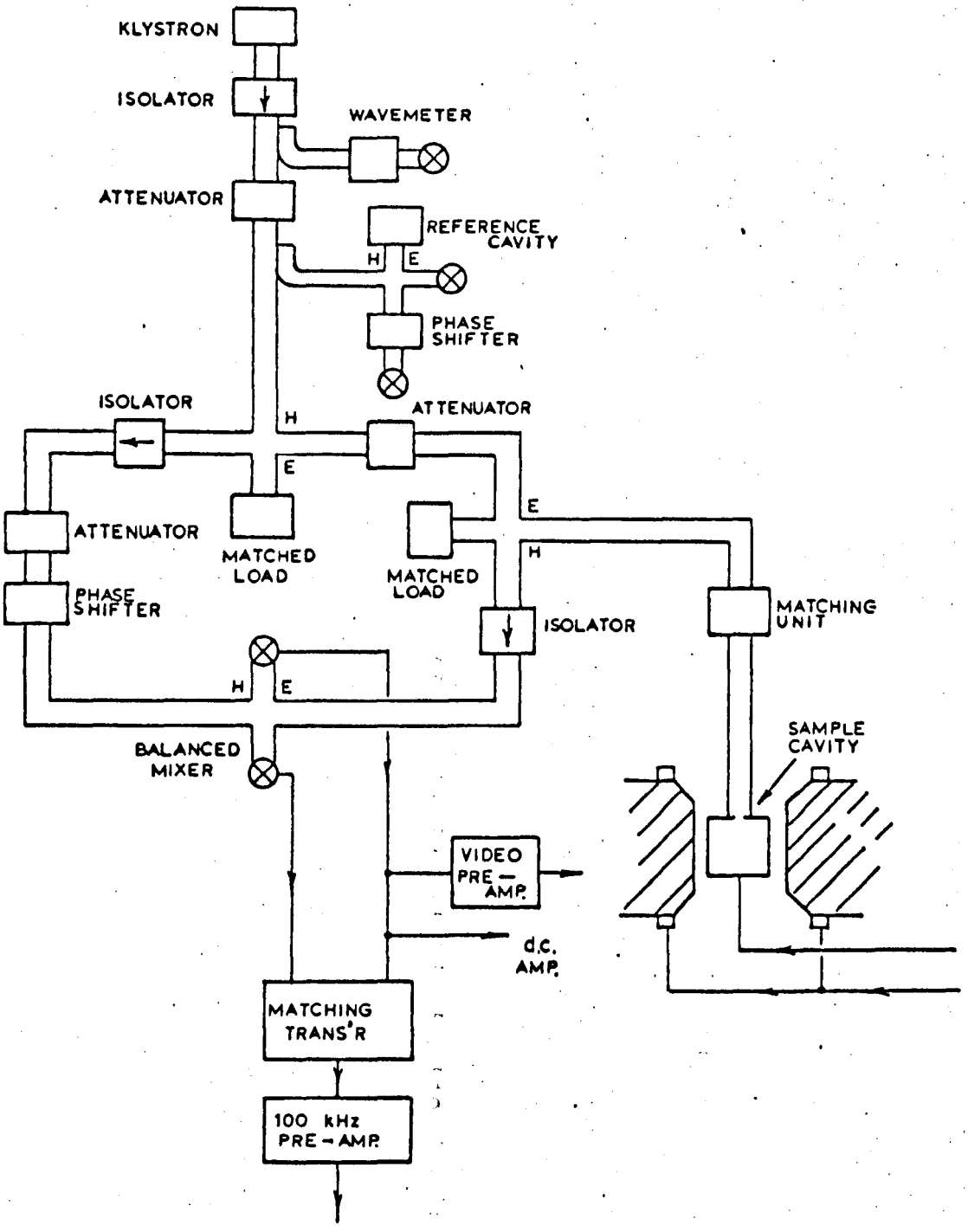

FIG. 5.2

The Spectrometer with Modification to Balanced Mixer Detection.

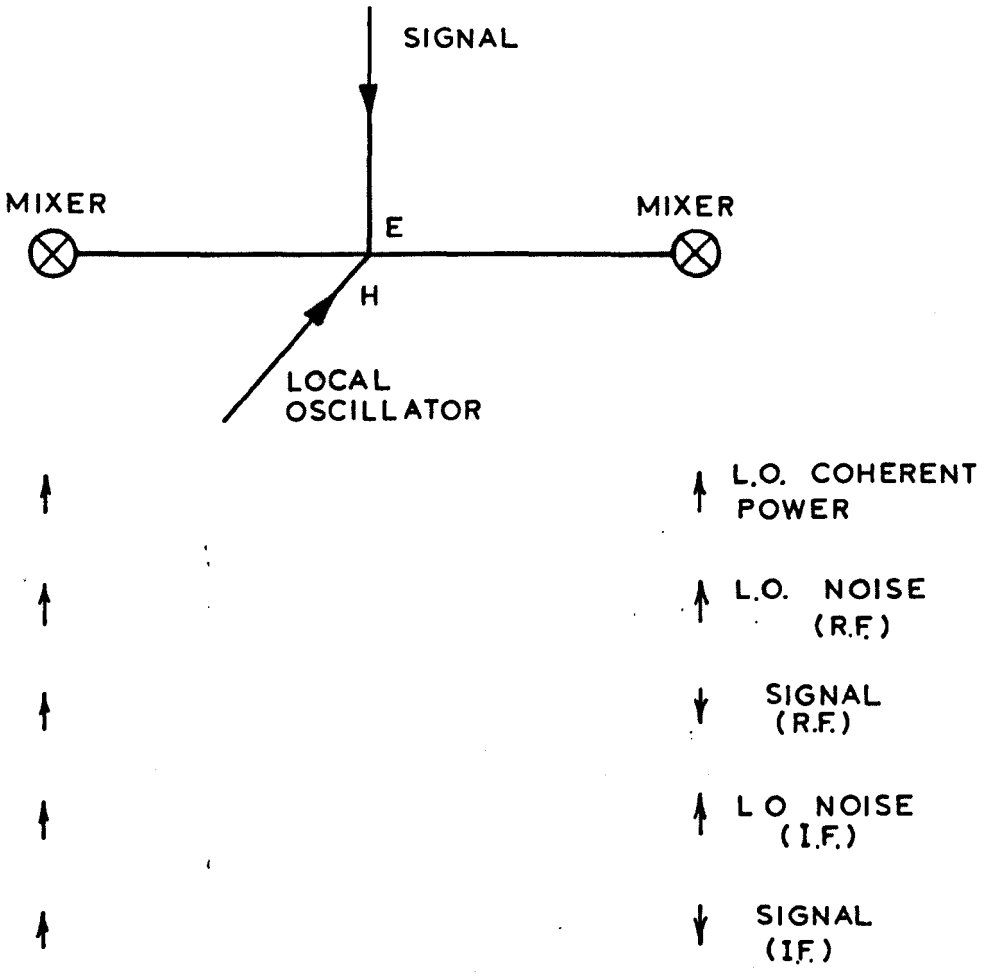

FIG. 5.3

The Magic Tee Balanced Mixer.

experimental advantage accruing, being that modulation coils external to the cavity could be used. As pointed out in Section 4.7 an increase in detector flicker noise would result, as would the power in the klystron sidebands, so it was decided to use a balanced mixer detection system[6,10,11]. Wilmshurst[12] has demonstrated the advantages of the balanced mixer compared with the unbalanced one with decreasing modulation frequency. A further advantage offered by this system is the ability to maintain spectrometer sensitivity with samples which saturate at low powers.

The modifications to the spectrometer are shown in Fig. 5.2. A magic tee was used for the balanced mixer, its configuration, and the phases of the signal and local oscillator (L.O.) waves are shown in Fig. 5.3. Note that if the mixer outputs are combined in a push-pull fashion, ideally, cancellation of the L.O. a.m. noise will result. The input transformer to the 100 kHz pre-amplifier was removed, and three similar coils used to construct the matching transformer, care being taken to ensure that the d.c. and high frequency impedances were identical, taking into account the derivation of the video and d.c. outputs across one of the mixers. With the mixer crystals available (again SLM8) a pair were found which when used individually gave signals within 1% for the same noise.

If the amount of L.O. noise suppression S, is defined as the ratio of the effective conversion loss for the signal to that for the L.O. noise, then[13]

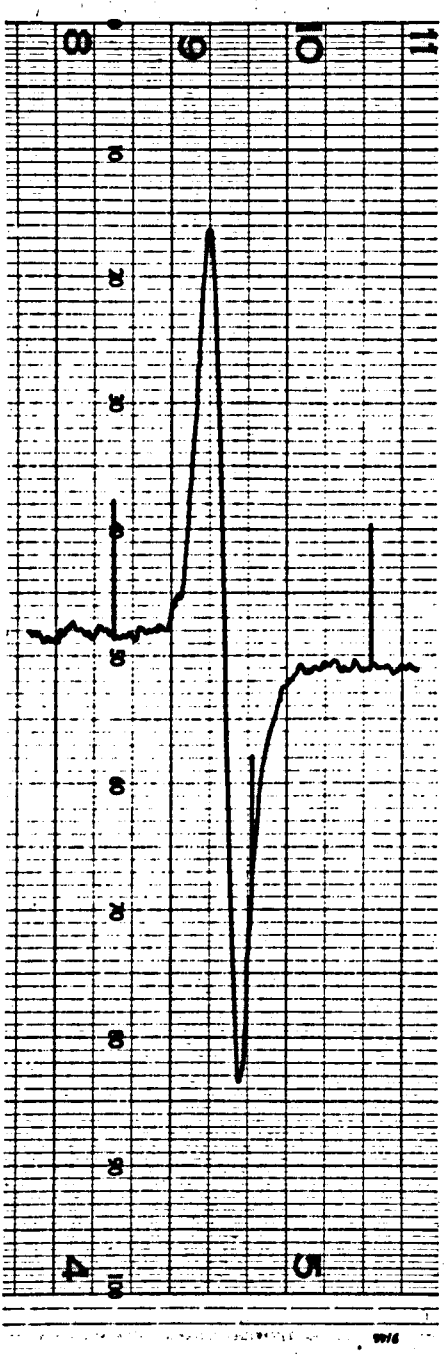

FIG. 5.4

The Spectrum of $1{\cdot}3.\ 10^{13}$ Conduction Electron Spins in Phosphorus-Doped Silicon.

$$S = \left[\frac{\left(\frac{L_1}{L_2}\right)^{\frac{1}{2}} + 1}{\left(\frac{L_1}{L_2}\right)^{\frac{1}{2}} - 1} \right]^2$$

where L_1 and L_2 are the conversion losses of the two mixers. Thus if the difference between the losses L_1 and L_2 is less than 3 dB, more than 15 dB of noise suppression will be obtained. Shigemoto[14] suggests 20 dB suppression to be typical, resulting in a noise figure degradation of 0.2 dB from L.O. noise for a 17 dB mixer noise figure. He further emphasizes that f.m. noise will not be suppressed.

The signal obtained from $1 \cdot 3 \cdot 10^{13}$ conduction electron spins in phosphorus-doped silicon (as prepared in a standard sample form by Gere[15]) is shown in Fig. 5.4. This spectrum was taken at 77°K with a bandwidth of $\frac{1}{1.5}$ Hz, the field markers being spaced by 16 gauss. A sensitivity of $6 \cdot 1 \cdot 10^{10}$ spins gauss^{-1} is calculated. Again converting to the conditions of Section 4.4, leads to a sensitivity of

$$4 \cdot 0 \cdot 10^{11} \text{ spins gauss}^{-1}. \qquad \ldots\ldots\ldots\ldots\ldots 5.6$$

The effective klystron noise figure in this configuration is governed by leakage of the balanced bridge containing the cavity. Using a figure of 30 dB, and calculating in a similar fashion to previous, yields

$$F_k = 3 \text{ dB}. \qquad \ldots\ldots\ldots\ldots\ldots 5.7$$

The comparative figure for the sensitivity in this case is

$$7 \cdot 5 \cdot 10^{9} \text{ spins gauss}^{-1}. \qquad \ldots\ldots\ldots\ldots\ldots 5.8$$

The conclusion is reached therefore that at a modulation frequency of 100 KHz little was gained by using a balanced mixer, apart from easing the tuning procedure to detect either absorption or dispersion. It was felt that in the time interval from measuring the sensitivity of the unbalanced system, there had been a degradation of the klystron in terms of power and noise, and thus some noise suppression was achieved. Had time permitted the addition of low frequency modulation, it is felt that the advantages of the balanced mixer system would have been more clearly demonstrated.

5.3 The Magnetic Field and its Measurement

The magnetic field was produced by a Newport Instruments Ltd., Type D, 8 inch, rotatable, water-cooled electromagnet. To achieve the necessary field, allowing a pole-gap of 5.4 cm for the metal cryostat tail, coned pole pieces of semi-angle 60° were used.

The Type C magnet power supply, by the same manufacturers, used a 3-phase rotary generator to isolate it from mains fluctuations, and with further current stabilization achieved ± 1 in 10^5 over a period of $\frac{1}{2}$ hour. This was equivalent to a field homogeneity of the order of 0.2 gauss over a restricted volume. In response to a linear voltage sweep from the spectrometer to the power supply, a linear current sweep could be applied to the magnet, although magnet saturation prevented the field sweep being linear with time, as is evident in Fig. 5.4.

The magnetic field may be measured in many ways; two of these methods will be briefly discussed and a third more thoroughly, since this was the method used by the author.

Calibrated samples or "g markers" are widely used, the most common being D.P.P.H.[16]. In its polycrystalline form it has a g value of 2.0036, and a linewidth of approximately 2.8 gauss. The "g marker" is placed in close proximity to the sample under study, or at least in the same magnetic field. Copper sulphate, lithium hydride, sugar[17], phosphorus-doped silicon[15], and a powder of manganese-doped strontium oxide[18], have also been proposed as "g markers" and as samples able to be prepared to give a known number of spins. The last example will additionally provide 6 lines of 1.6 gauss width spread over a field range of 420 gauss.

The use of Hall plates has not been popular as considerable precautions are necessary to maintain temperature stability. A system applicable to E.P.R. has been described[19], having an accuracy of approximately 10^{-3}, and one with an order of magnitude greater accuracy exhibited[20]. Manufacturers have incorporated them into their magnet control systems[21], and they have been used to measure the magnetic field in a volume containing liquid helium[22,23].

The earliest nuclear resonance circuits for magnetic field measurement of Rollin[24], and Pound and Knight[25], were superceded by that of Robinson[26]. This circuit reigned supreme for a considerable time, but has been replaced by transistorised oscillators (e.g., 27-31). The signal to noise ratio of these oscillators has been improved by frequency modulating within the linewidth, and using phase sensitive detection[32,33].

At room temperature the resonance of protons is normally observed. They may be incorporated within water (with added $Mn(NO_3)_2$ to reduce the spin relaxation time), rubber[34], or a composite sample[35] also

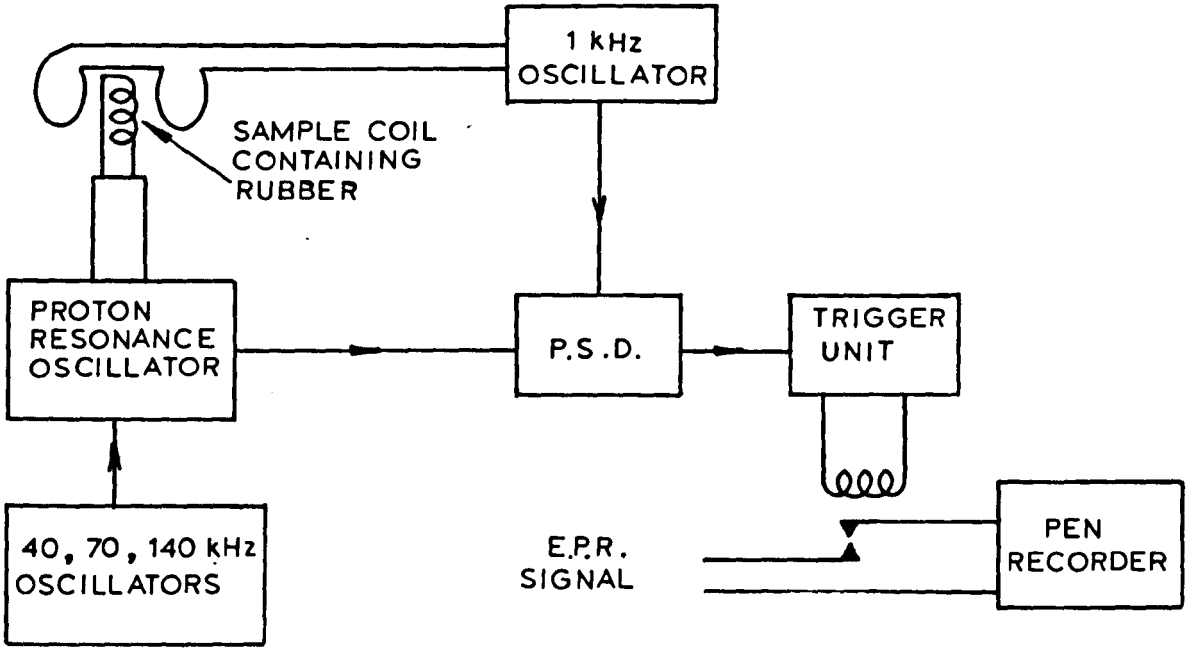

FIG. 5.5

The Field Marker System.

containing Li^7, which having a lower g factor extends the field range of the oscillator. By using Cs^{133} (36), F^{19} and Na^{23} (37), the technique can also be used at liquid helium temperatures. For protons the relationship between field and frequency is given by

$$H = 234.87 \times f \text{ (MHz) gauss,}$$

hence, as pointed out by Muha(38), if the digital counter used to monitor the frequency is gated at 2.3487 sec rather than 1 sec, a direct readout of the field may be obtained(39).

Many systems have been proposed able to provide field markers, some relying on the manual selection of the quarts crystals controlling the oscillator frequency(40), others achieving this frequency-stepping automatically(41). Bukin et al(42) have described a system which automatically tracks the magnetic field and derives markers from the beats between the oscillator and a heterodyne wavemeter. The author used the system described by Lancaster and Smallman(43), and it is shown in block diagram form in Fig. 5.5.

The proton resonance oscillator(26) was frequency modulated at one of three frequencies, nominally 40, 70 or 140 KHz, and the sidebands used to provide markers spaced by 9, 16 and 33 gauss respectively. A varactor diode (100 CS2, International Rectifiers Ltd.) was inserted into the tank circuit, providing means for varying the frequency of the oscillator, and for frequency modulation, through the application of d.c. bias and an alternating voltage, respectively. A second varactor diode in the parallel-tuned radio frequency amplifier stage has the same d.c. bias supply as that in the tank circuit, so simplifying "tracking". By modulating the field about the sample coil at 1 KHz and using phase

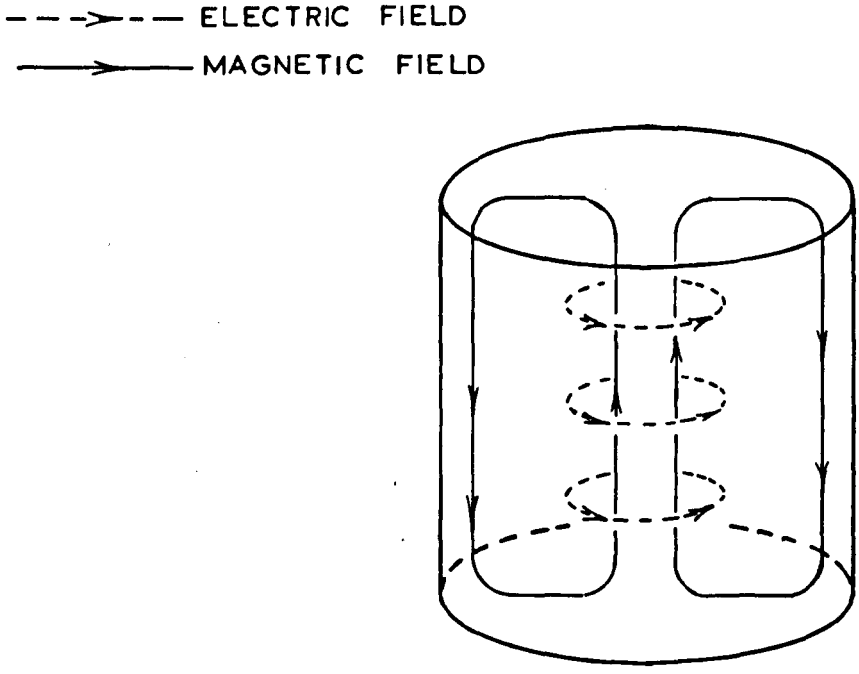

FIG. 5.6

TE_{011} Cylindrical Cavity Mode.

sensitive detection, signals were derived able to operate a relay which interrupted the signal to the pen recorder from the E.P.R. spectrometer. A Marconi Instruments Ltd. Counter/Frequency meter Type TF 1417/2 was used to determine the modulation frequency, which, with an Extension Unit Type TF 1434/2 could also be used to determine the resonance frequency.

Because of the reduced field homogeneity in the region of the sample due to the cryostats presence in the field, a small coil was used, tightly coupled to a rubber sample. A sufficiently strong signal was obtained to have several sidebands able to trigger the relay reliably, the spacing of the marker pulses being reproducible to $\pm$ 0.2 gauss. Had this not been possible, Breuer[44] has suggested the use of quadrupole compensating coils able to cancel field gradients up to 800 gauss cm^{-1}.

5.4 The Microwave Cavity

A cylindrical cavity resonating in the TE_{011} mode was chosen, the electric and magnetic field configurations being indicated in Fig. 5.6.

As the spectrometer operated at a high frequency field modulation of 100 KHz, at which the skin depth in metals is typically 250 μm (0.010"), modulation must either be introduced directly into the cavity, or means found to enable its penetration from outside. A metallic layer thinner than the above figure can be used[45], the walls can be wire-wound[46], or a dielectric rod used to space two metal end plates[47]. Initial efforts to construct a cavity in Araldite, silvering the surface chemically[45] were unsuccessful as a sufficiently high Q factor could not be obtained. The cavity finally developed is shown in Fig. 5.7.

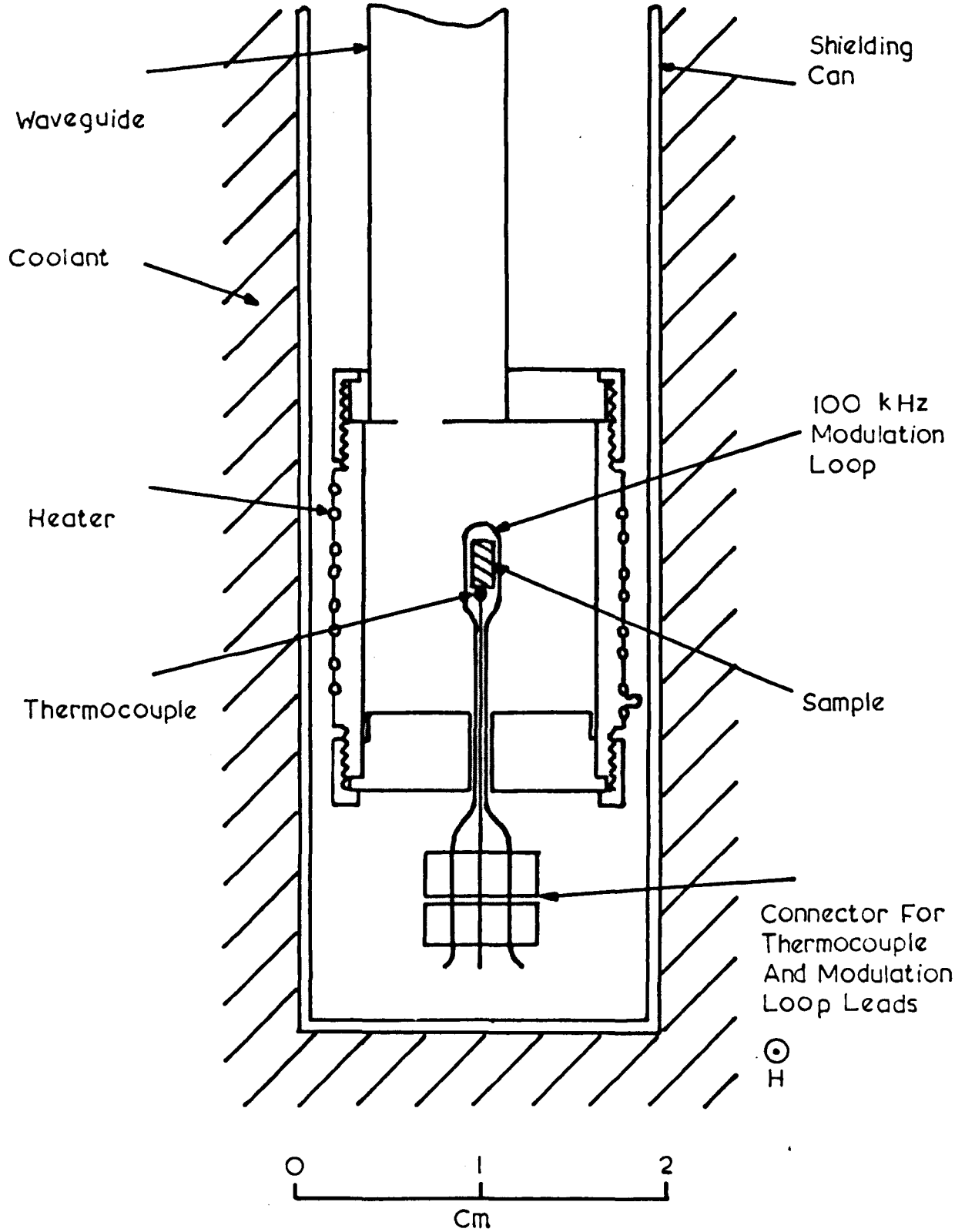

FIG. 5.7

The TE_{011} Experimental Cavity.

It was constructed in brass, and thermally isolated from room temperature by using copper-nickel waveguide. The diameter of the iris to give best coupling over the range of temperatures used was determined by trial-and-error.

Many systems allowing the coupling to be varied have been suggested[48]. Most have been designed for X band, so easing their construction, or they are not suitable for variable temperatures. The use of a beyond cut-off section of waveguide immediately before the cavity which is brought to above cut-off by the insertion of a dielectric plunger has been described by Gordon[49]. Experience showed that a P.T.F.E. plunger worked well at room temperature, but the considerable differential contraction of the P.T.F.E. and the electroformed copper waveguide when in a coolant, caused the coupling to be modulated by microphonics.

High frequency field modulation was achieved by incorporating a single loop of 30 S.W.G. copper wire within the cavity. Care was taken to remove all traces of enamel from the wire, since signals have been reported which can be traced to the possible low temperature charring of it[50]. Considerable care, and patience, was necessary to align this loop parallel to the cavity axis so preventing loss in Q due to the wire penetrating regions of higher electric field. The amplitude of the modulating field was determined by observing the signal amplitude with increasing field modulation, as indicated in Fig. 5.8. Smith[51] has calculated that for a Lorentzian line (as exhibited by the sample used) the peak signal from the phase sensitive detector occurs when $\frac{h_m}{\Delta H_{pp}} = 1.73$, where h_m is the field modulation amplitude, and ΔH_{pp} is the true linewidth between absorption derivative extrema. By determining ΔH_{pp} at low values of h_m, h_m may be calculated at the peak signal

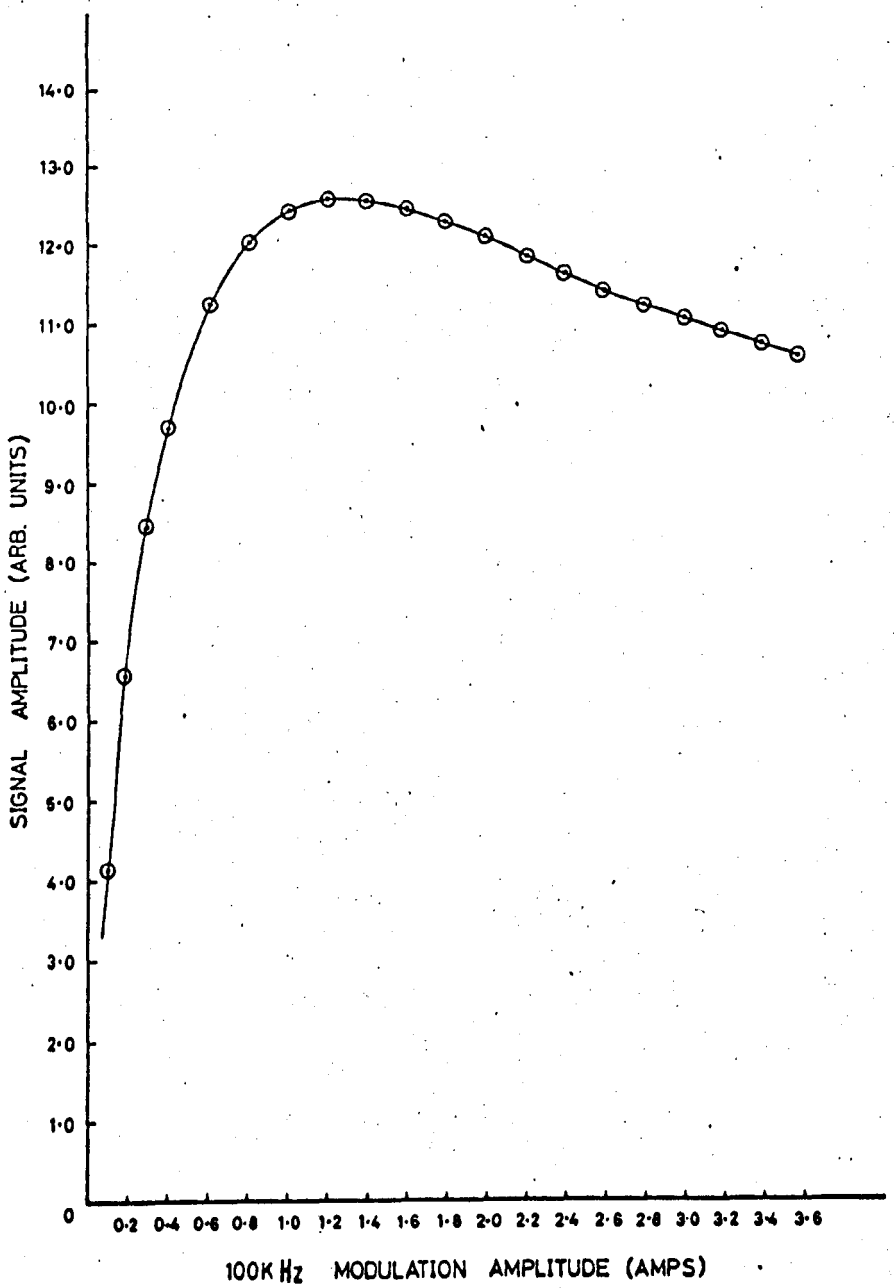

FIG. 5.8

Signal Amplitude as a Function of 100 k Hz Modulation Amplitude.

amplitude to be 4.8 gauss, which implies a maximum h_m of about 13 gauss.

The position of the temperature sensing element, a thermocouple, and the heater are indicated in Fig. 5.7. Further discussion of these elements is to be found in the next section. Reduced thermal contact between the cavity and coolant was achieved by enclosing it in an aluminium can, open at its upper end to the coolant gas.

With increasing temperature there is a corresponding decrease in the resistivity of the silicon, e.g., for a sample with $N_D \sim 2.10^{16}$ cm^{-3}, the resistivity decreases from 10^8 to 10^1 ohm cm in the temperature interval from 20 to 40°K. This was apparent in the decreasing cavity Q, since the sample, although small, penetrated the region of finite electric field. The overall or loaded Q, Q_L, for the cavity may be calculated by summing the reciprocals of the Q factors due to ohmic losses in the walls Q_u, losses arising from power leaking out of the cavity Q_r, and dielectric losses in the sample Q_s, i.e.,

$$\frac{1}{Q_L} = \frac{1}{Q_u} + \frac{1}{Q_r} + \frac{1}{Q_s}. \qquad \ldots\ldots\ldots\ldots\ldots 5.9$$

Over the temperature range of interest, Q_u and Q_r may be considered constant, such that a Q_L of 5000 would be exhibited without dielectric losses.

Now

$$Q_e = \omega_o \rho \mu \frac{\int_{V_c} |H|^2 \, dV_c}{\int_{V_s} |\delta|^2 \, dV_s}, \qquad \ldots\ldots\ldots\ldots\ldots 5.10$$

where H is the microwave magnetic field within the cavity, and δ is the

microwave electric field within the sample. If Equation 5.10 is evaluated for the cavity used[52] (see Section 4.4), ignoring the field perturbations of the cavity by the sample, and further assuming a cylindrical sample 3 mm long and 1 mm diameter situated centrally along the cavity axis, then

$$Q_\theta = 65\rho, \qquad \ldots\ldots\ldots\ldots 5.11$$

where ρ is the sample resistivity in ohm cm. Thus between 20 and 40°K Q_θ changes from approximately $6{\cdot}5.10^9$ to 650. This decreasing Q factor will become the dominating one at high temperatures, resulting in a decreased sensitivity, and hence increasing experimental errors.

5.5 Low Temperature Techniques

The sample temperature was sensed by a copper-constantan thermocouple situated within the cavity and in intimate contact with the sample. The e.m.f. generated, with respect to a reference junction in crushed melting ice E, was measured with a "CROPICO" potentiometer Type P3 (Croydon Precision Instrument Co.). Regular calibration at liquid helium, hydrogen and nitrogen temperatures, enabled the constants a, b, c in the expression[53]

$$E = a + bT + cT^2, \qquad \ldots\ldots\ldots\ldots 5.12$$

to be evaluated. The thermoelectric power increased from 6 to 10 $\mu V\ {}^\circ K^{-1}$ in the temperature interval 20 to 40°K.

Using three thermocouples rotated in position it was shown that an excess temperature of 1 to 2°K existed between the top and bottom of the cavity and its centre, i.e., the sample position.

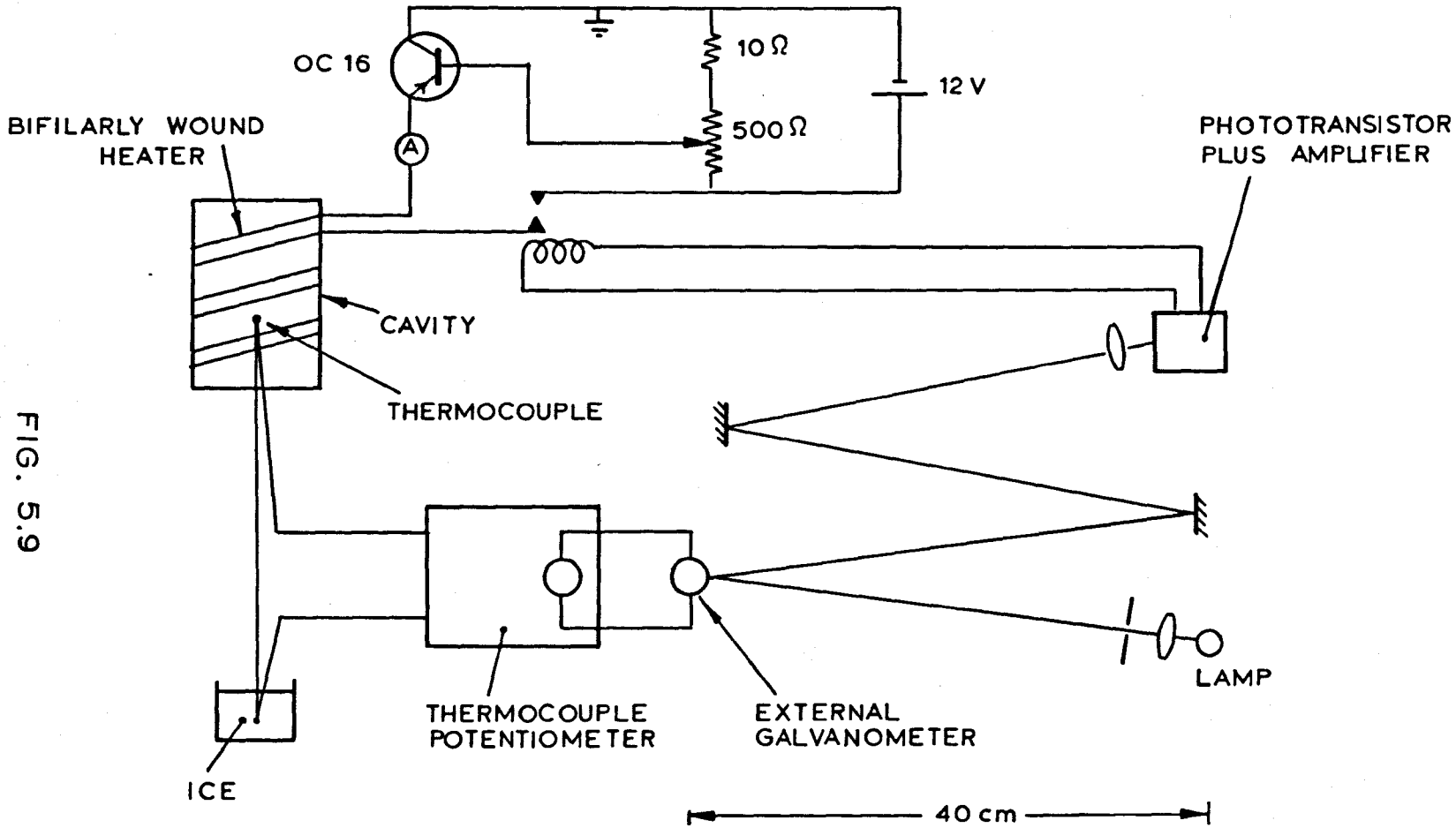

FIG. 5.9 Temperature Control System.

A silk-covered constantan heater was bifilarly wound upon the cavity, the current through it being controlled by the circuit indicated in Fig. 5.9. Many temperature control systems have been suggested[54-56], but that used is also indicated in the latter Figure. A mirror galvanometer was connected externally, in parallel, with the galvanometer of the thermocouple potentiometer and a beam of light was reflected from it onto a phototransistor forming part of a relay-drive circuit. This switched the current to the heater on and off. A temperature stability of $\pm$ 0.25°K was observed.

The cavity, with its surrounding can, was immersed in approximately 1½ litres of liquid coolant in the inner chamber of a tailed metal cryostat, manufactured by Oxford Cryogenics Ltd. Three carbon resistors attached to the outside of the can monitored the level of the coolant. In turn, these resistors formed one arm of a bridge, which after balancing with the resistor immersed in coolant, showed an unbalance upon its exit.

REFERENCES

1. H. M. Assenheim, Lab. Pract. 13 (1964) 1079.
2. W. G. Tuller, W. C. Galloway and F. P. Zaffarano, Proc. I.R.E. 36 (1948) 794.
3. N. A. Schuster, Rev. Sci. Instrum. 22 (1951) 254.
4. B. G. Bosch and W. A. Gambling, J. Brit. I.R.E. (1962) 389.
5. S. L. Johnson, B. H. Smith and D. A. Calder, Proc. I.E.E.E. 54 (1966) 258.
6. G. Feher, Bell System Tech. J. 36 (1957) 449.
7. T. Oxley, Mullard Tech. Commun. No. 78 (1965) 239.
8. H. A. Buckmaster and J. C. Dering, Proc. 14th Colloque AMPERE, Ljubljana (North Holland) 1966.
9. M. Weger, Bell System Tech. J. 39 (1960) 1013.
10. J. C. M. Henning, Rev. Sci. Instrum. 32 (1961) 35.
11. H. A. Buckmaster and J. C. Dering, Canad. J. Phys. 43 (1965) 1088.
12. T. H. Wilmshurst, J. Sci. Instrum. 1 (1968) 353.
13. R. V. Pound, Microwave Mixers (McGraw-Hill) 1948.
14. J. Shigemoto, Microwave J. 10 (1967) 77.
15. E. A. Gere, A Calibration Marker for Paramagnetic Resonance, 1961, Unpublished.
16. A. N. Holden, C. Kittel, F. R. Merritt and W. A. Yager, Phys. Rev. 77 (1950) 147.
17. R. H. Hoskins and R. C. Pastor, J. Appl. Phys. 31 (1960) 1506.
18. J. Rosenthal and L. Yarmus, Rev. Sci. Instrum. 37 (1966) 381.
19. H. Nagatomo and H. Iwasaki, J. Radio Res. Lab. (Tokyo) 12 (1965) 39.
20. Institute of Physics and Physical Society, Exhibition, 1969.
21. Fieldial, Varian Associates.

22. G. N. Harding, W. H. Mitchell and E. H. Putley, Solid-State Electronics 9 (1966) 465.

23. I. Hlasnik, F. Chovanec and M. Polak, Cryogenics 6 (1966) 89.

24. B. V. Rollin, Nature 158 (1946) 669.

25. R. V. Pound and W. D. Knight, Rev. Sci. Instrum. 21 (1950) 219.

26. F. N. H. Robinson, J. Sci. Instrum. 36 (1959) 481.

27. D. Donnally and T. M. Sanders Jr., Rev. Sci. Instrum. 31 (1960) 977.

28. W. L. Pierce and J. C. Hicks, Rev. Sci. Instrum. 36 (1965) 202.

29. F. N. H. Robinson, J. Sci. Instrum. 2 (1965) 653.

30. Y. Yang and Y. Chen, Rev. Sci. Instrum. 37 (1966) 1274.

31. E. A. Faulkner and A. Holman, J. Sci. Instrum. 44 (1967) 391.

32. N. C. Olsen, Nuclear Instrum. Methods 31 (1964) 237.

33. D. T. Edmonds, J. Sci. Instrum. 43 (1966) 63.

34. S. J. Rogers, J. Sci. Instrum. 38 (1961) 308.

35. L. S. Lerner, Rev. Sci. Instrum. 37 (1966) 680.

36. L. W. Rupp, Jr., Rev. Sci. Instrum. 37 (1966) 1039.

37. D. A. Hill and C. Hwang, J. Sci. Instrum. 43 (1966) 581.

38. G. M. Muha, Rev. Sci. Instrum. 36 (1965) 551.

39. Model 5330 A Programmable Preset Time-Base Counter, Hewlett-Packard Ltd. 1969.

40. J. C. M. Henning, J. Chem. Phys. 44 (1966) 2139.

41. A. Horsfield, J. R. Morton and D. G. Moss, J. Sci. Instrum. 38 (1961) 322.

42. I. I. Bukin, V. I. Kosyakov, V. L. Maksimov and E. V. Nedovodiev, Instrum. Expt. Tech. 2 (1966) 361.

43. G. Lancaster and A. G. Smallman, J. Sci. Instrum. 42 (1965) 341.

44. H. Breuer, Rev. Sci. Instrum. 36 (1965) 1666.

45. I. L. Firth, J. Sci. Instrum. 39 (1962) 131.

46. A. J. Estin, Rev. Sci. Instrum. 33 (1962) 369.

47. F. J. Rosenbaum, Rev. Sci. Instrum. 35 (1964) 1550.

48. R. S. Alger, Electron Paramagnetic Resonance (Wiley) 1968.

49. J. P. Gordon, Rev. Sci. Instrum. 32 (1961) 658.

50. L. Kent and J. R. Mallard, Nature 204 (1964) 396.

51. G. W. Smith, J. Appl. Phys. 35 (1964) 1217.

52. C. P. Poole, Jr., Electron Spin Resonance (Wiley) 1967 .

53. R. B. Scott, Temperature (Reinhold) 1941.

54. G. K. White, Experimental Techniques in Low Temperature Physics (O.U.P.) 1959.

55. A. C. Rose-Innes, Low Temperature Techniques (E.U.P.) 1964.

56. Harwell Temperature Controller, Oxford Instrument Co. Ltd., 1969.

Sample	N_D (cm^{-3})	Donor Impurity	N_A^* (cm^{-3})	Acceptor Impurity	Compensation Ratio $K = N_A/N_D$
A	$3.1.10^{15}$	P	$5.0.10^{14}$	In	0.16
B	$4.2.10^{15}$	P			
C	$2.3.10^{16}$	P	$6.2.10^{15}$	In	0.27
D	$5.2.10^{17}$	P			
E	$1.2.10^{17}$ to $1.0.10^{18}$	As			
F	5.10^{15} to 8.10^{15}	Sb			
G	$\sim 10^{14}$	Bi			

TABLE 6.1

The Characteristics of the Silicon Samples

(*Where no value for N_A is quoted the samples are nominally uncompensated.).

CHAPTER 6

RESULTS AND DISCUSSION ON THE TEMPERATURE DEPENDENCE OF THE E.P.R. SPECTRA OF DONORS IN SILICON

In Chapter 3 the various relaxation processes which have been observed in silicon as a function of temperature and donor concentration were outlined. It is apparent that samples having a phosphorus donor concentration $\lesssim 2.10^{18}$ cm^{-3} exhibit a marked spectral change in the interval from 20 to 77°K. At 20°K the spectrum is characteristic of bound donor electrons, while at 77°K conduction electron resonance predominates.

In this chapter are presented measurements made in the interval from 20 to 50°K where the hyperfine splitting is observed to decrease with increasing temperature, while simultaneously the linewidth increases and the lineshape changes. Subsequently the hyperfine lines are replaced by a wide single line which proceeds to narrow. The temperature dependence of the magnitude of the hyperfine interaction is described in terms of motional averaging, due to phonon induced transitions of the donor electron between the $1s(A_1)$ ground state and the triplet $1s(T_2)$ state. Some doubt remains as to whether this mechanism also explains the linewidth variation. An alternative mechanism for linebroadening by the exchange scattering of bound and conduction electrons is examined, along with the applicability of this process to the narrowing single line.

The characteristics of all the silicon samples used in the work reported in this thesis are given in Table 6.1, and by way of comparison

Donor	$\frac{a_D}{h}$ (MHz)	$\delta H_{A_1} = \frac{a_D}{g\beta}$ (Gauss)	$\Delta H_{\frac{1}{2}}$ (Gauss)	Nuclear Spin I_D	Percentage Abundance
Sb^{121}	186.8	66.8	2.3	5/2	57
Sb^{123}	101.5	36.3	2.3	7/2	43
P^{31}	117.5	42.0	2.5	1/2	100
As^{75}	198.4	70.9	2.9	3/2	100
Bi^{209}	1475.5	527.1	9.0	9/2	100

TABLE 6.2

Hyperfine Interactions and Linewidths of Different Donors in Silicon.

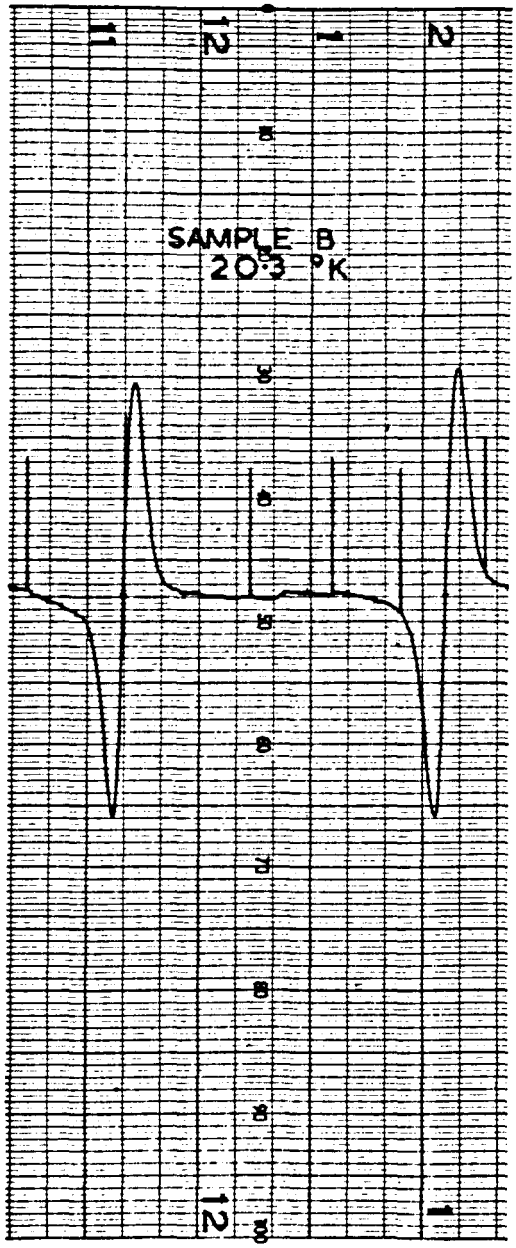

FIG. 6·1

E.P.R. Spectrum for Sample B :-
Phosphorus-Doped Silicon, $N_D = 4{\cdot}2.10^{15}\ cm^{-3}$.

the results of Feher[1] at 1.25°K are summarized in Table 6.2.

6.1 The E.P.R. Spectrum of Phosphorus-Doped Silicon in the Temperature Interval from 20 to 50°K

The results presented show the spectral changes observed in the temperature region from 20 to 50°K for a range of donor concentrations. All the samples evidenced two resolved hyperfine lines at 20°K. Since the degree of compensation could be relevant to the effects observed, this parameter was also varied.

Initial efforts to work with powdered samples, so preventing cavity damping as indicated in Section 5.4, were unsuccessful due to the presence of a surface state line which could not be removed by etching. This line occurred at $g \sim 2.006$ (see Section 3.6) and had a peak to peak width ~ 12 gauss. Unfortunately, it very slightly interfered with the low field hyperfine line and was still present, but much reduced, in some single crystal samples. Thus single crystal samples were used throughout, and quoted linewidths are of the high field line to eliminate any possible error due to this cause. The samples were mounted in good thermal contact with the thermocouple within the cavity, and measurements continued up to a temperature at which the signal became lost in the noise (see Section 5.4).

The observed spectra of phosphorus-doped silicon may be divided into two groups:

(i) $N_D < 10^{16}$ cm^{-3}, Samples A and B: The spectrum is of isolated, bound donor electrons, and typified by Fig. 6.1. In this and subsequent photographs of spectra, the derivative of absorption is shown as a function of magnetic field, the

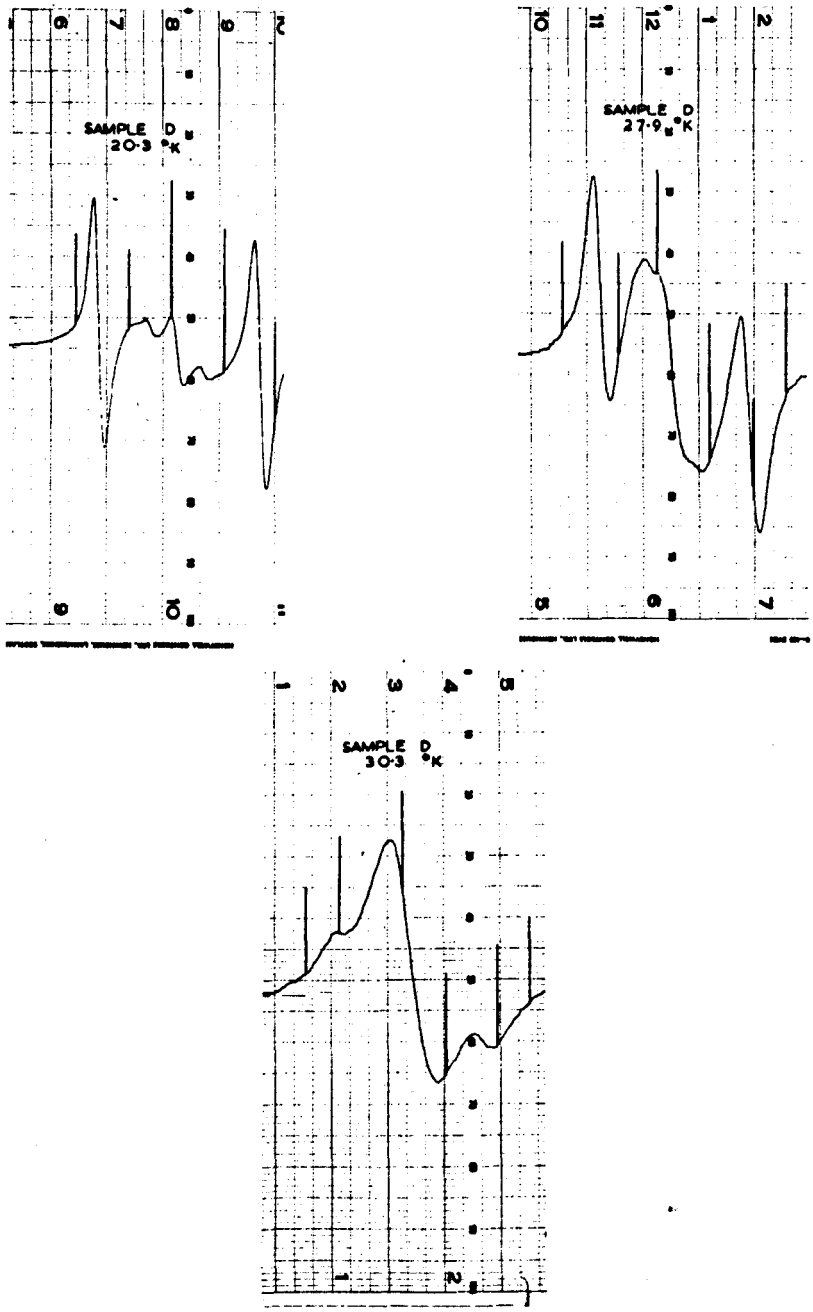

FIG. 6.2

The Variation with Temperature of the E.P.R. Spectrum of Sample D :- Phosphorus-Doped Silicon, $N_D = 5{\cdot}2 \cdot 10^{17}\ cm^{-3}$.

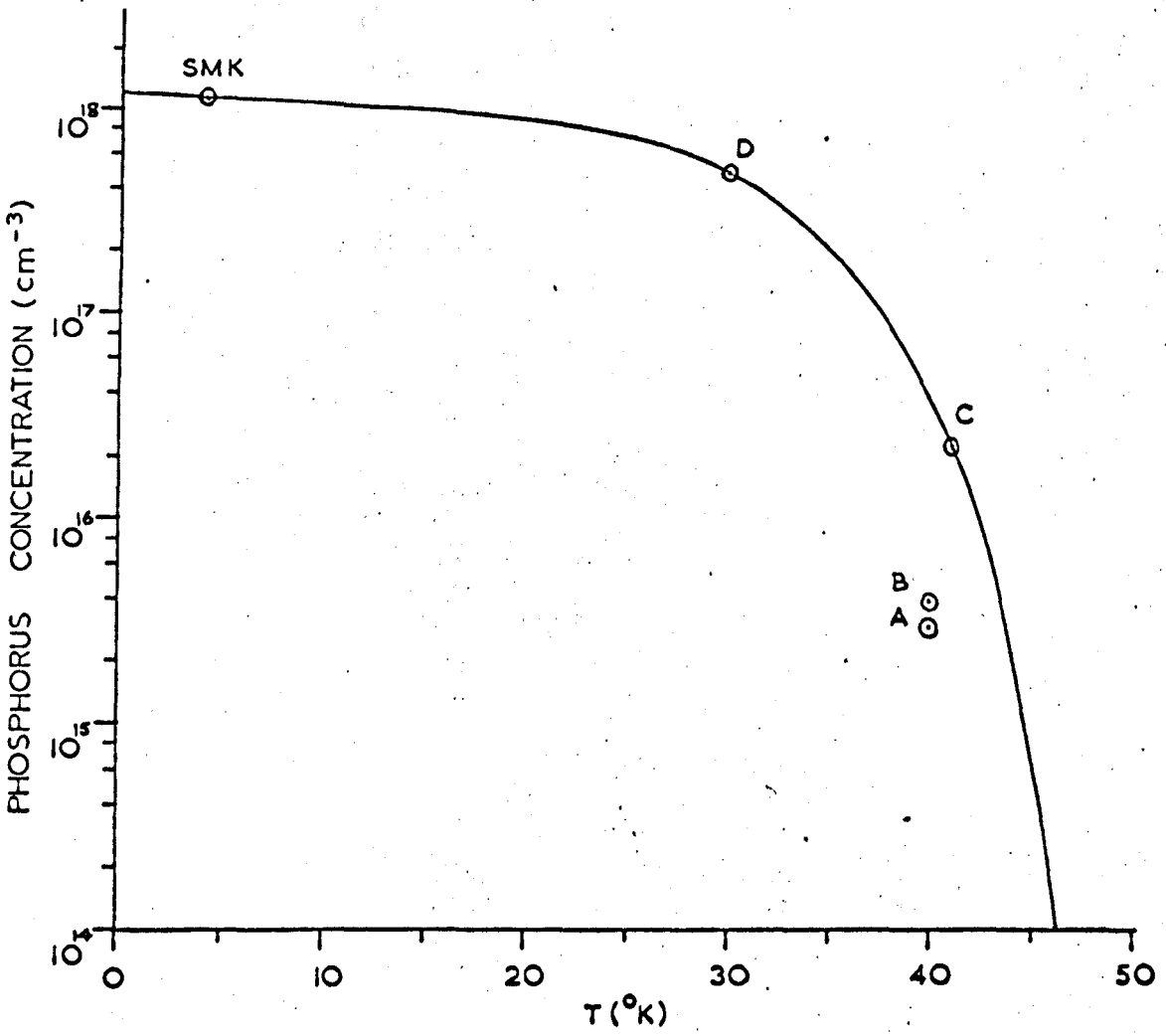

FIG. 6.3

This Figure Shows the Region (below the curve) in which Resolved Hyperfine Structure can be Observed in Phosphorus Doped Silicon.
SMK: W. Sasaki, S. Maekawa, J. Kinoshita[2]

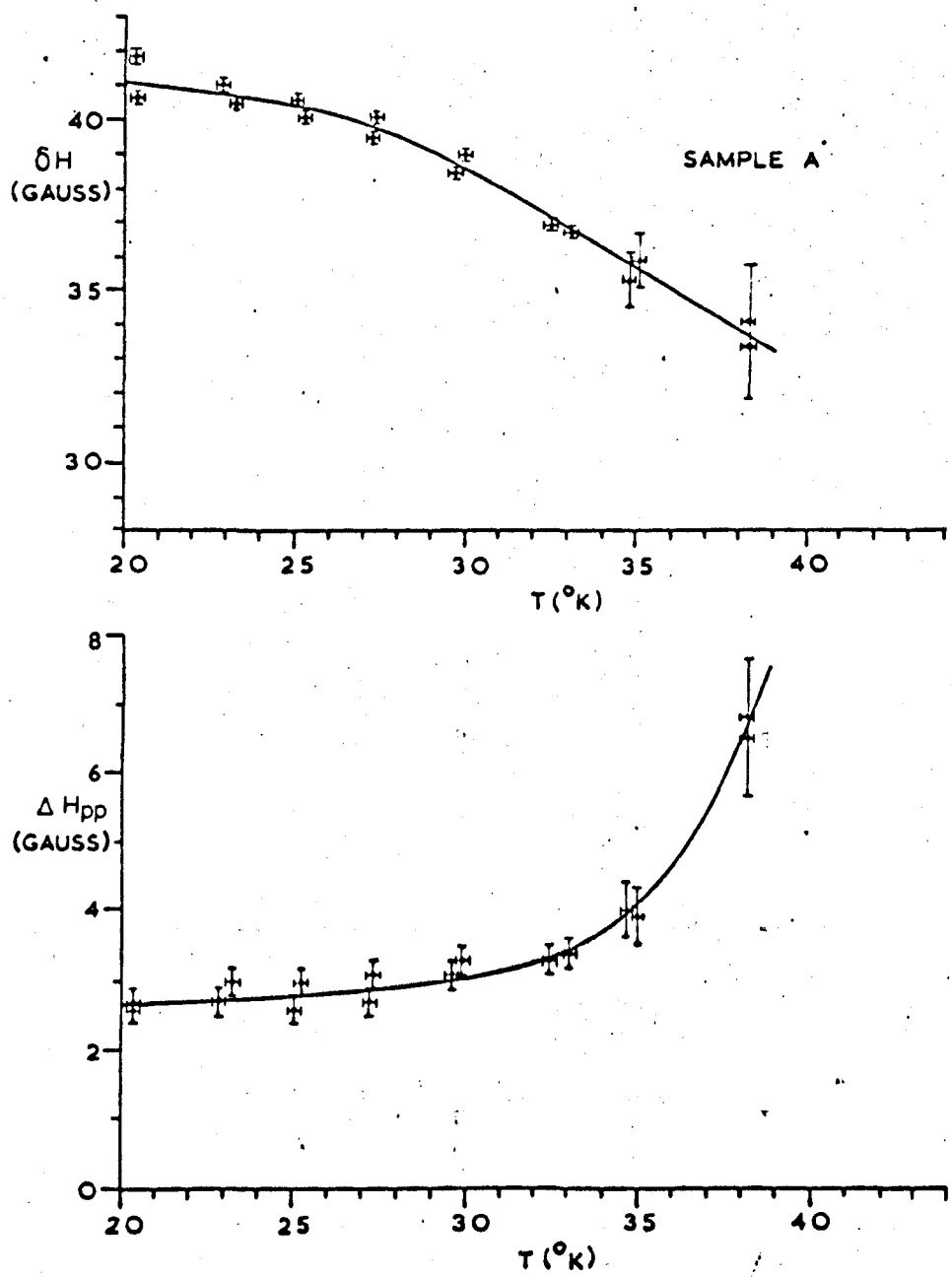

FIG. 6.4

Measurements of Hyperfine Interaction δH, and Linewidth ΔHpp for Sample A.

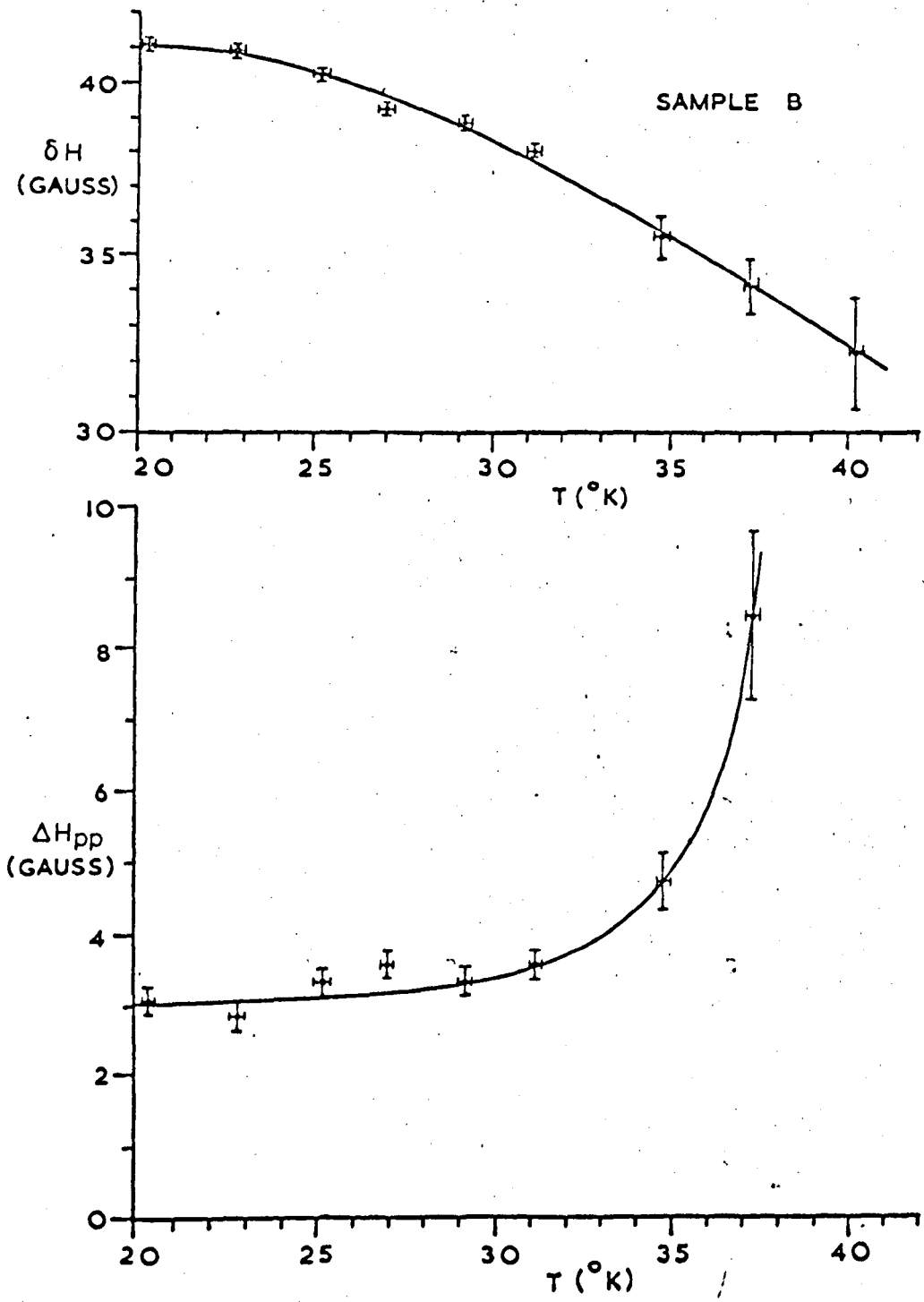

FIG. 6.5

Measurements of Hyperfine Interaction δH, and Linewidth ΔH_{pp}, for Sample B.

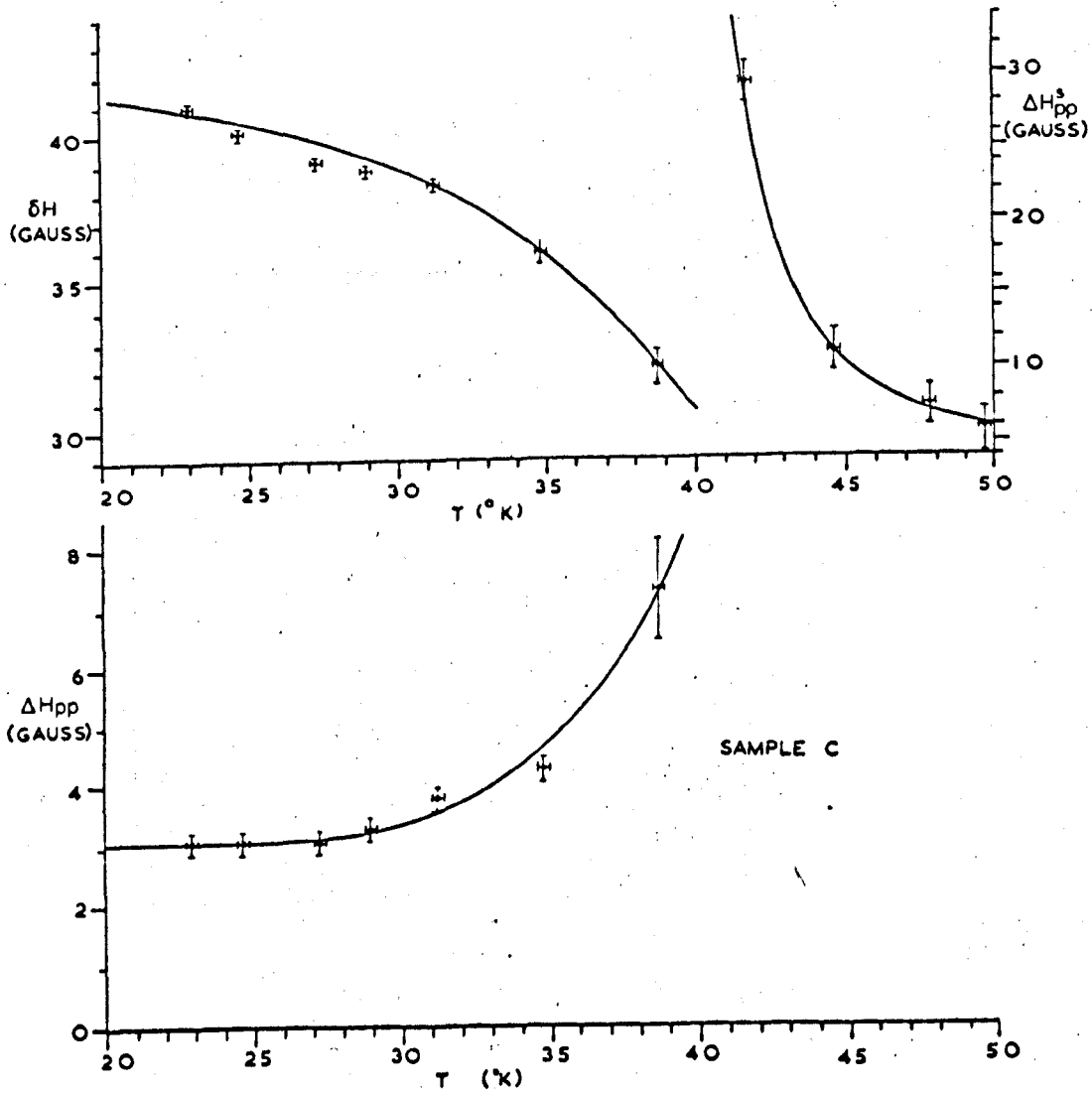

FIG. 6.6

Measurements of Hyperfine Interaction δH. Linewidth ΔH_{pp} and Width of Single Line ΔH^{s}_{pp}, for Sample C.

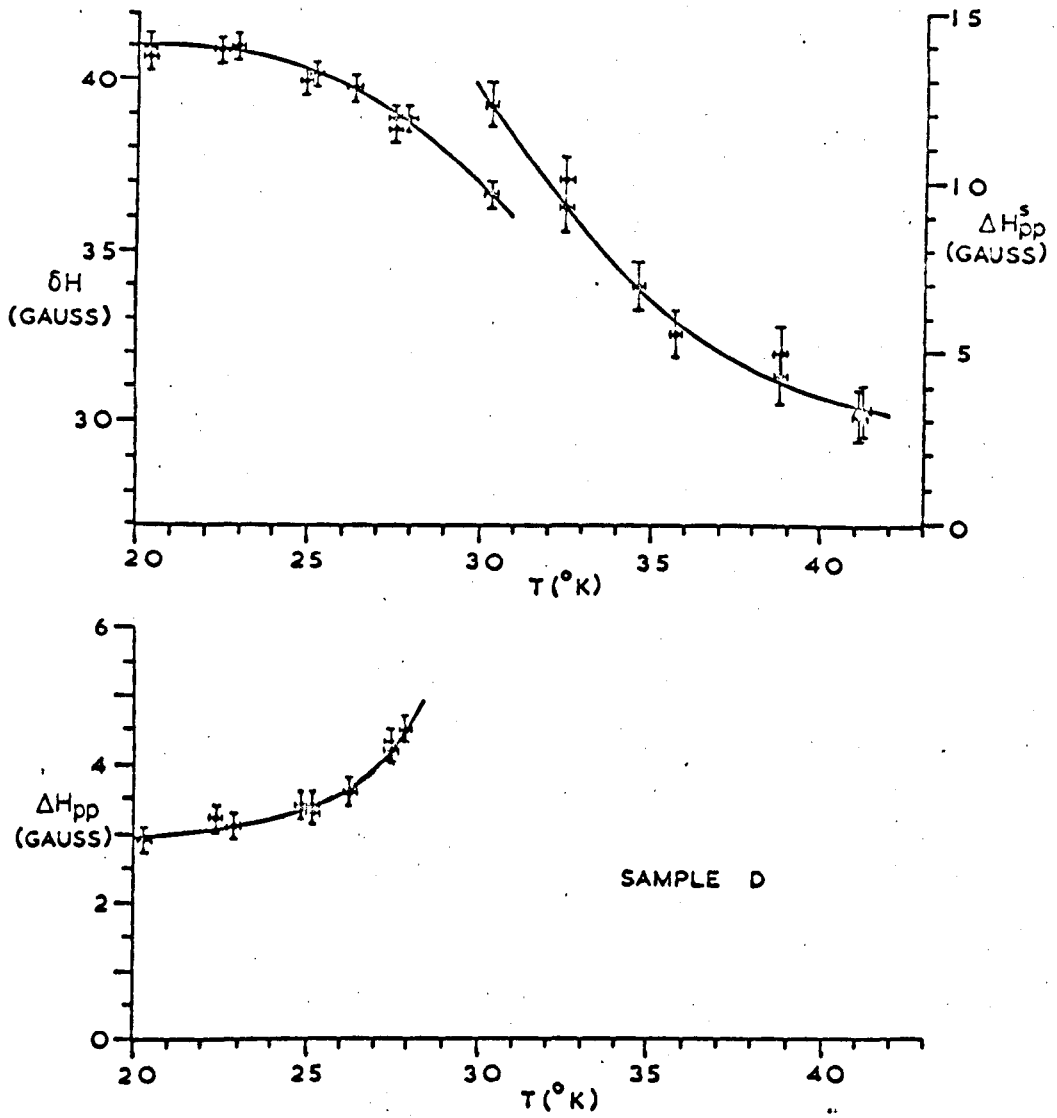

FIG. 6.7

Measurements of Hyperfine Interaction δH, Linewidth ΔH_{pp}, and Width of Single Line ΔH_{pp}^{s}, for Sample D.

short vertical bars being magnetic field markers. With increasing temperature these hyperfine lines broaden and move together.

(ii) $10^{16} < N_D < 10^{18}$ cm^{-3}, Samples C and D: For samples in this concentration range donor interaction is possible, but insufficient to form an impurity band. In this case cluster spectra are noted between the hyperfine lines, which themselves again broaden and move together with increasing temperature, while at the same time a broad line grows in the centre of the spectrum. Eventually the hyperfine lines disappear and the central line proceeds to narrow. Fig. 6.2 shows these changes taking place in a sample with N_D = $5.2.10^{17}$ cm^{-3}.

One aspect of the two groups of spectra has been combined in Fig. 6.3 and used to present graphically, in terms of N_D and temperature, the region in which resolved hyperfine lines may be observed. This region is contained below the curve. The points for Samples A and B were obtained by extrapolating to the temperature at which the linewidth $\to \infty$.

For the four samples A, B, C and D the quantitative measurements on the temperature dependence of the hyperfine splitting δH, the hyperfine linewidth between absorption derivative extrema ΔH_{pp}, and the width of the narrowing single line ΔH_{pp}^{s}, are given in Figs. 6.4 to 6.7 respectively. Lineshape determination by graphical integration was also carried out for some spectra. Bearing in mind $\frac{\Delta H_{\frac{1}{2}}}{\Delta H_{pp}} = 1.73$ and 1.18 for Lorentzian and Gaussian lines respectively, Sample A at 20°K had $\frac{\Delta H_{\frac{1}{2}}}{\Delta H_{pp}} =$

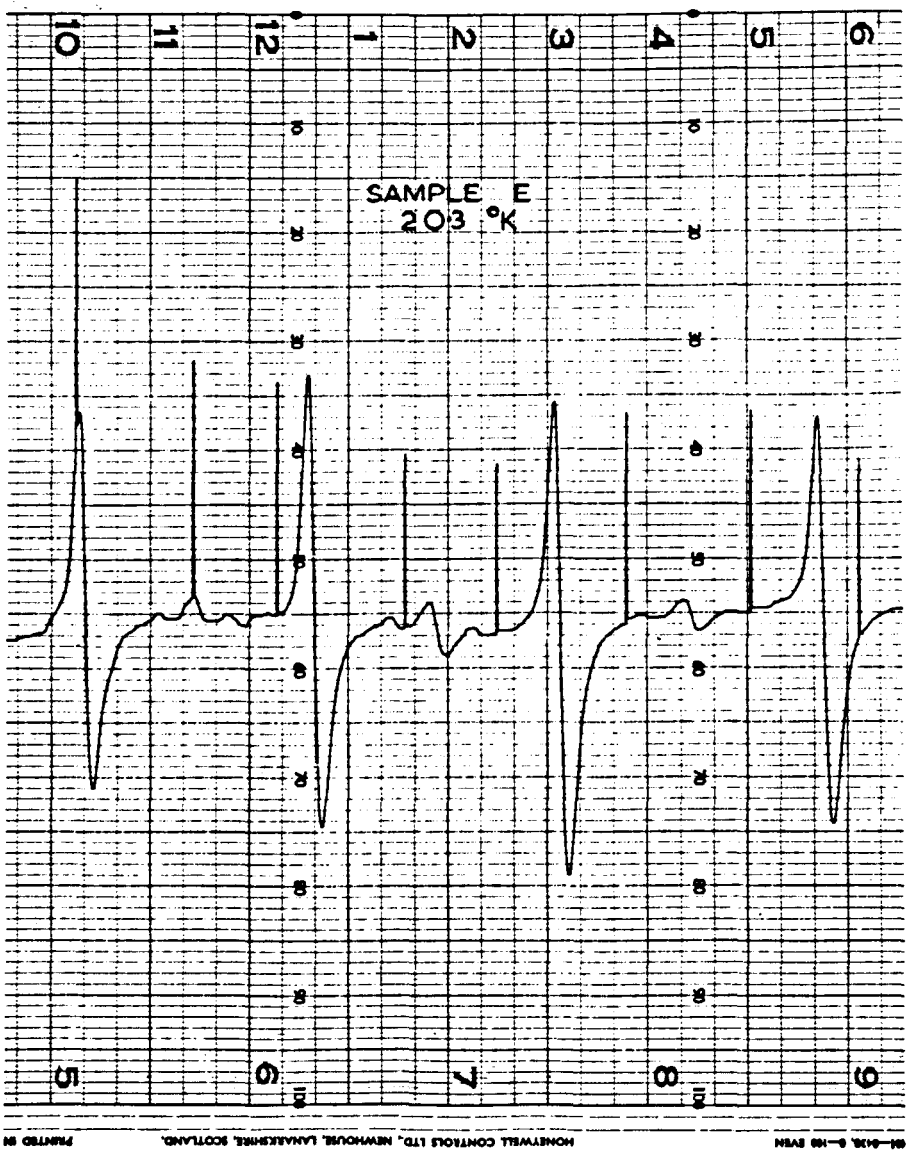

FIG. 6.8

E.P.R. Spectrum for Sample E:–

Arsenic-Doped Silicon, $1{\cdot}2 \cdot 10^{17} < N_D < 1{\cdot}0 \cdot 10^{18}$ cm^{-3}.

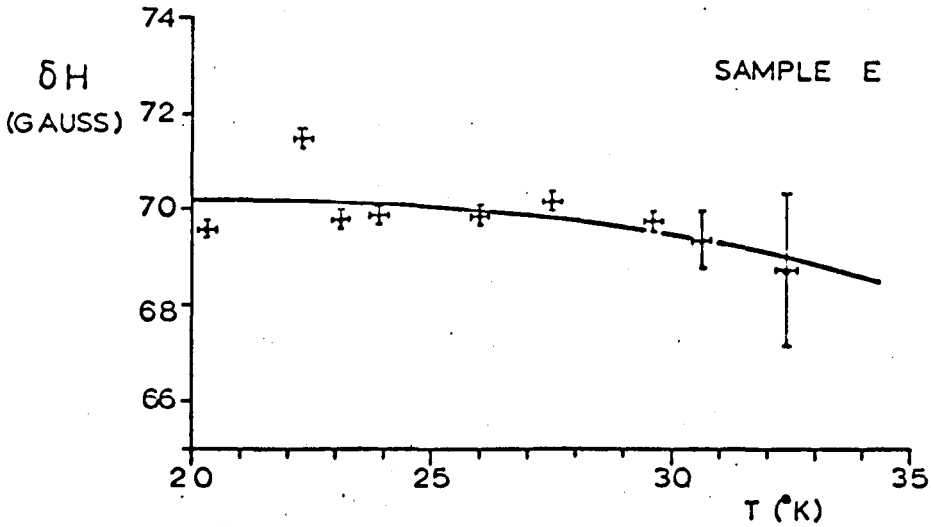

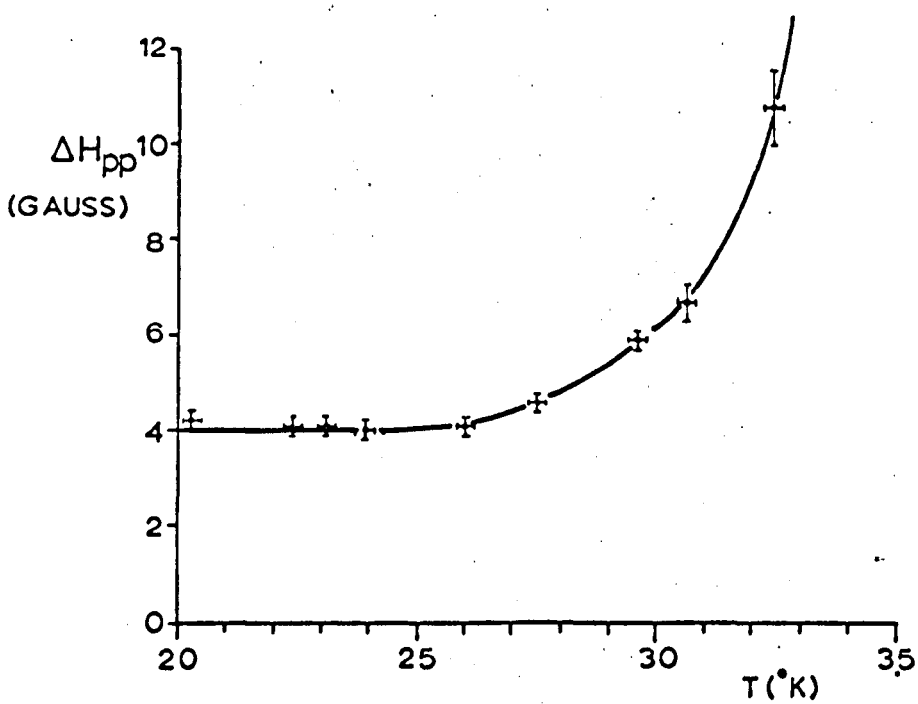

FIG. 6.9

Measurements of Hyperfine Interaction δH, and Linewidth ΔH_{pp} for Sample E.

1.28 ± 0.03, while for Sample D the narrowing single line showed no temperature variation of this ratio which was equal to 1.67 ± 0.08.

6.2 The E.P.R. Spectrum of Arsenic-Doped Silicon in the Temperature Interval from 20 to 35°K

Sample E is arsenic-doped, having $1 \cdot 2 \cdot 10^{17} < N_D < 1 \cdot 10^{18}$ cm^{-3}, and a typical spectrum is given in Fig. 6.8. As is apparent in Fig. 6.2 for phosphorus-doped Sample D, the spectrum of clusters of two and three donors may be distinguished between the hyperfine lines. The mid-spacing cluster line is in each case of two donors and the two subsidiary lines are of three. The intensities of the two-donor cluster lines are as expected from Section 2.9b i.e., 2-4-2, and the contribution of absorption by clusters at the isolated donor hyperfine lines is apparent through the greater intensity of the lines occurring at fields corresponding to $m_D = \pm \frac{1}{2}$ over those for $m_D = \pm \frac{3}{2}$.

For this sample there was no evidence of a surface state line sometimes observed for phosphorus-doped material. Also, contrary to material having a similar phosphorus concentration, with increasing temperature only a hyperfine linewidth increase and splitting decrease was noted, there being no significant growth of the cluster lines. This point will be discussed later in Section 6.7. Quantitative results are given in Fig. 6.9, where the average linewidth and hyperfine splitting are plotted. At 20°K the ratio $\frac{\Delta H_{\frac{1}{2}}}{\Delta H_{pp}} = 1.59 \pm 0.05$, which is more remote from a Gaussian lineshape than noted for phosphorus. This is consistent with observations by Feher[1], and explained through the higher ionization energy of arsenic donors, implying fewer Si^{29} nuclei encompassed within its orbit.

6.3 The E.P.R. Spectra of Antimony-and Bismuth-Doped Silicon

A spectrum could not be detected for antimony-doped silicon (Sample F) at 20°K. This is thought to be due to the short spin-lattice relaxation time at this temperature (estimated by extrapolation of the data of Castner[3] to be $\sim 10^{-9}$ sec), resulting in broad lines, which, combined with the relatively low donor concentration, prevented their detection. By pumping on the liquid hydrogen a temperature of 12°K was reached at which point a spectrum of fourteen lines was observed, consistent with the parameters in Table 6.2. This spectrum was similar to that at 4.2°K, but of reduced signal to noise.

Bismuth has an ionization energy which is really too large to be considered "shallow", and consequently the donor electron is closely bound. This Sample, G, was again rather low in donor concentration and in the region of $g = 2$ rather inconsistent results were obtained both at 4.2 and 20°K. The spectrum most common was of three lines, a broad one ~ 10 gauss wide, with two narrower ones, one overlapping the high field side of the broad one, and the other higher in field by ~ 40 gauss.

6.4 Potential Mechanisms for a Temperature-Dependent Hyperfine Interaction

The two possible processes which (at various times) were considered most likely to offer an explanation for the temperature-dependent hyperfine interaction are:

(i) The phonon-induced averaging of the ground state, either with excited states, or with respect to ionic position;

(ii) Electronic hopping between donor sites.

Exchange, either direct or indirect, is not thought to play a role in the present case. Direct exchange is of course present in the more highly doped samples, but for example in Samples A and B the exchange frequency[4] is $\frac{1}{2}$ 1 MHz which would be insufficient to provide the required averaging (see Equation 2.40 where $2\omega_o$ = 118 MHz). There would also be the question of any temperature dependence of the exchange interaction. Thermal expansion would tend to reduce the exchange frequency, and changes would be small. Kumar and Sinha[5] have postulated a temperature dependence through the phonon-induced mixing of excited orbital states into the ground orbital states. Good agreement is found for the line narrowing at very low temperatures observed in those samples displaying a single line, but the mechanism is in conflict with the usually adopted hopping process, and would still not be relevant to those samples of low doping. Indirect exchange via the conduction electrons has been studied theoretically[6,7] yielding the conclusion that the exchange frequency decreases with increasing temperature, the latter author[7] giving a relationship for an exchange coupling constant J' of the form

$$J' \propto \exp(-cT), \qquad \ldots\ldots\ldots\ldots 6.1$$

which is again in conflict with that required for the experimental results.

(a) The Admixture of States, and Averaging of a Single State, due to Phonons

Explicit temperature-dependent hyperfine interactions have been observed in two other systems, namely S-state ions (principally Mn^{2+})

in cubic environments[8], and F-centres[9].

Mn^{2+} ($3d^5$) exhibits an isotropic hyperfine spectrum due to core polarisation[10], the hyperfine field being of negative sign compared to that of an s electron with the same spin direction. Simanek and Orbach[11] proposed that a dynamic phonon-induced non-cubic crystal field mixes excited states of the form $3d^4$ ns into the ground $3d^5$ state. The admixed s states having spin parallel to the ground state will result in a net decrease of the hyperfine field.

The question of a temperature-dependent hyperfine interaction for transition metal and rare earth ions in general will be discussed later in Section 6.8.

An F-centre is an electron bound to a negative ion vacancy, so that its hyperfine interaction is due to those nuclei encompassed within the electron's orbit. Kravchenko and Vinetskii[12] have pointed out that vibrational motion of the ions due to phonons necessitates the averaging of the F-centre wave function at each ion site, resulting in temperature-dependent parameters.

Both the above theories[11,12] approximately predict a temperature dependence of the isotropic hyperfine constant a(T) (see Equation 2.46) according to

$$a(T) = a(T = 0)\ (1 \mp cT^n) \qquad \ldots\ldots\ldots\ldots\ 6.2$$

where the minus sign applies to the S-state ions, and the plus sign to F-centres. The exponent n is given by

$$\left.\begin{array}{ll} n = 4 & T < \theta_D \\ n = 1 & T > \theta_D \end{array}\right\}. \qquad \ldots\ldots\ldots\ldots\ 6.3$$

The results of Walsh et al[8] are in conflict with these predictions since they find $n \sim \frac{3}{2}$. No explanation of this difference is presently available. For F-centres in KCl, experiment and theory agree within experimental error.

By comparison with our results in silicon i.e., a 20% change in a(T) in a temperature variation of 20°K from 20 to 40°K, both the above mechanisms are very insensitive to temperature e.g., ~ 10% in 1000°K for S-state ions and ~ 3% for F-centres in the range 90 - 300°K. Hence the appropriateness of the above mechanisms is doubtful, but a discussion is postponed until Section 6.8.

(b) Electronic Hopping Between Donor Sites

The similarities in the spectral changes observed and those apparent in known cases of motional narrowing suggest that an explanation in these terms may be possible. If in the discussion of motional averaging given in Section 2.7 the relative motion of the paramagnetic ions and their surroundings is replaced by a "jumping" motion of the electrons between essentially stationary ions, Anderson's theory will still apply in principle. These stationary ions could be donor nuclei having different nuclear magnetic quantum numbers m_D.

A mechanism for such electron motion in samples of silicon having zero or small interaction between donors and requiring the minimum activation energy is that introduced in Section 3.5 i.e., phonon-induced electron hopping between electronically occupied and neighbouring unoccupied sites. The hopping frequency u for such motion is, as shown in Equation 3.18,

$$u \propto \Delta \coth \frac{\Delta}{2kT} \qquad \ldots\ldots\ldots\ldots\ldots 6.4$$

where Δ is the activation energy, which is a function of the degree of compensation as indicated in Equation 3.17. When the frequency of this jumping approaches that of the hyperfine splitting averaging should occur. This frequency must therefore be compared with that calculable from Anderson's theory. For phosphorus having $I = \frac{1}{2}$, and therefore only two values of $m_D = \pm \frac{1}{2}$, Equation 2.40 is directly applicable and may be re-written

$$f_e = \frac{1}{2\sqrt{2}} \frac{g\beta}{h} \left[\delta H_o^2 - \delta H^2 \right]^{\frac{1}{2}}, \qquad \ldots\ldots\ldots\ldots\ 6.5$$

where f_e is the jump frequency, and δH_o and δH are the hyperfine splittings at $T = 0^oK$ and T^oK respectively. Early results of Lacey and Lancaster[13] were interpreted in this fashion.

A further mechanism for the transference of electrons involves the excitation of the donor electron to the conduction band and its subsequent capture by a donor nucleus of different nuclear orientation. This process is obviously energetically less favourable, although the contribution of such a process to spin relaxation has been demonstrated[14].

(c) Averaging of the Ground State with Thermally Accessible Excited States

If during the time of one Larmor precession the electron whose resonance is being observed moves between the ground state and an excited state, then a mixed state will result. With a lifetime τ in that excited state the necessary restriction is

$$\omega_o \tau < 2\pi \qquad \ldots\ldots\ldots\ldots\ 6.6$$

where ω_0 is the microwave angular frequency. For two such levels within a few times kT of each other, thermal excitation will provide the stimulus for this mixing. This mechanism has been proposed by Watkins[15,16] to account for the temperature-dependent hyperfine interaction in stressed lithium-doped silicon in the temperature range 1.4 to 4°K.

Consider the situation in silicon for other shallow donors. The valley-orbit splitting is approximately equal to a few times kT in the temperature range of interest. As described in Section 3.2, of the donor ground states only the $1s(A_1)$ state has a non-zero $|\psi(o)|^2$ and therefore a finite contact hyperfine interaction. Of course, the $1s(E$ and $T_2)$ states being d- and p-like respectively do have a hyperfine interaction due to dipole-dipole coupling. But as this interaction varies as r^{-3} (see Equation 2.44) and the populations of these states are reduced from that of the $1s(A_1)$ state by the Boltzmann factor, the hyperfine interaction in these states may be neglected. Thus mixing of the $1s(A_1$, E and $T_2)$ states will consequently lead to a decrease in the observed isotropic hyperfine interaction. It may therefore be expected, from a naive point of view, that an averaged probability density will result, to which each state contributes in proportion to its probability of occupation. A simplified system for the donor ground states may be visualized in which the $1s(E$ and $T_2)$ states are replaced by a single five-fold degenerate state at Δ. As is evident from Fig. 3.3 this is not unreasonable, since for the donor phosphorus $1s(A_1) \rightarrow 1s(T_2) \sim 11.6$ meV while $1s(T_2) \rightarrow 1s(E) \sim$ 1.3 meV. The probabilities of an electron being in either of the two states are given by

$$P_{A_1} = \frac{N_{A_1}}{N_{A_1} + N_{E/T_2}} \quad \text{and} \quad P_{E/T_2} = \frac{N_{E/T_2}}{N_{A_1} + N_{E/T_2}} \qquad \ldots\ldots\ldots 6.7$$

where N_{A_1} and N_{E/T_2} are the average populations of those states. Hence the average probability density $|\psi(o)|^2$ is

$$|\psi(o)|^2 = P_{A_1} \cdot |\psi_{A_1}(o)|^2 + P_{E/T_2} \cdot |\psi_{E/T_2}(o)|^2, \qquad \ldots\ldots\ldots 6.8$$

which, by the incorporation of the relative populations

$$\frac{N_{E/T_2}}{N_{A_1}} = 5 \exp\left(-\frac{\Delta}{kT}\right) \qquad \ldots\ldots\ldots\ldots 6.9$$

gives finally

$$\delta_H = \frac{\delta_{H_{A_1}}}{1 + 5 \exp\left(-\frac{\Delta}{kT}\right)} \qquad \ldots\ldots\ldots\ldots 6.10$$

where $\delta_{H_{A_1}}$ is the hyperfine splitting of the $1s(A_1)$ state i.e., that apparent at $T = 0^{\circ}K$. The lifetime in the upper state may be calculated via the level widths, estimated by Castner[17] to be $\gtrsim 0.2$ meV, implying $\tau \lesssim 3.10^{-12}$ sec. Thus Q band measurements give $\omega_o \tau \sim 0.7$, so satisfying the condition Equation 6.6.

A more rigorous treatment of this phenomenon has been given by Dugdale, Lacey and Lancaster[18]. They propose a method for calculating E.P.R. spectra in the presence of motional narrowing which is more general than that of Kubo and Tomita[19]. A necessary requirement of the latter

authors' analysis is that the perturbation Hamiltonian $\mathcal{H}'$, representing the interaction between the paramagnetic centre and the phonons is small. Similarly the unperturbed Hamiltonian $\mathcal{H}_0$ is required to give rise to sharp resonance lines well separated from one another, and which therefore continue to be so under the influence of the perturbation. This enables an unambiguous association of the perturbed spectral lines with those of the unperturbed spectrum. In the case in hand, the perturbation gives rise to approximately a 20% change in the hyperfine interaction i.e., it cannot be considered small.

The analysis of Dugdale et al starts with the basic equations of Kubo and Tomita, and demonstrates that the above requirements for association of spectral lines may be relaxed. They note in their analysis that for terms which are non-vanishing in the limit of macroscopically large samples, a phonon creation-annihilation operator pair corresponding to any particular lattice mode occurs only once. Such operator pairs are associated with a factor $(\text{volume})^{-1}$, and during the analysis of the above authors the product of such operator pairs with the density of states function is required. Since this latter term is proportional to $(\text{volume})^{1}$, if the operator pairs occur more than once there will be uncompensated $(\text{volume})^{-1}$ factors, leading only to insignificant effects. Hence each such operator pair may be replaced by its thermal average value.

In applying the above analysis to phosphorus-doped silicon several assumptions will be made. Namely, that the Zeeman interaction is identical in all the ground states and is very much larger than the hyperfine interaction, and that the spin-orbit interaction within the triplet state is small such that only the secular part of the hyperfine interaction need be considered. The singlet, doublet and triplet states may be written

$|A_1\rangle$, $|E_1\rangle$, $|E_2\rangle$, $|T_{-1}\rangle$, $|T_0\rangle$ and $|T_1\rangle$ respectively, while $\hbar\Delta_E$, $\hbar\Delta_T$, $\hbar\omega_z$, $\hbar A$ and $\hbar\lambda$ are respectively the valley-orbit splittings of the ground state $|A_1\rangle$ from the doublet and triplet states, the Zeeman splitting, and the hyperfine and spin-orbit interaction constants. The unperturbed Hamiltonian $\mathcal{H}_0$ may then be written

$$\begin{aligned}\mathcal{H}_0 = {} & \hbar\omega_z S_z + 2\hbar A S_z I_z |A_1\rangle\langle A_1| \\ & + \hbar\Delta_E(|E_1\rangle\langle E_1| + |E_2\rangle\langle E_2|) \\ & + \hbar\Delta_T(|T_{-1}\rangle\langle T_{-1}| + |T_0\rangle\langle T_0| + |T_1\rangle\langle T_1|) \\ & + \hbar\lambda S_z(|T_1\rangle\langle T_1| - |T_{-1}\rangle\langle T_{-1}|) \\ & + \sum_i \hbar\omega_i \left(a_i^* a_i + \tfrac{1}{2}\right) \qquad \ldots\ldots\ldots\ldots 6.11\end{aligned}$$

where $\hbar\omega_i$ is a phonon energy associated with the creation and annihilation operators a_i^* and a_i. The coupling between the ground state and the doublet and triplet states is via the interaction of the orbital motion of the electron with the phonons. It may be written

$$\begin{aligned}\mathcal{H}' = {} & \sum_i (a_i^* + a_i)\left[P_i|A_1\rangle\langle E_1| + Q_i|A_1\rangle\langle E_2|\right. \\ & \left. + R_i|A_1\rangle\langle T_1| + S_i|A_1\rangle\langle T_0| + T_i|A_1\rangle\langle T_{-1}|\right] \\ & + \text{Hermitian conjugate terms.} \qquad \ldots\ldots\ldots\ldots 6.12\end{aligned}$$

Although Castner[17] has shown that at temperatures immediately below those of interest here spin-lattice relaxation is via spin-orbit interaction, this factor has been neglected above. Nevertheless, the solution

should accurately represent the resonance line positions, if not their widths.

As the calculation proceeds the shift of the unperturbed lines due to motional effects is shown to consist of two terms, one dominating when the ground and excited states lie within the phonon spectrum (the present case), and the other when this is not so. The temperature dependence of this latter term is very weak, as noted for the S-state ions and F-centres. At the next stage in the calculation it is necessary to introduce the spontaneous transition probabilities per unit time ω_E and ω_T for the $|A_1>/|E>$ and $|A_1>/|T>$ transitions. Likewise it is noted that the average occupation numbers of the resonant phonons are

$$n_E = \left[\exp\left(\frac{\hbar\Delta_E}{kT}\right) - 1\right]^{-1} \text{ and } n_T = \left[\exp\left(\frac{\hbar\Delta_T}{kT}\right) - 1\right]^{-1}. \quad \ldots\ldots\ldots 6.13$$

Castner[17] has estimated the spin-orbit splitting of the $|T>$ states to be 0.022 meV, implying $\hbar\lambda = 0.015$ meV for these p-like states. Similarly, from the level widths, he estimates $\hbar\omega_T \sim \hbar\omega_E = 0.2 - 0.3$ meV. Therefore, in angular frequency terms

$$\left.\begin{aligned} &\lambda = 2\cdot3.10^{10} \text{ sec}^{-1},\ \omega_T \sim \omega_E = 4\cdot6.10^{11} \text{ sec}^{-1} \\ &A = 3\cdot7.10^{8} \text{ sec}^{-1} \quad (\text{N.B. } A = \frac{a_D}{2\hbar}), \end{aligned}\right\} \quad \ldots\ldots\ldots 6.14$$

from which it may be concluded $\omega_T \sim \omega_E >> A$ and $\lambda >> A$. Incorporating these approximations and solving for the line having $m_D = +\frac{1}{2}$ (i.e., the low magnetic field line), a Lorentzian shaped resonance line in the neighbourhood of ω_z results, its position being given by

$$\omega = \omega_z - A\left[1 + \frac{2n_E}{(n_E + 1)} + \frac{3n_T}{(n_T + 1)}\right]^{-1}, \qquad \ldots\ldots\ldots 6.15$$

and its half-width at half-intensity by

$$\delta\omega = 2\omega_T n_T\left[1 - \frac{\omega_T^{\,2}(n_T + 1)^2}{\omega_T^{\,2}(n_T + 1)^2 + \lambda^2}\right]. \qquad \ldots\ldots\ldots 6.16$$

Since $\hbar(\Delta_E - \Delta_T) = 1.3$ meV[20] is small in comparison with $\hbar\Delta_T =$ 11.6 meV a weighted mean of $\hbar\Omega = 12.1$ meV may be used for the valley-orbit splitting. Bearing in mind that $\frac{\hbar\Omega}{kT} \geq 3$, Equation 6.15 may be finally simplified to yield

$$\omega_{m_D = +\frac{1}{2}} = \omega_z - A\left[1 + 5\exp\left(\frac{-\hbar\Omega}{kT}\right)\right]^{-1}. \qquad \ldots\ldots\ldots 6.17$$

Combining this with the equivalent solution for $m_D = -\frac{1}{2}$, the hyperfine splitting $\Delta\omega$ is seen to be

$$\Delta\omega = \frac{2A}{1 + 5\exp\left(-\frac{\hbar\Omega}{kT}\right)}, \qquad \ldots\ldots\ldots\ldots 6.18$$

i.e., in agreement with the simple approach Equation 6.10.

If the importance of the spin-orbit interaction of the triplet states upon the spin-lattice relaxation, and hence linewidth, is now acknowledged, Equations 6.11 and 6.12 must be appropriately modified by introducing the non-secular part of the spin-orbit interaction. Recalling the relative magnitudes of the quantities in Equation 6.14 along with an $\omega_z > 6.10^{10}$ sec^{-1} for X band and above, the solution yields Lorentzian-shaped lines in the low temperature limit i.e., $n_E \sim n_T \ll 1$. These lines are in the same

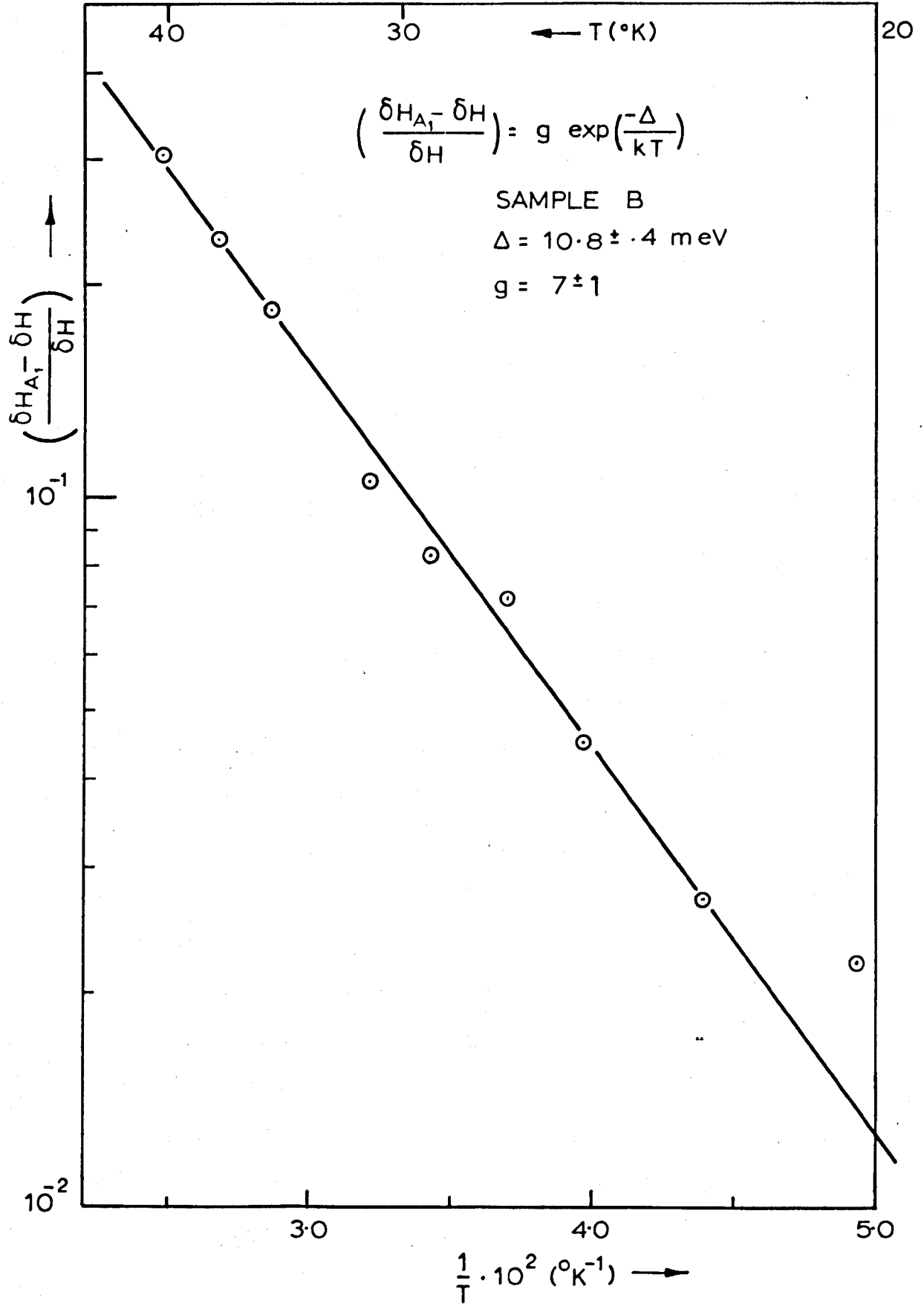

FIG. 6.10
Confirmation of the Dugdale et al Mechanism for Motional Narrowing.

positions as previously calculated, but the half-width at half intensity becomes

$$\delta\omega = \frac{2\lambda^2 n_T}{\omega_T}\left[2 + \left(\frac{\omega_z}{\omega_T}\right)^2\right]\left[1 + \left(\frac{\omega_z}{\omega_T}\right)^2\right]^{-1} \quad \text{..... 6.19}$$

Contrary to the previous estimate of the linewidth this result predicts a width weakly dependent upon magnetic field.

6.5 Analysis of the Experimental Results on the Temperature-Dependent Hyperfine Interaction

In drawing a comparison between the temperature dependence of the motional narrowing through hopping between donor sites and that through hopping between the various 1s ground states, note that the former predicts (Equations 6.4 and 6.5) a dependence which is not a function of the donor, but is a function of the degree of compensation and donor concentration, whereas the latter (Equations 6.10 and 6.18) is independent of the compensation and donor concentration, but predicts a donor dependence through the valley-orbit splitting. The samples in Table 6.1 go some way towards differentiating between the mechanisms, in that they encompass varying donor concentrations and degrees of compensation for one donor (phosphorus), and a range of donors from antimony to bismuth in increasing valley-orbit splitting. As previously described in Section 6.3 these two donors in particular did not provide useful results, but those of phosphorus and arsenic are thought sufficient to confirm the appropriate mechanism.

The re-arranged Equation 6.10 is plotted for Sample B in Fig. 6.10, where g is the degeneracy factor of the excited state at Δ. It appears

Sample	N_D (cm^{-3})	$K = \frac{N_A}{N_D}$	Δ (meV)	g
A	$3.1.10^{15}$	0.16	10.5 ± 0.6	6 ± 1
B	$4.2.10^{15}$		10.8 ± 0.4	7 ± 1
C	$2.3.10^{16}$	0.27	10.9 ± 0.9	$7 \, {}^{+3}_{-2}$
D	$5.2.10^{17}$		12.9 ± 0.9	$18 \, {}^{+9}_{-6}$

TABLE 6.3

The Weighted Valley-Orbit Splitting and Degeneracy of the 1s (E and T_2) states in Phosphorus-Doped Silicon.

to provide a correct solution to the experimental results. Similar least square solutions for all the phosphorus-doped samples are assembled in Table 6.3. The deduced values of Δ appear to lie a little below the weighted mean of 12.1 meV, while the measured degeneracy, taking errors into account, approaches five. Sample D is an obvious exception to both these generalizations.

A check was made upon the likely contribution of higher hydrogen-like states. For example, the next state is the $2p_0$ lying 34.1 meV above the $1s(A_1)$ state and having a degeneracy of six. The inclusion of this state would merely give rise to an additional exponential term in the denominator of Equation 6.10, and this would increase to only 1% of the original exponential term at 55°K.

The results for Sample B were also analysed according to Equation 6.5 (taking $g = 1.9885$[21]) to examine the relevance of Anderson's theory applied to electron hopping. Equations 6.4 and 6.5 require

$$f_e = c\,\Delta \coth \frac{\Delta}{2kT} \qquad \ldots\ldots\ldots\ldots\ 6.20$$

where c is a constant. Hence for each experimental measurement of f_e and corresponding T a graph may be plotted of c/Δ. A unique solution of this equation for c and Δ requires that for all the experimental points these graphs intersect at one point. No such intersection was found in the range $10^{-5} \leqslant \Delta \leqslant 10^{2}$ meV, and hence the hopping mechanism is discounted.

The dependence of the hyperfine interaction temperature variation on the donor species is apparent from a comparison of Figs. 6.7 and 6.9, which are for phosphorus - and arsenic-doped samples of similar donor

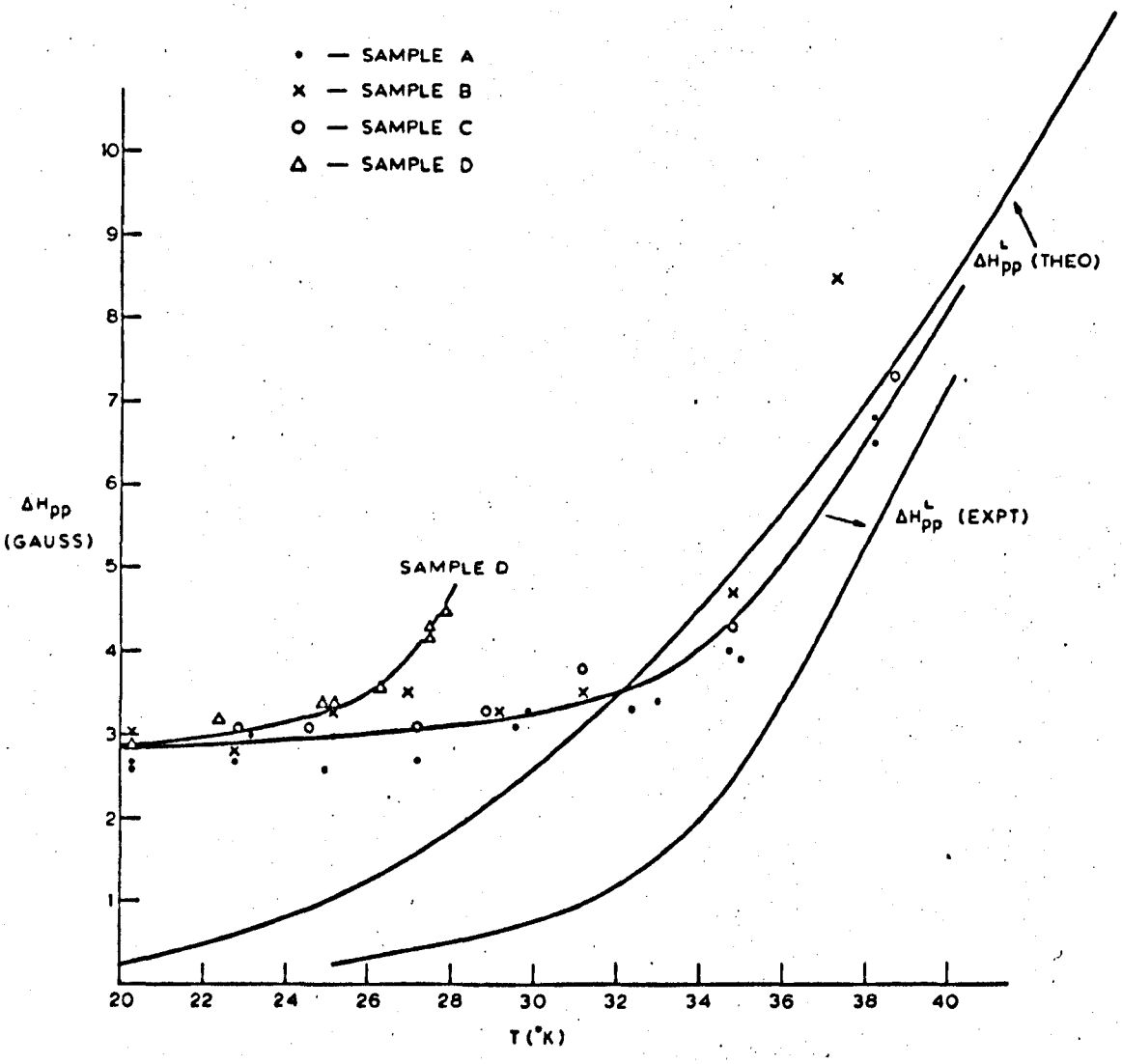

FIG. 6.11

A Comparison of the Theoretical and Experimental Linewidths of Phosphorus–Doped Silicon.

concentrations. They clearly indicate that the donor species determines the behaviour, rather than the donor concentration and compensation. This is consistent with the valley-orbit splitting of arsenic being approximately twice that of phosphorus, and is additional evidence of the inappropriateness of the hopping mechanism.

6.6 The Temperature-Dependent Hyperfine Linewidth

If the numerical values given in Equation 6.14 for phosphorus-doped silicon are inserted into the linewidth given by Dugdale et al (Equation 6.19), then for Q band measurements at 35 GHz the peak to peak width of the derivative of the Lorentzian line is

$$\Delta H_{pp}^{L} = \frac{270}{\exp\left(\frac{140}{T}\right) - 1} \qquad \ldots\ldots\ldots\ldots\ 6.21$$

where the weighted mean of the 1s (E and T_2) states has been used. Fig. 6.11 contains a comparison of this predicted behaviour and that found experimentally. The most obvious discrepancy occurs at temperatures below 30°K, where for three of the four samples the width is essentially constant, and equal to that of the Gaussian envelope. At 20°K the observed peak to peak width is 2.8 ± 0.2 gauss, which may be compared to the value given by Feher[1] of $\frac{2.5}{1.18} = 2.1$ gauss at 1.25°K. The latter author did in fact measure a linewidth in excess of this but applied a saturation correction, but through an estimation of the microwave magnetic field H_1 in the author's cavity[22] such a correction is not applicable here. Overmodulation at 100 KHz may also be dismissed as a broadening mechanism, since according to Smith (see Section 5.4) the correct ΔH_{pp} will be measured providing $\frac{h_m}{\Delta H_{pp}} < 0.3$, where h_m is the modulation amplitude.

This implies using Feher's above value that h_m should not be greater than 0.6 gauss, which condition was certainly satisifed by the experimental $h_m \sim 0.3$ gauss. Envelope broadening at 20°K due to the reduced spin-lattice relaxation time from 1.25°K may also be dismissed. Castner[3] measured $T_s \sim 5.10^{-7}$ sec at 20°K, implying a peak to peak spin packet width ~0.1 gauss, clearly insufficient to broaden the line from 2.1 to 2.8 gauss. The reason for the difference therefore remains unclear.

The other immediate observation upon Fig. 6.11 is the more rapid increase in linewidth of Sample D having $N_D \sim 5.10^{17}$ cm^{-3}. This is due to a much reduced relaxation time at this concentration due to fast relaxing pairs (see Section 3.4) with the consequent greater spin packet width, leading to observable envelope broadening at lower temperatures. Feher and Gere[14] observed that at 1.25°K the spin-lattice relaxation time decreases rapidly from 10^{+4} sec for a phosphorus concentration of 1.10^{16} cm^{-3}, to 10^{-6} sec for a concentration of 5.10^{17} cm^{-3}.

The temperature variation of the linewidth of the arsenic-doped Sample E is shown in Fig. 6.9. Again at 20°K a value in excess of that measured at 1.25°K by Feher is observed.

At present the comparison drawn in Fig. 6.11 is of the envelope of the increasing spin packet widths with the packet widths themselves as calculated from Equation 6.21. A technique for calculating the packet width from the measured width is therefore required. Castner[3] defines a quantity K by the relation

$$T_2 = T_1 = \left(\frac{2}{\sqrt{3}\,\gamma\,\Delta H_{pp}} \right) K\,(a), \qquad \ldots\ldots\ldots\ldots\ 6.22$$

where $$a = \frac{\Delta H_{\frac{1}{2}}^{L}}{\Delta H_{\frac{1}{2}}^{G}} = \frac{1.73\ \Delta H_{pp}^{L}}{1.18\ \Delta H_{pp}^{G}}, \qquad \ldots\ldots\ldots\ldots\ 6.23$$

and graphically displays K(a) for $1 \leqslant a \leqslant 10$. Hence the peak to peak envelope width

$$\left.\begin{aligned} \Delta H_{pp} &= \Delta H_{pp}^{L} \cdot K \\ \text{and} \qquad a &= 1.47 \frac{\Delta H_{pp}^{L}}{\Delta H_{pp}^{G}} \cdot \end{aligned}\right\} \qquad \ldots\ldots\ldots\ldots\ 6.24$$

Combining the above expressions gives

$$K = \left(1.47 \cdot \frac{\Delta H_{pp}}{\Delta H_{pp}^{G}}\right) \cdot \frac{1}{a} \cdot \qquad \ldots\ldots\ldots\ldots\ 6.25$$

From the experimental results $\Delta H_{pp}^{G} = 2.8$ gauss, therefore K is finally given by

$$K = (0.52 \cdot \Delta H_{pp}) \cdot \frac{1}{a}, \qquad \ldots\ldots\ldots\ldots\ 6.26$$

and $$\Delta H_{pp}^{L} = 1.9\ a. \qquad \ldots\ldots\ldots\ldots\ 6.27$$

Thus for an envelope width ΔH_{pp} the point of intersection of Equation 6.26 with Castner's curve may be found, and hence the Lorentzian packet width ΔH_{pp}^{L} derived. A comparison between these two quantities is given in Fig. 6.12. Returning to Fig. 6.11 it is now possible to compare like with like i.e., the calculated and experimental Lorentzian widths. It is apparent that the experimental value is less than the calculated at all temperatures and does not have such a smooth variation, although at temperatures below $\sim 32^{\circ}K$ the procedure for estimating ΔH_{pp}^{L} is more liable to error.

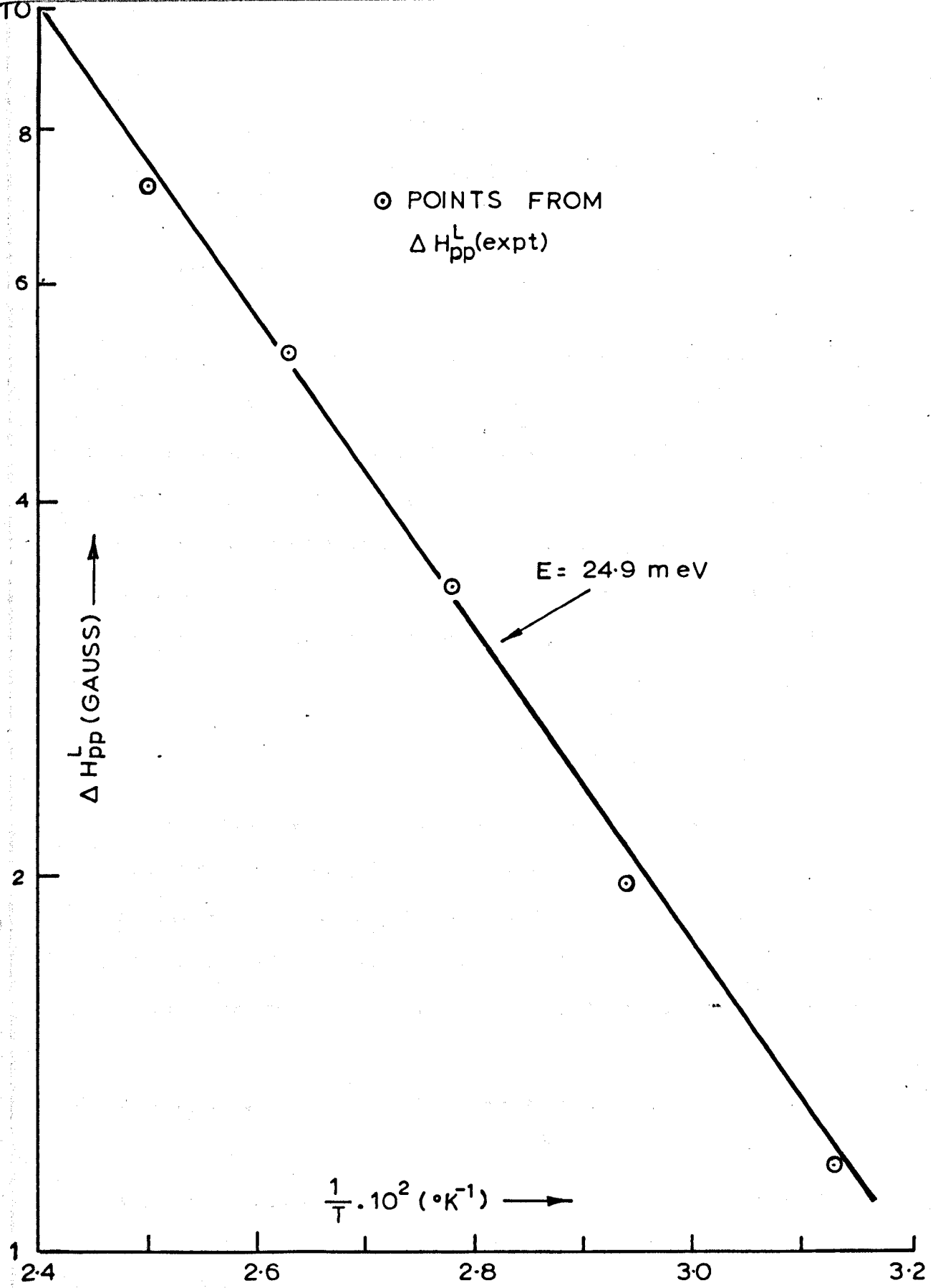

FIG. 6.13

Demonstration of the Importance of the Donor Ionization

A further plot of the derived Lorentzian peak to peak width variation with temperature as in Fig. 6.13 shows that

$$\Delta H_{pp}^{L} \propto \exp -\left(\frac{E}{kT}\right) \qquad \ldots\ldots\ldots\ldots 6.28$$

with E = 24.9 meV. A behaviour of this form was in fact predicted by Lépine[23] who has studied the spectral temperature variation of the donor phosphorus alone. His alternative explanation of this linewidth variation is through the exchange scattering of the donor electron by a conduction electron, and as a consequence of this the donor electron experiences resonance at ω_z and $\omega_z \pm A$. Providing the rate of exchange, ω_{ex}, is less than the hyperfine interaction, the linewidth is proportional to it. Since

$$\omega_{ex} = \sigma_{ex} v\, n_c \qquad \ldots\ldots\ldots\ldots 6.29$$

where σ_{ex} is the exchange cross section, v is the conduction electron average velocity and n_c is the conduction electron concentration, the linewidth is also proportional to n_c. By calculation, he demonstrates that the temperature dependence of the linewidth is identical with that of the relative number of electrons in the conduction band i.e.,

$$\Delta H_{pp}^{L} \propto \frac{n_c}{(N_D - N_A)} \qquad \ldots\ldots\ldots\ldots 6.30$$

where $(N_D - N_A)$ electrons are distributed over the hydrogen-like states and the conduction band. In his analysis Lépine approximates the hydrogen-like states to a system consisting of only the $1s(A_1, E \text{ and } T_2)$ states since the other states are within a few times kT of the conduction

band. From Smith[24], the conduction electron concentration is related to the donor ionization energy E_d by

$$n_c \propto \exp\left(-\frac{E_d}{2kT}\right). \qquad \ldots\ldots\ldots\ldots 6.31$$

Thus it is expected that

$$\Delta H_{pp}^{L} \propto \exp\left(-\frac{E_d}{2kT}\right). \qquad \ldots\ldots\ldots\ldots 6.32$$

This appears to be confirmed by the derived energy of 24.9 meV, which lies close to $\frac{E_d}{2}$ = 22.7 meV for phosphorus. (The donor ionization energies are given in Fig. 3.3. They are 45.3 and 53.5 meV for phosphorus and arsenic respectively.)

The results for arsenic also appear to confirm the above mechanism, although due to the deviation of the lineshape even at low temperatures from a true Gaussian, difficulty was found in extracting the true Lorentzian widths. For arsenic $\frac{E_d}{2}$ = 26.8 meV, a value little different from that for phosphorus. Thus, as experiment confirms, the linewidth variation for this donor is very similar to phosphorus, which would not be so should the process be dominated by the valley-orbit splittings, differing as they do by a factor of two.

6.7 The Linewidth Reduction in the Higher Temperature Interval

As noted in Section 6.1 those samples (C and D) having $10^{16} < N_D < 10^{18}$ cm^{-3} exhibited in the higher temperature region studied a single line which narrowed with increasing temperature. In this temperature region Lépine suggests that the increased number of conduction electrons results in the exchange rate ω_{ex} being greater than the hyperfine interaction, with the consequent appearance of a single line. The linewidth

is now a function of the relative number of electrons in the 1s (A_1) state n_{A_1}, and the conduction electron concentration, which assuming a constant ratio, with respect to temperature variations, of the half-width to peak to peak width (see Section 6.1) gives

$$\Delta H_{pp}^{s} \propto \left(\frac{n_{A_1}}{N_D - N_A}\right)\left(\frac{1}{n_C}\right). \qquad \ldots\ldots\ldots\ldots 6.33$$

With increasing temperature the first term will decrease while n_C will increase, giving a decreasing linewidth. Whereas with increasing donor concentration the first term increases while n_C again increases. The first term increases less rapidly than n_C, resulting in a decreasing linewidth with increasing donor concentration. Figs. 6.6 and 6.7 confirm this. The compensation in Sample C may also be contributing to the difference between the samples, in that at a fixed temperature there is little change in the relative population of the 1s (A_1) state but the number of conduction electrons is reduced.

It was noted in Section 6.2 that for the arsenic-doped Sample E no significant growth of the cluster lines was observed, such that the above narrowing single line was not detected. An explanation for this may lie in the following. The intensity of this line is proportional to the number of electrons bound to the donors, that is

$$\text{Intensity} \propto (N_D - N_A - n_C). \qquad \ldots\ldots\ldots\ldots 6.34$$

Now the width of the line is given in Equation 6.33 above, so that

$$\text{Amplitude} \propto \frac{(N_D - N_A - n_C)\,(N_D - N_A)\,n_C}{n_{A_1}}. \qquad \ldots\ldots\ldots\ldots 6.35$$

Therefore, if it is assumed that n_C is small, and that for the two donors arsenic and phosphorus, $(N_D - N_A)$ is the same, then

$$\frac{\text{Amp. As}}{\text{Amp. P}} = \left(\frac{n_{C_{As}}}{n_{C_P}}\right)\left(\frac{n_{A_1\,P}}{n_{A_1\,As}}\right). \qquad \ldots\ldots\ldots\ldots 6.36$$

Now there will be approximately equal numbers of electrons bound to the 1s (A_1) states in both cases, whereas it is easily estimated that at 30°K

$$\frac{n_{C_{As}}}{n_{C_P}} \simeq \frac{1}{5}. \qquad \ldots\ldots\ldots\ldots 6.37$$

Hence it is reasonably argued that the difference in donor ionization energies is sufficient to prevent the observation of this line in the arsenic-doped sample.

As the temperature increases further the resonance signal will increasingly be due to conduction electrons (see Section 3.6), so that the width of the observed single line will pass through a minimum. Lépine's measurements of this minimum suggest a further broadening mechanism is present. In the temperature region of this minimum the relative population of the 1s (E and T_2) states passes through a maximum. Now as previously mentioned in Section 3.4 Castner has demonstrated the importance of spin-orbit coupling in the 1s (T_2) states, such that three resonances are possible within these states. Lépine suggests that due to the rapid motion of electrons from the 1s (T_2) states to either the conduction band or the 1s (A_1) state only a resulting averaged single line is observed, and that this is the extra contribution at the minimum.

6.8 Conclusions and Suggestions for Further Work

The hopping motion of an electron between different energy states associated with it, be these of a donor in a semiconductor, or of an ion in a lattice, is confirmed as a mechanism able to give rise to a temperature dependence in the measured hyperfine interaction.

Consider two examples from the latter class. There is no fundamental reason why transition metal ions and rare-earth ions should not display a similar dependence, that is until the orders of magnitude of the relevant quantities are examined. The first excited state is approximately 1 eV above the ground state for transition metal ions. Thermal energies are thus insufficient to cause any mixing. Rare-earth ions present a different situation. Now the nearest excited state is only of the order of 10 meV away i.e., apparently of the right order of magnitude, but due to strong spin-lattice interaction spectra can only be observed at very low temperatures, again resulting in thermal energies insufficient for excitation.

For the bound donor electron the motion is between the 1s (A_1) ground state and the 1s (E and T_2) states. The estimated valley-orbit splitting through this mechanism for the donor phosphorus is slightly less than the weighted mean of the optically measured position of the 1s (E and T_2) states. This trend is also apparent in Castner's E.P.R. measurements of the Orbach relaxation, in that he estimates a value of 10.6 meV compared to an optical value of 11.6 meV for the 1s (A_1) → 1s (T_2) transition. No reason for this difference has so far been advanced. The results for the sample having a phosphorus concentration of 5.10^{17} cm^{-3} are rather different from the lower concentration results. At this concentration the electron is able to move between donors through

exchange in addition to the excitation within the 1s states.

The results for the arsenic-doped sample clearly demonstrate that the energies determining the temperature behaviour of the hyperfine splitting and the linewidth are different, so confirming the quantitative measurements on phosphorus-doped silicon. Similar quantitative measurements should be obtainable for antimony due to its similar valley-orbit and ionization energies. This leads to a proposal that an improved variable temperature cavity arrangement would be advantageous. A temperature range of 4.2 to 300°K would be ideal, perhaps achieved by better thermal isolation of the cavity from the refrigerant than in the method used by the author. As in many experiments results for bismuth are likely to prove different from those for the other donors. Its valley-orbit splitting is of the order of three times that of phosphorus, while its ionization energy is of the order of one and a half times that of the other donors. Thus higher temperatures are expected to be necessary before either the hyperfine splitting or the linewidth show any changes, although higher donor concentrations could be used before exchange would be evident.

Since the reduction in the hyperfine interaction is due to the averaging of the interaction of two states with and without finite values of $|\psi(o)|^2$, this averaging could be brought about at a fixed low temperature (e.g., $< 4.2^{\circ}K$, so minimizing kT) by illuminating the sample during resonance with radiation of a wavelength equivalent to that of the $1s\ (A_1) - 2p_o$ transition. This would provide additional evidence for the proposed mechanism, and if the hyperfine interaction reduction is not accompanied by a linewidth increase further weight is given to Lépine's proposal. Laser lines at the appropriate wavelength of 36 μm have been

observed in He, H_2O vapour and D_2O vapour.

Contrary to the theory of Dugdale et al the hyperfine linewidth appears to be dominated, in energy terms, by the ionization energy of the donor not its valley-orbit splitting. The theoretical estimate of Dugdale et al certainly gives an answer of the correct order of magnitude, but this is very much dependent on the values taken for the spin-orbit interaction in the 1s (T_2) states and the spontaneous transition probability 1s (A_1) - 1s (T_2) per unit time. Both of these quantities are presently inconclusively determined. The magnetic field dependence of the linewidth is a feature exclusive to the Dugdale et al theory, so that accurate measurements made say at 10 GHz and 140 GHz (these being the present practical limits) could provide one further test of the latter theory. Measurements by Lancaster at 10 GHz to compare with those reported here at 35 GHz did not allow any conclusions to be drawn due to magnitude of the experimental errors.

Since Lépine's theory predicts a linewidth proportional to the velocity of the conduction electrons and their concentration, several experiments may be proposed which could be carried out at fixed temperature. The sample could be illuminated at a sufficient energy to excite an increased number of conduction electrons, or the average velocity could be increased by application of an electric field. In this last case samples of higher donor concentration, or at the higher temperatures in which the hyperfine splitting is still observable, might result in excessive power dissipation. This could be overcome by pulsing the applied electric field at a frequency lower than that of the high frequency field modulation and gating the input to the spectrometer in synchronism, so that the resonance is examined only during those

periods in which the electric field is applied.

Similar hydrogen-like states for donors exist in other materials e.g., GaAs and GaP. Very precise optical measurements of these states have been made on high purity GaAs, but like GaP no results have been published on the E.P.R. of "shallow" bound donor electrons. For these cases are really the reverse of that for silicon, in that whereas the silicon lattice contains ~ 5% nuclei having a magnetic moment and the common donors have 100% abundance of nuclei with spins, the reverse is true for GaAs and GaP. Due to the spatial extent of the electron orbit this therefore leads to undetectably broad lines, and only for one deep donor, oxygen, has bound resonance been confirmed. It is thus unlikely that similar effects to those reported here will be observed in these materials.

REFERENCES

1. G. Feher, Phys. Rev. 114 (1959) 1219.
2. W. Sasaki, S. Maekawa and J. Kinoshita, J. Phys. Soc. Japan 22 (1967) 928.
3. T. G. Castner, Jr., Phys. Rev. 130 (1963) 58.
4. D. Jérome and J. M. Winter, Phys. Rev. 134 (1964) 1001.
5. N. Kumar and K. P. Sinha, Zeits für Physik 197 (1966) 26.
6. J. F. Janak, J. Phys. Chem. Solids 27 (1966) 1571.
7. B. I. Kochelaev, Soviet Phys. - Solid State 7 (1966) 2315.
8. W. M. Walsh, Jr., J. Jeener and N. Bloembergen, Phys. Rev. 139 (1965) 1338.
9. H. Seidel, Zeits für Physik 165 (1961) 218.
10. V. Heine, Phys. Rev. 107 (1957) 1002.
11. E. Simanek and R. Orbach, Phys. Rev. 145 (1966) 191.
12. V. Ya. Kravchenko and V. L. Vinetskii, Opt. Spectry. 18 (1965) 37.
13. S. D. Lacey and G. Lancaster, Phys. Letts. 22 (1966) 386.
14. G. Feher and E. A. Gere, Phys. Rev. 114 (1959) 1245.
15. G. D. Watkins, Conference on Solid State Physics, Manchester (1967).
16. G. D. Watkins and F. S. Ham, Phys. Rev. B 1 (1970) 4071.
17. T. G. Castner, Phys. Rev. 155 (1967) 816.
18. D. E. Dugdale, S. D. Lacey and G. Lancaster, J. Phys. C 4 (1971) 654.
19. R. Kubo and K. Tomita, J. Phys. Soc. Japan 9 (1954) 888.
20. R. L. Aggarwal and A. K. Ramdas, Phys. Rev. 140 (1965) 1246.
21. D. K. Wilson and G. Feher, Phys. Rev. 124 (1961) 1068.
22. D. K. Wilson, Phys. Rev. 134 (1964) 265.
23. D. J. Lépine, Phys. Rev. B 2 (1970) 2429.
24. R. A. Smith, Semiconductors (C.U.P.) 1961.